Simulating groundwater and surface water flow and solute transport in tile-drained landscapes

Thèse

Vinicius Ferreira Boico

Doctorat interuniversitaire en sciences de la Terre
Philosophiæ doctor (Ph. D.)

Québec, Canada

UNIVERSITÉ LAVAL

Simulating groundwater and surface water flow and solute transport in tile-drained landscapes

Thèse

Vinicius Ferreira Boico

Sous la direction de :

René Therrien, directeur de recherche

Résumé

Dans des conditions de climat humide et lorsque les sols sont peu perméables, les systèmes de drainage souterrains sont généralement utilisés pour contrôler le niveau de la nappe phréatique et améliorer la production agricole. Cependant, les drains souterrains modifient à la fois les voies d'écoulement hydrologique et les taux de transport des nutriments des terres cultivées vers les eaux de surface, pouvant détériorer la qualité des eaux souterraines et de surface. De plus, des macropores sont souvent présents dans les sols composés de till argileux, ce qui génère un flux d'eau rapide et riche en nutriments de la surface du sol vers les drains souterrains. Une approche rentable pour réduire le lessivage des nutriments provenant de l'agriculture consiste à imposer des restrictions uniquement dans les zones vulnérables à la contamination de l'eau. Ces zones peuvent être identifiées à l'aide de modèles hydrologiques distribués. Les résultats obtenus sur de petits bassins versants expérimentaux doivent être simplifiés pour être appliqués à des échelles plus grandes, généralement requises pour l'élaboration de politiques. L'objectif de cette étude était d'examiner les avancées et les limitations de l'inclusion des drains souterrains dans les modèles d'écoulement de surface et souterrain. Les objectifs spécifiques étaient de i) démontrer l'utilisation des estimations de conductivité électrique spécifique (CE), pour améliorer les simulations hydrologiques dans un champ drainé, ii) étudier l'efficacité d'un modèle hydrologique et de transport de soluté tridimensionnel pour simuler un test de traçage de bromure (Br) dans un champ drainé et iii) évaluer différents modèles conceptuels de drains souterrains et d'hétérogénéité du sol pour la simulation numérique du drainage dans un bassin versant agricole au Danemark. Les résultats suggèrent que la simulation de la profondeur de la nappe phréatique peut être améliorée par l'inclusion d'hétérogénéités basées sur des estimations de la CE. L'approche des *seepage nodes* était appropriée pour simuler les débits de drainage, cependant la précision des simulations était meilleure pour les modèles à l'échelle du terrain. À l'échelle du bassin versant, le fait de ne représenter que les drains principaux est approprié pour pouvoir utiliser des maillages plus grossiers et pour simuler le débit des cours d'eau et les faibles profondeurs des eaux de surface dans les zones drainées. Des résultats similaires ont été obtenus lorsque les *seepage nodes* ont été appliqués sur l'ensemble des zones agricoles, sans tenir compte de l'emplacement spécifique des drains souterrains. Cette dernière approche peut être appliquée lorsque les drains souterrains ne sont pas cartographiés, ce qui est généralement le cas. Une représentation simplifiée de l'hétérogénéité et de la macroporosité peut expliquer les différences entre ls valeurs observées et simulées des charges hydrauliques, débits de drainage et processus de transport de solutés. Les approches de modélisation étudiées dans cette thèse peuvent améliorer la représentation de la dynamique de l'écoulement souterrain et les simulations du transport de substances agrochimiques lessivées des champs cultivés, telles que le nitrate et phosphate.

Abstract

Under humid climate conditions and for low-permeability soils, subsurface tile drains are usually employed to lower the water table and enhance agricultural production. However, tile drains alter both the hydrologic flow pathways in agricultural catchments and the rates of nutrient transport from cropland to surface water bodies, potentially impairing the groundwater and surface water quality. Furthermore, macropores are often present in clayey till soils, generating rapid and nutrient-rich water flow from the ground surface to the tile drains. A cost-effective approach to reduce nutrient leaching from agriculture is to impose restrictions only in vulnerable areas to water contamination, which can be identified using distributed hydrological models. Results on small experimental catchments need to be simplified for application on larger scales, usually required for policy-making purposes. The objective of this study was to investigate the outcomes and limitations of including tile drains in surface and subsurface flow models. Specific objectives were to i) demonstrate the use of electrical conductivity (EC) estimates to improve hydrological simulations in a tile-drained field, ii) investigate the efficiency of a three-dimensional hydrological and solute transport model to simulate a bromide (Br) tracer test in a tile-drained field and iii) assess different conceptual models for tile drains and soil heterogeneity for the numerical simulation of tile drainage in an agricultural catchment in Denmark. The results suggest that the simulation of the water table depth can be improved by the inclusion of heterogeneities based on EC estimates. The seepage nodes approach was suitable to simulate drain discharge, however the accuracy of the simulations was better for the field-scale models. At the catchment scale, representing only the main drains was suitable to reduce the mesh refinement and simulate stream flow and low surface water depths in drained areas. Similar results were obtained when seepage nodes were applied all over the agricultural areas, without considering the specific location of tile drains. The later approach can be applied when tile drains are not mapped, which is usually the case. The misrepresentation of heterogeneity and macroporosity may explain the differences between observed and simulated hydraulic heads, drain discharge and solute transport processes. The modeling approaches investigated in this dissertation can improve subsequent simulations of tile drainage and the transport and fate of leached agrochemicals such as nitrate or phosphate.

Contents

List of figures

List of tables

To Bibimax…

"Educar-se é impregnar de sentido cada momento da vida, cada ato cotidiano." Paulo Freire

Acknowledgments

I would like to acknowledge all of the support I have received from when I first arrived in Québec City to complete this PhD. This has been a long journey from September 2016 to April 2022. Worldwide, I found support from professors, researchers, friends, colleagues, associations, employees, and my parents.

To my supervisor, René Therrien, I would like to express my sincere appreciation for his generous and continuous support, expert guidance, and constructive advice. I'm also grateful to René for giving me the chance to present our research at various international conferences. The fulfillment of this dissertation was made possible thanks to his guidance and support… Thank you René!

I'm grateful to my former professors in hydrogeology and related areas, especially my Master's thesis supervisor Edson Wendland, and John Molson from *Université Laval*, for the encouraging guidance through this incredible and multidisciplinary area.

I would also like to acknowledge the funding provided by the Innovation Fund Denmark and the Natural Sciences and Engineering Research Council of Canada. Research stays in Denmark were only possible with extra funding from MITACS (Canada) and the Quebec Water Research Center (CentrEau). A research stay in the Helmholtz Centre for Environment Research (UFZ) was funded by a scholarship from the *Fonds de recherche du Québec – Nature et technologies* (FRQNT). CentrEau also provided financial support for attending national and international conferences.

I thank my colleagues from Université Laval who supported me in the hydrological modeling with HydroGeoSphere, PEST and scientific writing and reviewing. I also thank for the enjoyable social environment and interesting discussions, academic or not. Thank you Hugo Delottier, Cécile Coulon, Masoumeh Parhizkar, Nathan Young, Flore Sergeant, Julie Perreault, Alexandre Mandizabal, Walter L. A. Quijano, Laura Gatel, Sophie Dagenais, Alexandra Germain, Jonathan Fortin and many others. Special thanks to Ana Carolina Miranda who is a valuable friend and was close to me with warm and funny conversations (and good food sometimes).

I would like to thank Anker L. Højberg, Bo V. Iversen, Heidi C. Barlebo, Mads Steiness, Ioannis Varvaris, Triven Koganti, Rasmus Petersen and Anne L. Hansen, in Denmark for the warm welcome and continued support during my many stays in GEUS and Aarhus University. I thank Jan Fleckeinstein and Guilherme Nogueira, for the academic support and great hospitality in Germany during pandemic times. I also would like to recognize the administrative support from the secretary from different

departments/institutions (Isabelle, Guylaine, Camilla, Viviane, Barbara) and professors and researchers (René, Anker, Bo, Jan) with the bureaucracy of the various VISA processes – thank you!

Thank you to Roxane four our many pomodoros together in Canada and Germany, and of course the lovely friendship and all the hagebutten :). And thank you all my beloved friends (Vilmantas, Bené, Jasson, Charles, Steffie, Philou, Salvador, Caio, Clara, MH, Alice, Rafael, Camille, Doug, Miri, Bibimax, Johana, Juliana, Ju, Fram, Isa, Bel, Bea, Jean, Recife) and brother who were with me during the elaboration of this PhD.

And thank you Mom and Dad, for being there, virtually or personally, and for always supporting me in my academic journey and other adventures :).

Without all these supports, this dissertation would have not been possible.

Preface

This PhD dissertation is mainly written as a series of articles, in accordance with the guidelines given by the Faculty of Sciences and Engineering, Université Laval. Vinicius F. Boico was the first author and René Therrien was the supervisor of the three articles included in Chapters 4 to 6. Vinicius F. Boico was responsible for the conceptualization, methodology, investigation, writing the original draft, reviewing, visualization and project administration. René Therrien was responsible for the supervision, software, resources and funding acquisition.

The co-authors of the articles were: Anker L. Højberg (resources and funding acquisition), from the Department of water resources, Ramboll, Copenhagen, Denmark; Bo V. Iversen (data curation and funding acquisition), Triven Koganti (investigation and data analysis) and Rasmus J. Petersen (investigation) from the Department of Agroecology, Aarhus University, Tjele, Denmark; Ioannis Varvaris (data analysis) from the Department of Civil & Environmental Engineering, University of Wisconsin-Madison, Madison, EUA; Jan H. Fleckenstein (resources and investigation) and Guilherme Nogueira (investigation), from the Department of Hydrogeology, UFZ, Leipzig, Germany; Hugo Delottier (methodology), from the Centre for Hydrogeology and Geothermics, Neuchâtel, Switzerland; and Nathan L. Young (revision), from the Department of Geology and Geological Engineering, Université Laval, Quebec City, Canada. All authors contributed to the critical review and editing process.

A brief description of the articles is provided.

Chapter 4 is an article published in the Journal of Hydrology in January 2022:

Boico, V. F., Therrien, R., Højberg, A. L., Iversen, B. V., Koganti, T., Varvaris, I. (2022). Using depth specific electrical conductivity estimates to improve hydrological simulations in a heterogeneous tile-drained field. Journal of Hydrology, 604. doi:10.1016/j.jhydrol.2021.127232.

Chapter 5 is an article in preparation for submission:

Boico, V. F., Therrien, R., Fleckeinstein, J., Nogueira G., Iversen, B. V., Petersen R. J. 3D surface-subsurface modeling of a bromide tracer test in a macroporous tile-drained field: improvements and limitations.

Chapter 6 is an article published in the Journal of Hydrology in September 2022:

Boico, V. F., Therrien, R., Delottier, H., Young, N. L., Højberg, A. L. (2022). Comparing alternative conceptual models for tile drains and soil heterogeneity for the simulation of tile drainage in agricultural catchments. Journal of Hydrology, 612(Part A). doi:10.1016/j.jhydrol.2022.128120

Introduction

Subsurface drainage systems consisting of tile drains are usually employed to lower the water table, reduce soil saturation, and enhance agricultural production in soils with low permeability and for humid climatic conditions. However, tile drains alter both the hydrologic flow pathways in agricultural catchments (Hansen et al., 2013; King et al., 2014; Thomas et al., 2016; Werner et al., 2016) and the rates of agrochemicals transport (fertilizers, pesticides and herbicides) from cropland to surface water bodies (Amado et al., 2017; Radcliffe et al., 2015; Rozemeijer et al., 2010b; Stamm et al., 2002). As a result, tile drains facilitate the transport of leached chemicals from the application area to surface or coastal waters with a short residence time, compared to the natural subsurface flow system in a catchment (Figure 0.1). Furthermore, the presence of macropores in clayey-till soils increases the rate at which nutrient-rich water is routed from the ground surface to tile drains.

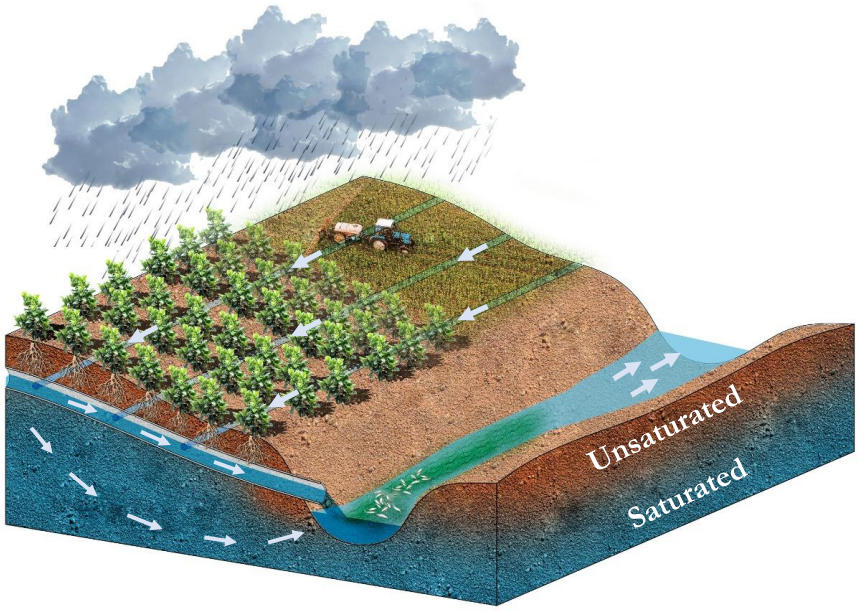

Figure 0.1 - Water flow paths in a tile-drained agricultural field. This illustration shows the tile drain flow after a rainfall event. Drain discharge in agricultural areas convey water with high concentration of agrochemicals to the surface water bodies. Excessive amounts of nutrients in the water bodies cause eutrophication and hypoxia destroying the aquatic ecosystem.

Excessive nutrient enrichment (eutrophication) of water bodies causes toxic algal blooms, as well as a loss of oxygen and biodiversity, in streams, lakes, and coastal areas (Carpenter et al., 1998). European waters are already affected by high concentrations of nutrients from inland water bodies (groundwater, rivers and lakes) to transitional and coastal waters and ecosystems in open seas (European Environment Agency, 2005). In Denmark, 90% of the total nitrogen load to fjords and coastal waters in 2012 was from diffuse sources, such as agriculture (Wiberg-Larsen et al., 2013). Since 1985, national regulations have

been implemented to reduce nitrogen losses from farming (Kronvang et al., 2008), and a reduction of 45% of yearly nitrogen surplus was obtained from 1990 to 2012 (Jensen et al., 2013). However, a further reduction of 25 to 50% is still needed to reach the European Union objectives (Refsgaard, 2014, 2019). A cost-effective approach to reduce nitrate leaching from agriculture is to impose restrictions only in areas vulnerable to water contamination (Refsgaard et al., 2014, 2019), which can be identified using distributed hydrological models, provided the models have sufficient resolution to make predictions at small spatial scales.

The potential negative environmental impacts of tile drainage systems were studied in the Transport and Reduction of Nitrate in Danish landscapes at various Scales (TReNDS project, www.nitrat.dk). The overall objective of TReNDS was to develop the scientific foundation, field technologies and modeling concepts for cost-effective quantitative assessments of nitrate transport and reduction required for spatially-differentiated regulation on agrochemicals application. This project was created in response to the EU Water Framework Directive (WFD, European Union, 2008), which prompted the development of integrated hydrological models for the assessment of regulations to reduce nitrate pollution. The TReNDS project objectives addressed in the present dissertation were i) to improve the understanding of the impact of drainage systems on water flow and solute transport for different hydrogeological settings, and ii) to develop upscaling approaches to enable the representation of local-scale processes in catchment-scale hydrological modeling.

Reliable estimates of nutrient travel times from application areas to the surface water system are essential for the evaluation of the water quality response due to changes in agricultural practices and nitrogen mitigation measures (Vervloet et al., 2018; Meals et al., 2010). As tile drains provide a rapid flow pathway between agricultural areas and downstream recipients, the fast flow in the drainage network must be modeled with sufficient accuracy. Such models will also provide a better understanding of the hydrological processes affecting runoff generation in these areas (O'Connell et al., 2007). The implementation of tile drainage systems in hydrological models was suitable for simulating drain discharge (De Schepper et al., 2015, 2017; Thomas et al., 2016) and solute transport in tile drainage water (Colombani et al., 2016; Mollerup et al., 2014) and to improve simulations of hydraulic heads (Hansen et al., 2013) and the stream discharge (Hansen et al., 2013, Kiesel et al., 2010, Koch et al., 2013). However, improvements in hydrological models with tile drains are required for: tile drainage integration into catchment-scale models; accurate water flow and nutrient transport simulations through heterogeneous tile-drained soils; and the development of new concepts to represent the dynamics of tile drainage and to increase model resolution to be used for differentiated regulation. Furthermore, results and methodologies developed in small experimental catchments often need to be simplified for application in the larger-scale simulations that are typically used for policy-making purposes (Refsgaard et al., 1999).

The purpose of this research was to advance coupled groundwater and surface water flow modeling in tile-drained landscapes by allowing for a physically-based, yet computationally-efficient simulation of hydrological and solute transport processes. Existing modeling concepts were investigated to improve hydrological and solute transport simulations in terms of accuracy, simplicity, reproducibility, and simulation times. First, the research aimed to demonstrate the capability of electrical conductivity estimates to improve hydrological simulations in a heterogeneous tile-drained field. Second, the model performance to simulate a bromide tracer test was evaluated by implementing macroporosity in a dense tile-drained field. Third, different conceptual models for tile drains and soil heterogeneity for the numerical simulation of tile drainage in an agricultural catchment were compared and evaluated.

Chapter 1

Literature review

1.1 Tile drainage in agricultural areas

Subsurface drainage is used in agricultural areas worldwide to improve the root growth conditions and organic matter decomposition (Ali, 2011). Many countries in Europe and North America, as well as Egypt, Pakistan, China, Turkey and India have large tile-drained agricultural areas (Nijland et al., 2005). In Canada, the USA and northern Europe, the regional landscape and near-surface geology were shaped by several ice advances and retreats during the Wisconsinian glaciation in North America (Lemieux et al., 2008) and the Weichsel and Saale glaciations in Europe (Houmark-Nielsen and Kjaer, 2003). The unconsolidated glacial sediments deposited during these glaciations, particularly tills and glaciolacustrine clays, favored the formation of poorly to very-poorly drained soils, which can limit agricultural production due to the presence of shallow water tables and high water contents, depending on climate and land slope conditions (Rodvang and Simpkins, 2001). In Denmark, clay soil drainage with tiles started around 1850, and currently approximately 50% of the agricultural area is artificially drained, with 8 to 20 meters of distance between the drains (Olesen, 2009). In Iowa (USA), the installation of subsurface drains and surface ditches started around 1890 and, by around 1930, 2.5 million hectares of Iowa were part of drainage districts (Schilling et al., 2012, 2019).

1.2 Tile drainage definition and classification

Subsurface drains are permeable pipes installed underground and connected into a subsurface system to remove the excess water from the topsoil. They are usually installed close to the surface (usually between depths of 1.0 to 1.5 m). Generally called tile drains, the buried pipe drains may be made of plastic, concrete or clay (Ali, 2011). The water enters concrete and clay pipes through small spaces between the tiles. In plastic pipes, water enters through perforations distributed over its length (Ali, 2011). The main drainage facilities within an agricultural area usually consist of field or lateral drains; collector drains that collect water from the field drains; main drains, that collect water from two or more collectors, and a drainage outlet (Ritzema, 1994; Figure 1.1a). Due to the complexity of the tile drainage network, the nomenclature may be simplified to lateral drains and main (or collector) drains, that conduct water out of the field to the drainage outlet (Bouarfa and Zimmer, 2000; Sunohara et al., 2016; Thomas et al., 2016; Yue 2010). The drainage outlet discharges water to a surface water body (stream or ocean), to wetlands, or to an

open ditch. Figure 1.1b shows an example of tile drainage systems in the Fensholt catchment, in Denmark.

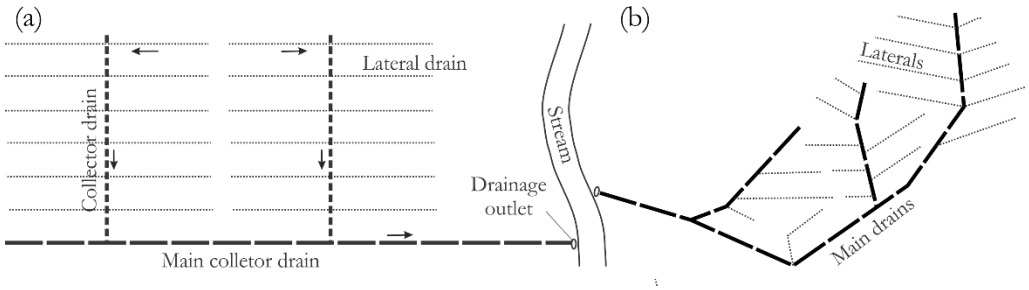

Figure 1.1 – Plan views illustrating (a) Types of tile drains within an agricultural area according to Ritzema (1994) and (b) example of a tile drainage system in the Fensholt catchment, Denmark, using a simplified nomenclature.

Subsurface drainage systems are differentiated into conventional and controlled systems (Evans et al., 1995). Conventional drainage systems are composed of a simple drainage network without any complementary equipment. In controlled drainage systems, the network has additional equipment to control drainage flow, such as flashboard risers, pits, tanks and drop logs (Evans et al., 1995).

1.3 Hydrology of humid tile-drained agricultural areas

The hydrological response of a tile drainage system results from complex interactions between the input of rainfall (or irrigation), the land characteristics, and the drainage system (Robinson and Rycroft, 1999). Infiltration depends on antecedent conditions, vegetation, roughness, and compactness of the soil surface, which also influences the water flow to the drainage systems. The volume of water entering the soil is limited by the infiltration capacity of the soil. After infiltration, water may be temporarily stored in the unsaturated zone (vadose zone) until it reaches the water table (saturated zone). Volumes of precipitation greater than the infiltration capacity, or infiltration water that cause the water table to rise to the ground surface, will subsequently initiate overland flow or surface ponding. Depressions on the surface may store surface water, promoting focused infiltration in localized areas. Groundwater will flow in response to a hydraulic gradient across the water table and may discharge to surface water bodies as baseflow. Tile drain flow is generated when the water table rises above the elevation of the drains and can be considered a component of baseflow. The sketches presented in Figure 1.2 represent the main hydrological processes that govern uncontrolled tile drainage as used to maintain groundwater at a desired level within an agricultural field.

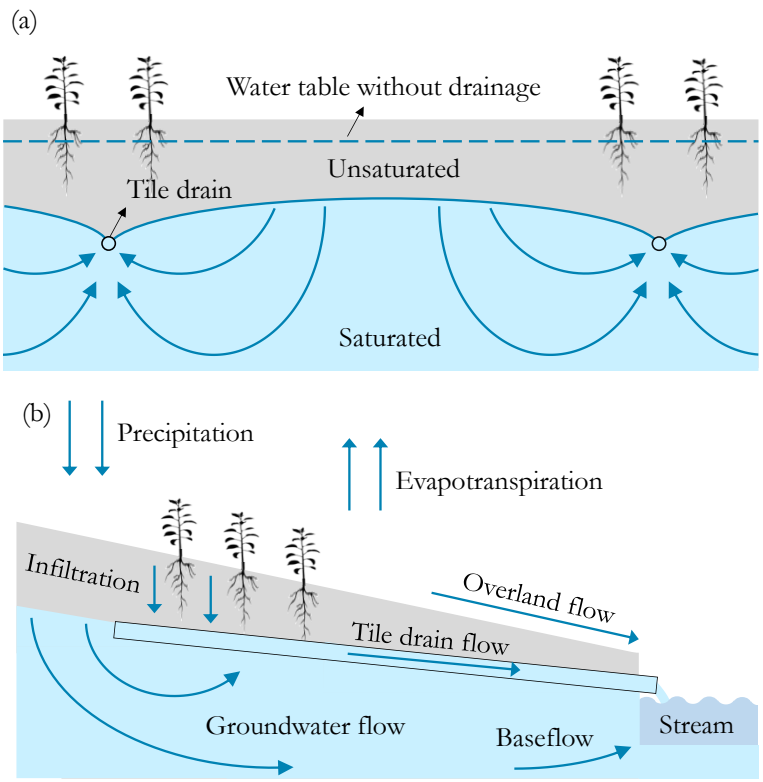

Figure 1.2 – Sketches of the (a) water table with and without a subsurface drainage system and (b) main hydrological processes in a tile-drained field discharging to a stream.

Conversion from natural drainage to artificial subsurface drainage for agriculture has had a significant impact on the hydrologic flow pathways in agricultural catchments (Blann et al., 2009; Hansen et al., 2013; King et al., 2014; Thomas et al., 2016; Werner et al., 2016). Field monitoring and model simulations suggested that tile drainage flow increases annual baseflow in streams, with seasonal increases in spring and summer (Schilling and Libra, 2003; Schilling et al., 2008). Compared to undrained land, tile drainage and the change in land use to agriculture increases peak runoff rates and losses of nutrient and sediment (Skaggs et al., 1994). However, the increased magnitude of the runoff peaks and nutrient loads depend heavily on land use changes, type of drainage system, agricultural practices, fertilizer usage, crops, soil and climate. Robinson and Rycroft (1999) and Skaggs et al. (1994) proposed two competing theories where i) tile drainage can increase stream flow peaks by removing water from the subsurface and conveying it to the outlet faster than the lateral subsurface flow in undrained soils or ii) reduce flow peaks (and flooding downstream), since surface water infiltrates faster and is released to the outlet over a longer period compared to surface runoff. Recent research has shown that peak stream discharge is lower and that less variability in the flow curve duration was observed in drained compared to undrained catchments (Boland-Brien et al., 2014). Sloan et al. (2017) observed that tile drains reduce peak flows of some medium-sized flood events but had minimal effect for the largest events of the year. The authors also stated that stream peak flow at the catchment outlet varies with the spatial distribution of drained fields.

Discharge flow from tile drains can vary greatly in a catchment, depending on the tile-drained area, soil properties, precipitation and evapotranspiration (Eastman et al., 2010; King et al., 2014). Furthermore, many authors have shown that changes in tile drain depth and spacing have a considerable effect on tile outflow and nitrate losses (Kirkham, 1949; Davis et al., 2000; Skaggs and Chescheir, 2003; Kladivko et al., 2004; Nangia et al., 2010). In a modeling study in Denmark, De Schepper et al. (2017) estimated that 74% of the Fensholt catchment discharge originates from tile drains. In an experimental field in the Netherlands, the contribution of drains to the catchment discharge was estimated to be around 80% (Rozemeijer et al., 2010a) and in Finland, Nouisiainen et al. (2015) found that yearly volumes of tile drainage effluent corresponded to around 33% of precipitation in a tile-drained field. In a tile-drained region in Ontario, Canada, Macrae et al. (2007) found that the contribution of tile drainage in watershed discharge ranged from 0 to 90%. In the United States, Logan et al. (1980) found that annual rainfall recovered in tile drainage ranged from 4 to 18% in Iowa, 0 to 40% in Minnesota and 0 to 66% in Ohio. In more recent tile drainage modeling studies in Iowa, Arenas-Amado et al., (2017) reported that tile drainage accounted for 15-43% of streamflow in a northeast Iowa watershed from April to November, and Schilling et al. (2019) estimated that tile drainage accounted for approximately 46 to 54% of annual discharge in the Boone River and provided most of the flow in the river during the March to June period. In Ohio, King et al. (2015) reported that tile drainage provided 56% of a small watershed.

Nutrient transport and reduction processes in agricultural landscapes are influenced by hydrology. Understanding the impact of tile drainage on the streamflow is important to estimate how pollutant discharge from tile drains differs from natural groundwater flow to streams. In natural systems, groundwater flows through riparian zones where water contaminants, such as nitrate, are reduced by biological processes (Clément et al., 2003; Davis et al., 2011; Hill et al., 1996, 2019). However, tile drainage bypasses riparian zones, discharging excessive amounts of pollutants from upland agricultural fields directly to surface water. Considering the magnitude of contaminant loads from tile-drained landscapes, evaluation of nitrate transport to surface water should consider the percentage of baseflow derived from subsurface drainage flow compared to other sources (Schilling et al., 2008).

1.4 Numerical modeling of tile-drained areas

The availability, cost and processing capacity of computers have evolved during the last decades, improving the science and practice of numerical modeling of groundwater flow and transport processes (Konikow, 2011). Over the past 20 years, the applications of fully-integrated three-dimensional (3D) hydrologic models have increased due to a better mathematical representation of the hydrological processes, parameterization and cost-effective computational resources (Berg et al., 2019). These models can be used to develop scenarios to evaluate the effectiveness of mitigation strategies such as constructing vegetated strips, wetlands, depressions and drainage systems, and implementing best agricultural practices (Tang et al., 2012).

Data to support hydrological modeling studies on tile drainage impacts are often scarce, as farm drainage is often carried out privately and at small scales, and drain installation is usually neither centrally recorded nor easily visible (Robinson and Rycroft, 1999). Precise measurement of flow path contributions and high-frequency monitoring in tile-drained areas as performed by Rozemeijer et al., (2010b) and van der Velde et al., (2010) is difficult and often impossible, as the extensive equipment used for installation and monitoring required to do so is often financially prohibitive. Although they cannot replace field investigations, numerical models are very useful to improve the understanding of the hydrology of tile-drained catchments.

Several different methods for representing tile drains in a more computationally efficient way have been developed and tested. Fipps et al. (1986) were among the first authors to implement subsurface drains as boundary conditions in a two-dimensional (2D) numerical solution. They tested four methods: modeling a hole equal in size to the radius of the drain, the single-node approach using a specified flux, or a specified head, and the resistance adjustment method, where the hydraulic conductivities of the elements around the drains are adjusted. Based on this study, MacQuarrie and Sudicky (1996) developed a one-dimensional equation of drainage flow in a three-dimensional variably saturated model, equivalent to an open channel flow equation. Under transient drainage water flow, the Boussinesq equation for two-dimensional unconfined flow can also be applied. Variably-saturated subsurface water flow in hydrological models is commonly solved by Richards' equation. Under steady-state conditions, subsurface drainage water flow can be solved by i) Hooghoudt's equation, which considers radial water flow under and towards the drains, and horizontal water flow above them; ii) Kirkham's equation, developed for drainage flow in a ponding context and iii) Ernst's equation, where radial flow is considered above and below the drains.

Physically-based models have been widely used for simulating water flow and solute transport through the saturated and unsaturated zones in tile-drained fields, and several numerical codes are available for

use at different scales and dimensionality. One-dimensional models may represent tile drains as a sink node boundary condition (SWAP, Kroes et al., 2017), by solving Hooghoudt's equation (ADAPT, Kalita et al., 1998; ANSWERS, Bouraoui et al., 1997; DRAINMOD, Skaggs, 1978, 2012) or by water balance methods (SaltMod, Oosterbaan, 2002). Two-dimensional, physically-based models usually calculate tile drainage by Hooghoudt's equation, such as MHYDAS-DRAIN (Tiemeyer et al., 2007) and AnnAGNPS (Yuan et al., 2006) and the Boussinesq equation, such as SIDRA (Lessaffre and Zimmer, 1988). Tile drainage has also been modeled as a high-permeability equivalent porous medium using ANTHROPOG (Carluer and De Marsily, 2004) and as morphologically connected structures of low flow resistance with CATFLOW (Klaus and Zehe, 2011; Zehe et al., 2001). A list of hydrological models suitable for tile drainage modeling is presented in Table 1.1.

In three-dimensional models, tile drainage can either be simulated as an equivalent layer of high hydraulic conductivity (SWMS-3D, Carlier et al., 2007; HydroGeoSphere, De Schepper et al., 2015; Thomas et al., 2016) or as one-dimensional line elements in (HydroGeoSphere, De Schepper et al., 2015; MODHMS, Panday and Huyakorn, 2004). However, the most common method for representing tile drainage is the use of sink nodes (or seepage nodes), which is supported by MODFLOW (Langevin et al., 2017), MODHMS , FLUSH (Warsta et al., 2013), HYDRUS (Šimůnek et al., 2009), FEMWATER (Lin et al., 1997), HydroGeoSphere (HGS, Aquanty Inc., 2017) and MIKE-SHE/MIKE 11 (Refsgaard and Storm, 1995). When seepage nodes are used, each seepage node is assigned a pressure head (or hydraulic head) value and the drainage flow rate is calculated from the hydraulic gradient and a conductance term (similar to a leakage coefficient). Seepage nodes are usually deactivated under unsaturated conditions and can only extract water from the model. HYDRUS, however, can represent drains as sinks or sources of water. Drainage water in MIKE-SHE/MIKE 11, MODHMS and HydroGeoSphere can be routed to specific locations defined by the modeler, such as wetlands or streams (Christiansen et al., 2004). Preferential flow through macropores in tile drained fields can be simulated in MHYDAS-DRAIN, FLUSH, HYDRUS, MIKE-SHE/MIKE 11, MODHMS and HydroGeoSphere.

The complexity and number of hydrological domains (surface, subsurface, dual continuum, etc.) represented in these models differ considerably. For instance, DRAINMOD is a root zone model; MHYDAS-DRAIN, SWAT, and ANTHROPOG are surface and root zone models where groundwater is represented by a reservoir model; SWMS 3D is a variably-saturated subsurface model; and MIKE SHE, MODHMS, and HydroGeoSphere are fully integrated three-dimensional models coupling surface and subsurface domains.

Table 1.1 - Non-exhaustive list of hydrological models suitable for tile drainage modeling. The model dimension (Dim.) and scale (F = field, C = catchment) is presented. The governing equations to solve surface, subsurface and drain domains or the water balance parameters (in italics) are shown

Model	Dim.	Scale	Overland	Subsurface	Drain	Reference
ADAPT	1D	F	-	Richards	Hooghoudt/Kirkham	Kalita et al. (1998)
AnnAGNPS	2D	C	Curve number*	Darcy	Hooghoudt	Yuan et al. (2006)
ANSWERS	1D	F	-	Brooks-Corey	Hooghoudt	Bouraoui et al. (1997)
ANTHROPOG	2D	F	-	Darcy	Richards (equivalent medium)	Carluer and De Marsily (2004)
CATFLOW	2D	F	Saint-Venant†	Richards	Richards (connected structures)	Zehe et al. (2001)
DRAINMOD	1D	F	-	Richards	Hooghoudt/Kirkham	Skaggs (1978, 2012)
FEMWATER	3D	F	-	Richards	*Sink*	Lin et al. (1997)
FLUSH	3D	F	Saint-Venant†	Richards	*Sink*	Warsta et al. (2013)
HydroGeoSphere	3D	Any	Saint-Venant†	Richards	Hazen-Williams	Aquanty Inc. (2017)
HYDRUS	3D	Any	-	Richards	*Sink/Source*	Šimůnek et al. (2006)
MHYDAS-DRAIN	2D	F	Hortonian flow	*Reservoir*	Hooghoudt	Tiemeyer et al. (2007)
MIKE SHE/MIKE 11	3D	Any	Saint-Venant†	Richards	*Sink*	Refsgaard and Storm (1995)
MODFLOW	3D	Any	-	Darcy	*Sink*	McDonald and Harbaugh (1988)
PESTDRAIN	2D	F	*Reservoir*	Boussinesq	Boussinesq	Branger et al. (2009)
SaltMod	1D	F	*Water balance equation*			Oosterbaan (2002)
SIDRA	2D	F	-	Boussinesq	Boussinesq	Lessaffre and Zimmer (1988)
SUTRA	3D	Any	-	Darcy	*Sink*	Voss and Provost (2010)
SWAP	1D	F	*Reservoir*	Richards	Hooghoudt	Kroes et al. (2008)
SWAT	2D	C	Curve number*	*Reservoir*	*Sink*	Arnold et al. (1998)
SWMS-3D	3D	F	-	Richards	Richards (equivalent medium)	Šimůnek et al. (1995)

∗ The curve number values for surface runoff are calculated based on Soil Conservation Service curves developed by the U.S. Department of Agriculture (1972). † Diffusion wave approximation to the Saint-Venant equation.

De Schepper et al. (2015) investigated the applicability of various tile drainage modeling concepts using the HydroGeoSphere code by varying some parameters, such as the drain type, time interval for precipitation and conceptual model for the subsurface (single and dual continuum). They stated that i) the concept of discrete drain pipes is suitable for tile drainage flow modeling, but it may lead to very long simulation times; ii) the model representing tile drains as equivalent medium requires calibration to reproduce the water budget at the field or catchment scale; iii) hourly precipitation input produced more pronounced drainage peaks and iv) simplifying the drainage network into the main collecting pipes represents an alternative to reduce the mesh density and reduce computational times. Hansen et al. (2013) used a coupled groundwater-surface water model based on the MIKE SHE code. Their results showed that including tile drain data in the calibration improved the performance for hydraulic heads and stream discharge, but only on a large-scale. Furthermore, the model was not able to describe the local-scale

dynamics of tile drain discharge. Hansen et al. (2009) combined a root zone model (DAISY) with MIKE SHE/MIKE11 and obtained consistent results for the nitrogen fluxes in the river system, but not for daily discharge values. Regarding the finite element grid configuration, Tarboton and Wallender (2000) stated that fine spacing is necessary in the vicinity of the drain to ensure stable numerical solutions for the modeling of multiple drains and solute transport.

1.5 Macroporosity in tile-drained soils

Macropores or fractures in low hydraulic conductivity soils are preferential flow pathways that can increase the velocity of water flow and advection-dominant solute transport to the tile drains (Šimůnek et al., 2003). Macroporosity in tile-drained soils can create events of high solute or particle concentrations in drainage water endangering the surface water quality (Akay and Fox, 2007; Frey et al., 2016; Júnior et al., 2004; Rosenbom et al., 2015; Stamm et al., 1998, 2002). Preferential flow often occurs in the absence of hydraulic equilibrium (Jarvis et al., 2007) and arises from a contrast in conductance between different types of flow paths (Nimmo et al., 2012). Under nonequilibrium flow, water infiltrates too fast to equilibrate with slowly moving water in the bulk of the soil matrix (Jarvis et al., 1998b). Jarvis et al. (2020) stated that the potential for non-equilibrium water flow and solute transport in macropores depends on factors related to the structural formation and degradation of the macropore network, such as soil biota activity, soil properties, site factors (drying intensity, vegetation, etc.) and management (tillage, cropping, etc.).

Preferential water flow and transport in macroporous soils have been accurately simulated using the dual continuum approach (Varvaris et al., 2018; 2019, Bishop et al., 2015; Abbaspour et al., 2001; Frey et al., 2012; 2016, Klaus and Zehe, 2011, Gärdenäs et al., 2006), which can be used to analyse field-scale tracer experiments (Rosenbom et al., 2009). The dual continuum formulation in HydroGeoSphere involves two separate continua of pore sizes representing the porous media (micropores) and the macropores, where mass transfer between the macropore and porous media continua is described using first-order transfer terms (Aquanty Inc., 2017; Šimůnek et al., 2003). Preferential flow through macropores has been addressed by dual continuum and Richards' equation-based models with good performance for water flow and solute transport in tile drains (Bishop et al., 2015; Frey et al., 2012, 2016; Gärdenäs et al., 2006; Gerke and Köhne, 2004; Gerke et al., 2007; Pot et al., 2005). Non-equilibrium transport can be simulated by the dual porosity, dual permeability and the single porosity with immobile zone concepts. More details about the application of the dual continuum approach in tile-drained areas are presented in Chapter 5.1.

1.6 Sensitivity analysis and calibration

Heterogeneity of the subsurface properties and data scarcity are inherent to groundwater modeling. When defining the geological structure of a model and setting hydraulic parameter values, many generalizations and simplifications contribute to model uncertainty (Refsgaard et al., 2012). A sensitivity analysis and calibration against the variables of interest (heads, discharge, concentrations, etc.) can be performed to compensate for inevitable (unknown) errors in the model structure and parameters and improve the model fit to the observations. A sensitivity analysis investigates how the variation in the model simulations can be attributed to variations of model parameters. The modeler can then estimate sensitive parameters, that have a significant influence on the model output, and insensitive parameters, that have low or negligible effect on simulations (Anderson et al., 2015). Some parameters may be correlated, when the variation in one parameter can be offset by variations to others such that the model simulations are not appreciably changed. Predictions however may be sensitive to correlated parameters found during calibration. During the calibration process, the sensitive parameters are varied manually, by trial-and-error, or automatically, using a parameter estimation software. The model is considered calibrated when the simulations reproduce the observations sufficiently well, and the parameters are reasonable, based on expert knowledge about the system (soft knowledge). However, several different parameter sets and model structures may be acceptable in reproducing the observations (equifinality, Beven et al., 2001) due to uncertainties in the model parameters and structure. Some suggestions to reduce equifinality, improving the reliability of model simulations, include the collection of more observation data, zonation, and reduction of the parameters range (Zhou et al., 2014). Equifinality in tile drainage modeling is addressed in Sections 4.5.7 and 5.4.8.5.

Chapter 2

Study sites

Tile drainage was simulated for two drainage areas (D5 in Chapter 4 and D7 in Chapter 5) and the Fensholt catchment (Chapter 6). The Fensholt catchment (6 km^2) is located in the eastern region of the Jutland peninsula in Denmark (Figure 2.1). The Fensholt catchment has been studied to investigate the water and nutrient balance, tile drain flow and efficacy, numerical modeling techniques and geology (De Schepper et al., 2017; Hansen et al., 2019a; Hansen et al., 2019b; Noorduijn et al., 2021; Petersen et al., 2020a; Petersen et al., 2020b; Prinds et al., 2020; Prinds et al., 2019, Varvaris et al., 2018, 2019, 2021a, 2021b).The upper geology is dominated by clayey till of Weichselian age and by freshwater peatland around the main stream. Tills that confine the aquifers in most of the studied area have a clayey matrix of low hydraulic conductivity and they are embedded with sand bodies. Preferential flow occurs in Danish tills due to fractures, root holes and other zones with high hydraulic conductivity (Hinsby et al., 2006). The stratigraphy consists of Paleogene and Neogene sediments covered by a sequence of Pleistocene glacial deposits. The Paleogene layers are formed of fine-grained marl and clay, which have a low permeability. The Neogene layers above consist of a Miocene sequence of marine origin, typically up to 40 m thick. The formation is clay-dominated but with interbedded sand units, which can be more than 10 m thick (Hansen et al., 2014). The climate condition is characterized by mild winters, cool summers and frequent precipitation (He et al., 2015).

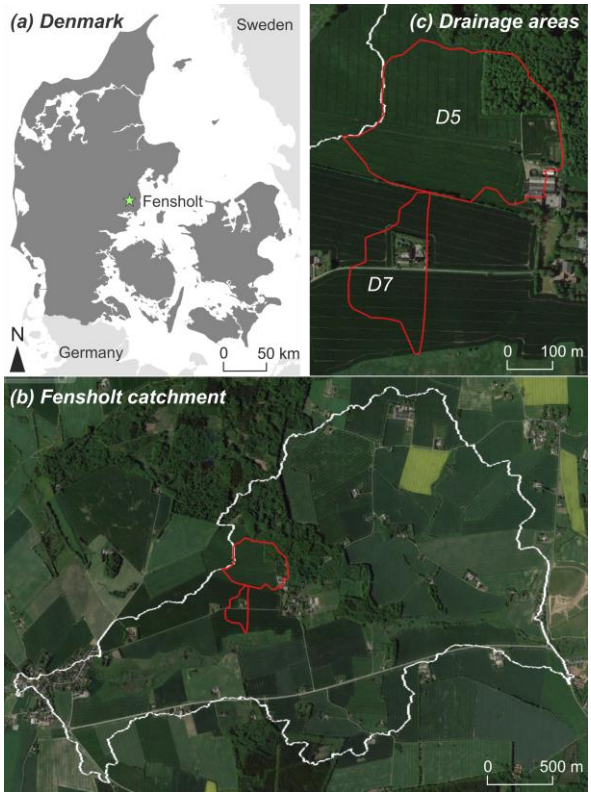

Figure 2.1 - (a) Location of the Fensholt catchment in Denmark (55°59' N, 10°5' E), (b) satellite view (Google Earth, 2019) of the Fensholt catchment with the drain discharge areas D5 and D7 highlighted, and (c) zoom to the drainage areas D5 and D7.

The main water body in Fensholt is the Stampemølle Bæk, which flows towards the east and ends in the Odder River. Agriculture is the main land use in the catchment, followed by forest, urban areas and roads, wetland and peatland (Nielsen et al., 2000). Its topography varies from 40 to 100 m above mean sea level. Two drainage areas within the Fensholt catchment (D5 and D7 in Figure 2.1) were modeled in this research. The use of depth-specific electrical conductivity estimates to improve hydrological models was investigated in the drainage area D5 (0.14 km²). The drainage area D7 (0.04 km²) was modeled for the investigation of a bromide tracer test in the macroporous tile-drained field. Photos from agricultural lands, tile drains, a tile drainage outlet, clayey till soil and a non-drained area in the Fensholt catchment are illustrated in Figure 2.2. More detailed information about the Fensholt catchment is presented in Section 6.2.1, and additional information about the drainage areas D5 and D7 is presented in Sections 4.2.1 and 5.2.1, respectively.

Figure 2.2 – (a) Agricultural land, (b) clayey till soil in D5, (c) tile drains, (d) non-drained area, and (e) outlet of a tile drainage network in the Fensholt catchment.

Chapter 3

Model application

3.1 Modeling methodology

The development of a fully-integrated hydrological-solute transport model developed in this research involved: data collection; definition of the conceptual model for surface-subsurface water flow and solute transport; design of the numerical model (initial and boundary conditions, parameters, input data) for the drainage areas and catchment; model calibration using stream and drain discharge data, groundwater levels and bromide concentrations at the outlet of a drainage system; evaluation of the calibration for reasonable parameter values. Figure 3.1 presents the workflow of the hydrological and solute transport modeling. Although not presented in the figure, the field and catchment data and soft knowledge (information that is not evaluated directly by model output) inform every step of the modeling workflow, especially the design of the conceptual model, parameterization of the numerical model, and model calibration and evaluation (Anderson et al., 2015).

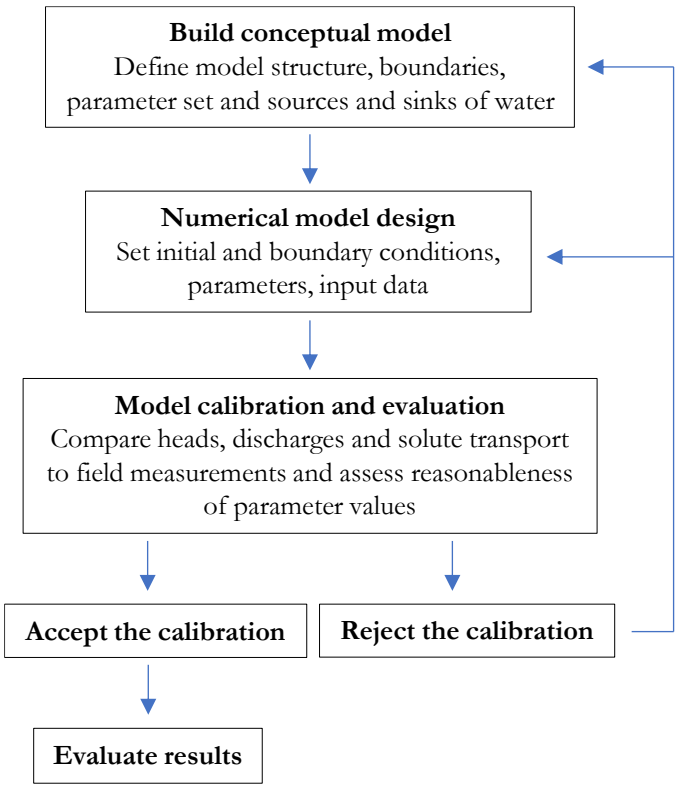

Figure 3.1 – Workflow of hydrological and solute transport modeling. Almost all steps are informed by field data and soft knowledge. Adapted from Anderson et al. (2015).

3.2 Numerical model

In this study, three-dimensional simulations of the hydrogeological system were performed using the physically-based numerical model HydroGeoSphere (Aquanty Inc., 2017; Therrien et al., 2010). HydroGeoSphere combines groundwater flow, surface water flow and solute transport between the 3D subsurface porous medium, 2D surface and in fractured media and 1D hydraulic feature elements. The governing flow equations are discretized with the control volume finite element method and the resulting non-linear equations are solved by applying the Newton-Raphson linearization method. The matrix equations are solved implicitly at each non-linear iteration until convergence.

3.2.1 Overland flow

Transient surface water flow is represented in the model by the simplified diffusion-wave approximation to the Saint-Venant equation (Equation 3.1), which is a two-dimensional depth-averaged flow equation. The development of this equation assumes that there is no inertia and adopts depth-averaged flow velocities, a vertical hydrostatic pressure distribution, mild slopes and dominant bottom shear stresses, and is written as:

$$-\nabla(d_o q_o) - d_o \Gamma_o \pm Q_o = \frac{\partial \phi_o h_o}{\partial t} \tag{3.1}$$

where d_o is the depth of flow [L], q_o is the fluid flux on the surface domain [L/T], Γ_o is the fluid exchange rate with the subsurface domain [1/T], Q_o is a volumetric flow rate per unit area that represents external sources and sinks [L/T], ϕ_o is the surface flow domain porosity, which is one for a flat plane and varies from zero to one for an uneven surface, and h_o is the water surface elevation [L], which is equal to $z_o + d_o$, where z_o is the bed (land surface) elevation [L].

3.2.2 Subsurface flow

The subsurface flow equations are solved for variably-saturated conditions. The general form of Richards' equation for 3D transient subsurface water flow solved by HydroGeoSphere is (Therrien, 2010):

$$-\nabla(w_m q) + \sum \Gamma_{ex} \pm Q = w_m \left(S_w S_S \frac{\partial h}{\partial t} + \theta_S \frac{\partial S_w}{\partial t} \right) \tag{3.2}$$

where w_m is the volumetric fraction of the total porosity [-] occupied by the porous medium, Q is the flux exchange between the porous medium and outside of the domain [1/T], that represents a source (positive) or a sink (negative) to the system. Γ_{ex} is the volumetric fluid exchange rate between the subsurface and the other domains [1/T], such as drains and dual continuum. S_S is the specific storage coefficient [1/L]. The fluid flux q is described by

$$\mathrm{q} = -\mathrm{K}\,\mathrm{k_r}\,\nabla(\psi + z) \tag{3.3}$$

where ψ is the pressure head [L], z is the elevation [L], $\mathrm{k_r} = \mathrm{k_r}(S_w)$ is the relative permeability of the porous media [-] with respect to the water saturation $S_w = \theta/\theta_s$, θ and θ_s are total porosity [-] and saturated water content [-], respectively. The compressibility effect of the specific storage in the right-hand side of the general form of Richards' equation (Equation 3.2) in unsaturated conditions is assumed to be negligible compared to the effect of changes in saturation (Cooley, 1971; Neuman, 1973). The coupling of water flow between model domains is simulated by the dual node approach, which is based on a Darcy flux transfer between two domains.

3.2.3 Solute transport

Solute transport is calculated with a 3D solute transport equation in a variably-saturated porous matrix:

$$-\nabla(qC - \theta_s S_w D \nabla C) + \sum \Omega_{ex} \pm Q_c = \frac{\partial(\theta_s S_w C)}{\partial t} \tag{3.4}$$

where C is the solute concentration [M/L^3], D is the hydrodynamic dispersion [L^2/T] that incorporates the effects of diffusion and mechanical dispersion, Ω_{ex} is the mass exchange rate of solute per unit volume [M/L^3/T] that occurs between the domains (subsurface, surface, tile drains, etc.) and Q_c represents a source or a sink to the porous medium system [M/L^3/T], specified from the boundary conditions. The solute exchange terms between two different domains are defined by a numerical superposition principle, assuming continuity of solute concentration.

3.2.4 Tile drainage flow

Tile drains can be simulated in HydroGeoSphere as one-dimensional (1D) features, where the fluid flux is explicitly simulated (discrete drain), or using the seepage boundary condition. The discrete drain is described by relating the flow of water and hydraulic properties of the pipe to the rate of total head loss caused by friction. The seepage nodes (nodes set as seepage boundary conditions) are given a zero-pressure head condition when the water table rises above the node elevation (Aquanty Inc., 2017) and function as a no-flow boundary condition if the water table drops below the seepage nodes elevation. De Schepper (2015) compared both approaches, where the discrete drain flow was calculated by the Hazen-Williams equation, and the drains segments were replaced by nodes set with a seepage boundary condition. The seepage nodes approach simulated similar drain discharge and hydraulic heads to the 1D line elements approach for stationary and transient flow. Furthermore, the seepage nodes approach as simple to be applied in a catchment-scale modeling study, resulting in reasonable simulation times (De Schepper et al., 2017). De Schepper (2015) concluded that the seepage drainage option is suitable for simulating water flow in the porous medium towards the drains (lateral drainage water flow). However, the physical properties of the pipe were not specified and pipe flow and drainage routing, with potential

pressurized flow, were not considered. In the present study we adopted the seepage nodes approach, formulation of which is explained in Section 6.3.6 of Chapter 6.

3.2.5 Coupling surface-subsurface water flow

The dual node scheme is used here to couple surface and subsurface water flow. In this scheme, the water exchange term is calculated based on the hydraulic head difference between two domains using the Darcy flux relation. The exchange term in the dual node approach is defined by:

$$\Gamma_{pm \rightarrow olf} = -(\mathrm{k_r})_{exch} K_{exch} \frac{(h_o - h)}{l_{exch}} \tag{3.5}$$

where $\mathrm{k_r}$ is the relative permeability [-], K_{exch} is the saturated hydraulic conductivity [L/T], and l_{exch} is the coupling length [L] for fluid exchange.

3.2.6 Interception and evapotranspiration

HydroGeoSphere simulates interception by vegetation and buildings and actual evapotranspiration based on the potential evapotranspiration boundary condition applied at the model surface. Interception is a storage factor proportional to the type of land cover and the development stage of the vegetation. Rain is intercepted, stored and then available for depletion by evaporation (Guerrits et al., 2010). The interception varies from zero to the maximum interception storage capacity S_{int}^{Max} (Kristensen and Jensen, 1975):

$$S_{int}^{Max} = c_{int}(LAI) \tag{3.6}$$

where c_{int} is the canopy storage parameters [L] and LAI is the leaf area index [-]. Evapotranspiration corresponds to the sum of transpiration and evaporation. Transpiration (T_p) is calculated by (Kristensen and Jensen, 1975):

$$T_p = f_1(LAI)\, f_2(\theta)\, RDF\, (E_p - E_{can}) \tag{3.7}$$

where $f_1(LAI)$ is a function of leaf area index [-], $f_2(\theta)$ is a function of moisture content (θ) [-], RDF is a root distribution function [-], E_p is the reference evapotranspiration [L] and E_{can} is the evaporation by vegetation [L]. Evaporation (E_s) at the soil surface and along a prescribed depth (B_{soil}) in the subsurface domain is calculated by:

$$E_s = a^*\big(E_p - E_{can}\big)[1 - f_1(LAI)]\, EDF\, (B_{soil}) \tag{3.8}$$

where EDF is an evaporation distribution function limiting evaporation from the soil surface to B_{soil}, and a^* is a wetness factor [-] calculated as:

$$a^* = \begin{cases} \dfrac{(\theta - \theta_{e2})}{(\theta_{e1} - \theta_{e2})} & for\ \theta_{e2} \le \theta \le \theta_{e1} \\ 1 & for\ \theta > \theta_{e1} \\ 0 & for\ \theta > \theta_{e2} \end{cases} \tag{3.9}$$

where θ_{e1} is the moisture content [-] above which full evaporation can occur and θ_{e2} is the limiting moisture content [-] below which evaporation is zero. Further details of the governing equations and solution methodology are presented in Aquanty Inc. (2017) and Therrien et al. (2010).

3.2.7 Error analysis

The combination of trial-and-error and automatic parameter optimization by the software PEST (Doherty, 1994, 2018) was investigated in the calibration process. The trial-and-error method consists of adjusting each set of model parameters manually by successive simulations until the best overall agreement between model results and observed values is achieved. PEST is a software package for parameter estimation and uncertainty analysis of environmental models, which provides utilities for linear and nonlinear error-variance and uncertainty analysis in highly parameterized modeling contexts. The accuracy criteria during the calibration procedure were determined graphically (hydrographs, depth to water table and breakthrough curves) and error analysis of the drain discharge, hydraulic heads and solute discharges. The errors were calculated by the mean absolute error (MAE), root mean square error (RMSE), Nash–Sutcliffe efficiency (NSE, Nash and Sutcliffe, 1970) and the Kling-Gupta efficiency (KGE, Gupta et al., 2009):

$$MAE = \frac{\sum_{i=1}^{n} |(\phi_{sim} - \phi_{obs})_i|}{n} \tag{3.10}$$

$$RMSE = \sum_{i=1}^{n} \sqrt{\frac{(\phi_{sim} - \phi_{obs})_i^2}{n}} \tag{3.11}$$

$$NSE = 1 - \frac{\sum_{i=1}^{n} \left(Q_{sim,i} - Q_{obs,i}\right)^2}{\sum_{i=1}^{n} \left(Q_{obs,i} - \overline{Q_{obs}}\right)^2} \tag{3.12}$$

$$KGE = 1 - \sqrt{(r-1)^2 + \left(\frac{\sigma_{sim}}{\sigma_{obs}} - 1\right)^2 + \left(\frac{\overline{Q_{sim}}}{\overline{Q_{obs}}} - 1\right)^2} \tag{3.13}$$

where ϕ_{sim} and ϕ_{obs} are the simulated and observed values, n is the total number of observations, i is the index of each measurement, Q_{sim} and Q_{obs} are simulated and observed discharges, r is the linear correlation between observations and simulations, σ_{sim} and σ_{obs} are the standard deviation in simulations and observations, $\overline{Q_{sim}}$ and $\overline{Q_{obs}}$ are the mean of simulated and observed discharge. The NSE and KGE equal to 1 indicate perfect correspondence between simulations and observations.

NSE<0 and KGE<-0.41 indicate that the model simulation results are poorer than the mean of the observations (Knoben et al., 2019).

The model was considered calibrated when the optimal parameter values are achieved, but limited to the computational times for successive simulations, reasonableness of the parameter values, and random or systematic errors in the input data, boundary conditions and model structure.

Chapter 4

Using depth specific electrical conductivity estimates to improve hydrological simulations in a heterogeneous tile-drained field

Utilisation d'estimations de conductivité électrique spécifique en fonction de la profondeur pour améliorer les simulations hydrologiques dans un champ drainé

V. F. Boico, R. Therrien
Department of Geology and Geological Engineering, Université Laval. Quebec City, Canada.

A. L. Højberg
Department of water resources, Ramboll. Copenhagen, Denmark.

B. V. Iversen, T. Koganti
Department of Agroecology, Aarhus University. Tjele, Denmark.

I. Varvaris
Department of Civil & Environmental Engineering, University of Wisconsin-Madison. Madison, EUA.

Reference:

Boico, V. F., Therrien, R., Højberg, A. L., Iversen, B. V., Koganti, T., Varvaris, I. (2022). Using depth specific electrical conductivity estimates to improve hydrological simulations in a heterogeneous tile-drained field. Journal of Hydrology, 604. doi:10.1016/j.jhydrol.2021.127232

Résumé

Les études examinant l'effet de l'hétérogénéité du sol sur la dynamique de la nappe phréatique et sur le débit des drains, à l'aide de modèles tridimensionnels intégrant écoulements de surface et souterrains, sont limitées. L'objectif de ce chapitre est de démontrer l'utilisation d'estimations de conductivité électrique spécifique en fonction de la profondeur pour améliorer les simulations hydrologiques dans un terrain drainé. Les zones de sol riches en argile ont été identifiées en utilisant des estimations de conductivité électrique. Un modèle comprenant les zones argileuses peu perméables dans les couches de sol jusqu'à une profondeur de 1,2 m a été comparé à un modèle plus simple supposant des couches de sol homogènes. Les deux modèles ont simulé un écoulement de drainage qui se compare bien aux observations. Cependant, l'inclusion des zones argileuses a amélioré la simulation des charges hydrauliques et de fluctuation de la nappe phréatique, et généré des zones inondées plus représentatives de celles observées pendant les saisons humides.

Abstract

Studies on the effect of topsoil heterogeneity on shallow water and drainage dynamics by fully-coupled 3D surface water and groundwater flow modeling are limited. The objective of this chapter is to demonstrate the use of depth specific electrical conductivity estimates to improve hydrological simulations in a tile-drained field. Clay-rich soil zones were identified in a tile-drained field using depth specific electrical conductivity. One model that included the low-permeability clayey zones in the soil layers down to a depth of 1.2 m was compared to a simpler model that assumed homogeneous soil layers. Both models simulate drain discharge that compares well to the observations. However, including the clayey zones improves the simulation of hydraulic heads, and water table fluctuations, and generates flooded areas that are more representative of those observed during the wet seasons.

4.1 Introduction

The spatial variability of the structure and hydraulic properties of soils can have a great impact on water flow and solute transport. However, it is often poorly known, and the uncertainty associated with the parameterization of soil structure and properties in hydrological models can be large. This uncertainty then propagates to predictions of hydrological models.

To reduce uncertainty and improve simulations with process-based hydrological models, several authors have explicitly incorporated subsurface heterogeneity (Atchley and Maxwell, 2011; Ali et al., 2014; Hansen et al., 2019). In agricultural tile-drained fields, the water table geometry and, consequently, water discharge from tile drains are to a high extent controlled by the hydraulic properties of the soils and the deeper geological units (Akay et al., 2008; Bednorz et al., 2016; De Schepper et al., 2017; Kennedy et al., 2012; Hansen et al., 2008) and by the configuration of the tile drain network (De Schepper et al., 2015). For instance, Eastman et al. (2010) compared subsurface drain discharge for several agricultural sites and observed greater discharge for clay loam soils compared to sandy loam soils. Hansen et al. (2013) simulated coupled groundwater-surface water flow in tile-drained areas and found that an insufficient representation of local subsurface heterogeneity is one of the limiting factors for adequately reproducing observed hydraulic heads and local-scale drain discharge dynamics. Haws et al. (2005) used effective homogeneous soil properties to simulate flow and transport in tile-drained macroporous agricultural fields and concluded that assuming soil homogeneity hindered the reproduction of observed tile drainage and solute discharges. In addition to allowing a better representation of flow dynamics, accounting for different flow route contributions by including tile drains and soil heterogeneity is also deemed essential for the accurate simulation of solute transport (van Der Velde et al., 2010), nitrate leaching (Bednorz et al., 2016) and seasonal in-stream nitrate concentration (Wriedt et al., 2007). In one study, Refsgaard et al. (2019) showed that geological heterogeneity in tile-drained fields resulted in substantial local spatial variations in nitrogen reduction in groundwater and surface water.

Borehole data is usually available for the estimation of the soil parameters. However, the natural variability in the soil hydraulic parameters is too large for reliable estimation of soil heterogeneity only based on locally and widely spaced borehole data. This limitation can be addressed by correlating local measurements to an auxiliary variable that represents the spatial distribution of the parameters (Blöschl et al. 1995). Geophysical methods, such as electrical conductivity (EC) surveys, are well suited to detect spatial soil heterogeneity at very high resolution (Kruger et al., 2013). Georeferenced soil EC measurements have proven suitable for mapping soil properties such as texture, water content, organic matter, and cation exchange capacity in non-saline soils (Corwin and Lesch, 2004; Heil and Schmidhalter, 2012; Huang et al., 2017; Koganti et al., 2017; Sheets and Hendricks, 1995). Recent advances in

electromagnetic induction (EMI) instruments and the development of sophisticated inversion routines have enabled on-the-go measurement of apparent electrical conductivity (EC_a) at multiple depths, allowing the determination of depth specific EC estimates. These estimates can be related to soil properties, such as salinity, soil water and clay contents (Huang et al., 2016; Koganti et al., 2018; Robinet et al., 2018, Møller et al., 2021) and can provide three-dimensional mapping of these properties (Koganti et al., 2018; Khongnawang et al., 2019). Hence, EMI is a promising tool to quantify the depth-dependent zonation of soil parameters.

Using bulk soil EC_a measurements in a tile-drained field, Varvaris et al. (2018) illustrated that the clay-size fraction increased with depth. They identified depression zones and the presence of a shallow low-permeability layer. Hansen et al. (2019a) used resistivity data for sediments down to 3.5 m below ground surface, based on EMI measurements, to set up a 3D hydrological model to simulate drain flow at the field scale. They associated a zone of higher resistivity to a higher sand content and used it to delineate in their model a zone of high hydraulic conductivity from 0 to 3.5 m in depth. There is still, however, only a few published studies where depth specific EC estimates, generated from the inversion of EC_a data measured by an EMI instrument have been used to delineate soil heterogeneity for integrated hydrological simulations. Furthermore, to the authors knowledge, there are no studies where heterogeneous soil zones in tile-drained areas were delineated based on EC estimates for the investigation of hydrological simulations, as opposed to a homogeneous soil layers model.

The objective of the present study is to demonstrate the use of depth specific EC estimates to improve hydrological simulations in a tile-drained field. We hypothesize that including clay-rich zones using EC estimates in a 3D coupled surface-subsurface hydrological model of a tile-drained field would improve the model performance, resulting in a more accurate description of the local water table level, drain discharge, groundwater–surface water exchange, and surface runoff. We used the integrated surface-subsurface hydrological model HydroGeoSphere (Aquanty Inc., 2017), which simulates the interaction between groundwater and surface water and the possible redistribution of water by exfiltration followed by runoff and re-infiltration. The Chapter focuses on a highly heterogeneous tile-drained field in Denmark. The methodology consisted in 1) delineating clay-rich zones at different depths using soil EC estimates, with a vertical resolution of 20 cm, and borehole soil texture analyses, 2) simulating coupled surface water, groundwater and tile drain flow in a tile-drained field for a reference model with homogeneous soil layers and a second model with heterogeneous soil layers defined from the EC estimates, and 3) analyzing the flow components for the two model conceptualizations and comparing observed and simulated hydraulic heads and drain discharge.

4.2 Methods and data

4.2.1 Site description

The study site is located in an agricultural region about 20 km south of the city of Aarhus, Denmark (55°59'N 10°4'E, Figure 4.1). It covers an area of 14 ha and is within the larger Fensholt catchment, whose area is 6 km². The study site is tile-drained with a network configuration shown in Figure 4.1c. The local climate is characterized by mild winters, cool summers, and frequent precipitation (He et al., 2015). The landscape consists of rolling hilly terrain with ground elevation ranging from 72 to 95 m above mean sea level. Approximately 83% of the site area is used for agricultural activities.

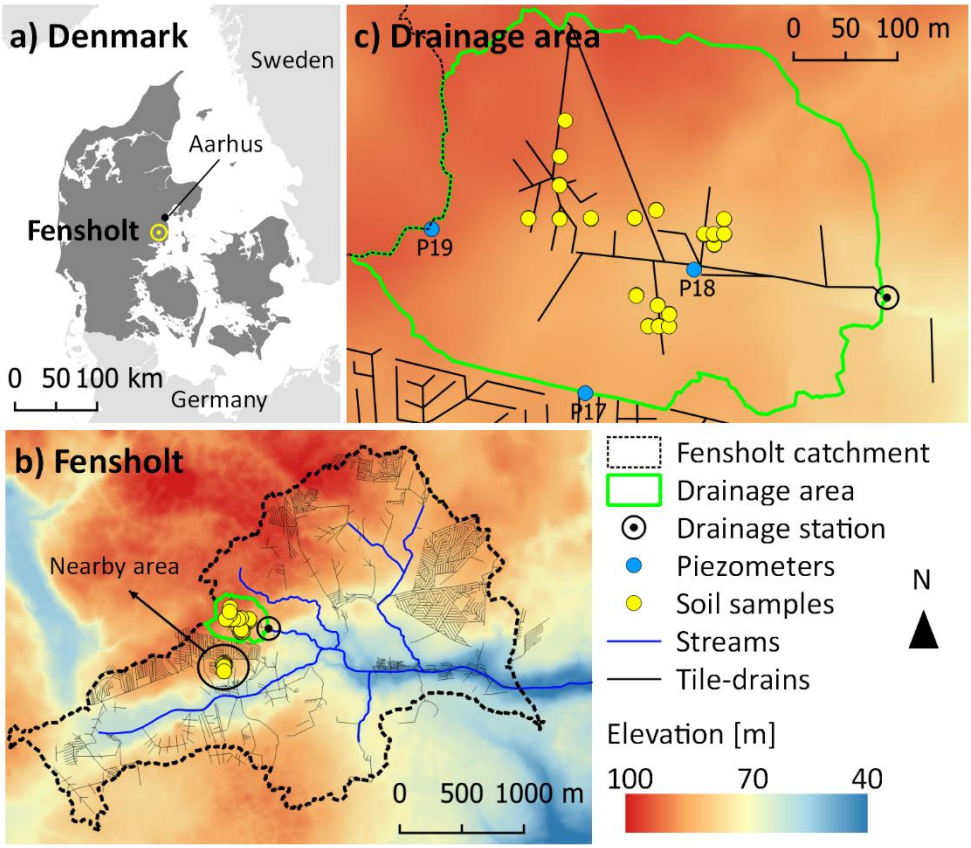

Figure 4.1 - (a) Location of the Fensholt catchment in Denmark (55°59' N, 10°5' E), (b) location of the studied drainage area, stream system and soil samples (c) mapped tile drains within the drainage area, piezometers and the drainage monitoring station. The ground surface elevation based on a 1.6 m digital elevation model is shown as background in (b) and (c).

4.2.2 Hydrologic data

Tile drain discharge at the site was measured daily at the outlet, indicated by the drainage station in Figure 4.1c, by an electromagnetic flow meter (KROHNE Optiflux 3070 flow meter, Krohne Messtechnik GmbH, Duisburg, Germany). The water table is shallow in the area (De Schepper et al., 2017; Hansen et al., 2019; He et al., 2014) and three piezometers (P17, P18 and P19 shown in Figure 4.1c), screened from ground surface to a depth of 2 m, were installed to manually measure water table levels twice a month. The piezometers were already installed at the field site, prior to our study, as part of the iDRÆN project of Aarhus University (see more in www.idraen.dk). Rainfall events were not studied because the hydraulic head observations were not available at a sufficiently fine temporal resolution (e.g., daily).

Precipitation data were obtained from a meteorological station situated 3 km southwest of the study area. Total annual precipitation for 2014 and 2015 was 909 and 1134 mm, respectively. Potential evapotranspiration was estimated with the Penman-Monteith equation using data from a meteorological station in Foulum, Denmark (56°29'N 9°35'E), 62.5 km from the study area.

4.2.3 Soil data

Varvaris et al. (2018) collected a total of 76 soil samples from various depths at locations shown in Figure 4.1c and determined the soil texture for sixteen of these samples. The main soil textures are coarse sandy loam, sandy clay loam, and clayey loam, according to the USDA soil texture classification. The clay content increases with depth due to pedological clay illuviation processes, leading to an expected decrease in permeability with depth. The redistribution of soil particles according to the hydro-topographical gradients results in high clay and organic matter contents in depression zones. The average thickness of each soil horizon was determined from borehole descriptions.

The soil water retention (SWR) curves were determined for 31 undisturbed 100 cm^3 soil samples. From that total, 16 samples were excavated from the topsoil at the site and 15 samples were taken at three different depths (0-20 cm, 28-48 cm and 85-105 cm) at a nearby area immediately south of the drainage area (Figure 4.1b). The soil cores were placed in a sandbox and slowly saturated with ascendant water. They were then drained to different pressure heads utilizing a sandbox (-30 and -100 cm H_2O), hanging water column (-300 cm H_2O) and a ceramic pressure plate apparatus (-1000 cm H_2O). The dry bulk density was determined by oven-drying the soil samples at 105 °C for 24 hours. The volumetric water content at each pressure head (θ, cm^3 cm^{-3}) was determined from the weight of the soil sample after each drainage step. Afterwards, the van Genuchten parameters (α and n) were estimated using the soil water retention and the variably saturated hydraulic conductivity as input in the RETC software (van Genuchten et al., 1991). The saturated hydraulic conductivity was measured at different depths at the

nearby area with the constant-head method as described by Iversen et al. (2004), using undisturbed 6280 cm^3 soil samples.

We used the single-transmitter multi-receiver EMI instrument operating at a frequency of 9 KHz DUALEM-21S (Dualem Inc., Milton, ON, Canada) for measuring the bulk soil EC_a at various depths. In this instrument, a transmitter coil is located at one end and is shared by two pairs of receiver coils in both horizontal coplanar (HCP) and perpendicular (PRP) orientations. For the HCP configurations, the transmitter-receiver separation distances are 1 and 2 m and for the PRP configurations, they are 1.1 and 2.1 m, respectively. The quadrature-phase and in-phase signal responses of the EMI sensor are representative of the EC_a and the apparent magnetic susceptibility of the soil (McNeill, 1980). Each of the four coil configurations results in the sensing of different soil volumes represented in the EC_a measurements (Dualem Inc., 2008; Callegary et al., 2012).

The DUALEM sensor was mounted on a sled (at a height of 0.3 m above ground) attached to an all-terrain vehicle, with real-time data georeferencing using Real-Time Kinematic Global Navigation Satellite System (RTK/GNSS) and the data were collected on transects spaced approximately 8 m apart. The Aarhus Workbench software (Auken et al., 2009) was used for both automatic and manual data processing and for inversion. The data were first automatically processed to remove negative EC_a values and to correct for the offset between the RTK/GNSS setup and the individual channels. The signal-to-noise ratio was improved by averaging the data using an appropriate sounding distance (3 m) and running mean width (6 m). The raw data was then manually inspected to remove noise caused by anthropogenic coupling induced by features such as metal cables or field-monitoring installations. The changes made to the raw data are incorporated into the averaged data generated by the automatic processing step. To better represent the EC distribution with depth and to estimate the average EC for the desired soil depths (i.e. 0–20 cm, 20–40 cm, 40–60 cm, 60–80 cm, 80–100 cm and 100–120 cm), we inverted the processed EC_a data with a quasi-3D spatially constrained inversion algorithm (Auken et al., 2015; Viezzoli et al., 2008). The inversion was necessary because the depth sensitivities of HCP and PRP arrays are nonlinear. Measured EC_a is therefore a depth-weighted average (e.g. Callegary et al. 2007; Tolboll and Christensen, 2007) and hence is a complicated representation of the true EC variability (Christiansen et al., 2016). We refer the reader to Christiansen et al. (2016) for a comprehensive overview of data processing and inversion of the DUALEM measurements using the Aarhus Workbench software.

4.2.4 Geology and Hydrogeology

The surficial geology consists of a 20 to 50 m thick cover of Quaternary glacial deposits, composed of both clayey and sandy sediments. The lithology of the clay sediments varies from glaciolacustrine clay to clayey till containing distributed and relatively small units of sandy glacial deposits of glaciofluvial origin.

The geology and hydrogeology of both the Fensholt catchment and study site have been previously characterized and conceptual models for the subsurface geology were developed (He et al. 2014; De Schepper et al. 2017; Varvaris et al. 2018; Hansen et al. 2019). He et al. (2014) used geophysical and borehole data to develop multiple stochastic representations of the subsurface geology for a larger catchment that covers about 100 km^2 and includes the study site. The soil and geological model proposed by He et al. (2014) was used by De Schepper et al. (2017), who developed a 3D hydrological model using HydroGeoSphere for the Fensholt catchment.

For the top 1.3 m of soil at the study site, Varvaris et al. (2018) demonstrated that the single-porosity model performed as well as the dual-permeability model for simulating drainage outflow. In a modeling study focused on an area close to our study site (Figure 4.1b), Varvaris et al. (2021b) show that including macropores in 2D hydrological models improved the fit between simulated and observed bromide concentrations in tile drains. Their results suggest that macropores can play a dominant role in water and solute transport in loamy structured tile-drained fields.

4.3 Model application

4.3.1 Numerical model

The HydroGeoSphere model (Aquanty Inc., 2017) was used for 2D surface and 3D subsurface hydrologic simulations for the tile-drained field. HydroGeoSphere uses the control volume finite element method to simulate fully coupled surface water, groundwater, and tile drainage flow. Two-dimensional surface water flow is simulated by solving the diffusion-wave approximation of the Saint-Venant equation. Three-dimensional variably-saturated groundwater flow is described by the modified form of Richards' equation:

$$-\nabla q + \sum \Gamma_{ex} \pm Q = S_w S_S \frac{\partial h}{\partial t} + \theta_S \frac{\partial S_w}{\partial t} \tag{4.1}$$

where Q is a volumetric source (positive) or sink (negative) [1/T], Γ_{ex} is the volumetric fluid exchange rate [1/T] between the subsurface and the other simulation domains, such as the surface domain, S_S is the specific storage coefficient [L^{-1}], $S_w = \theta/\theta_s$ is the porous medium volumetric saturation [-] and θ and θ_s are the volumetric water content [-] and volumetric water content at saturation [-], respectively. The fluid flux q [L/T] is described by:

$$\mathrm{q} = -\mathbf{K}\, \mathrm{k_r}\, \nabla(\psi + z) \tag{4.2}$$

where ψ is the pressure head [L], z is the elevation head [L], $\mathbf{K}$ is the hydraulic conductivity tensor [L/T], and $\mathrm{k_r} = \mathrm{k_r}(S_w)$ is the relative permeability of the porous media [-], which is a function of its saturation.

HydroGeoSphere simulates interception and actual evapotranspiration (AET) as mechanistic processes as described in Panday and Huyakorn (2004) and Aquanty Inc. (2017). The Newton-Raphson iterative method is used to linearize and solve the discretized nonlinear equations. A maximum saturation variation of 0.05 between successive time steps was specified for the variable time stepping procedure in HydroGeoSphere (Aquanty Inc., 2017). The initial time step was 60 s and time steps were limited to a maximum of 1 h.

4.3.2 Surface domain

The horizontal boundaries of the surface flow domain coincide with the water contributing area for the outlet of the tile drainage system. To discretize the surface flow domain, a 2D triangular mesh was generated with the AlgoMesh software (Figure 4.2). The topography was generated by interpolating a 1.6 m resolution digital elevation model onto the surface mesh. In the vicinity of the drains, the triangular elements of the mesh were refined with a maximum segment length equal to 10 m and an element area ranging from 2 to 35 m². The number of nodes and triangular elements in the 2D surface mesh were 1481 and 2856, respectively.

The overland flow parameters specified for the surface domain are provided in Table 4.1. The concepts of rill storage height (H_R) and obstruction storage height (H_O) in HydroGeoSphere were applied to implicitly represent the micro-topography of the soil surface. The coupling length (L_C) listed in Table 4.1 represents the thickness of the interface between the subsurface and the surface domains.

Table 4.1 - Overland flow parameters assigned to the surface domain: Manning roughness coefficient (n), Rill storage height (H_R), Obstruction storage height (H_O), Coupling length (L_C)

Parameter	Value	Source
n [$s/m^{1/3}$]	0.2	Li et al. (2008)
H_R [m]	0.005	Cochand et al. (2018)
H_O [m]	0.03	Cochand et al. (2018)
L_C [m]	0.01	Goderniaux et al. (2009)

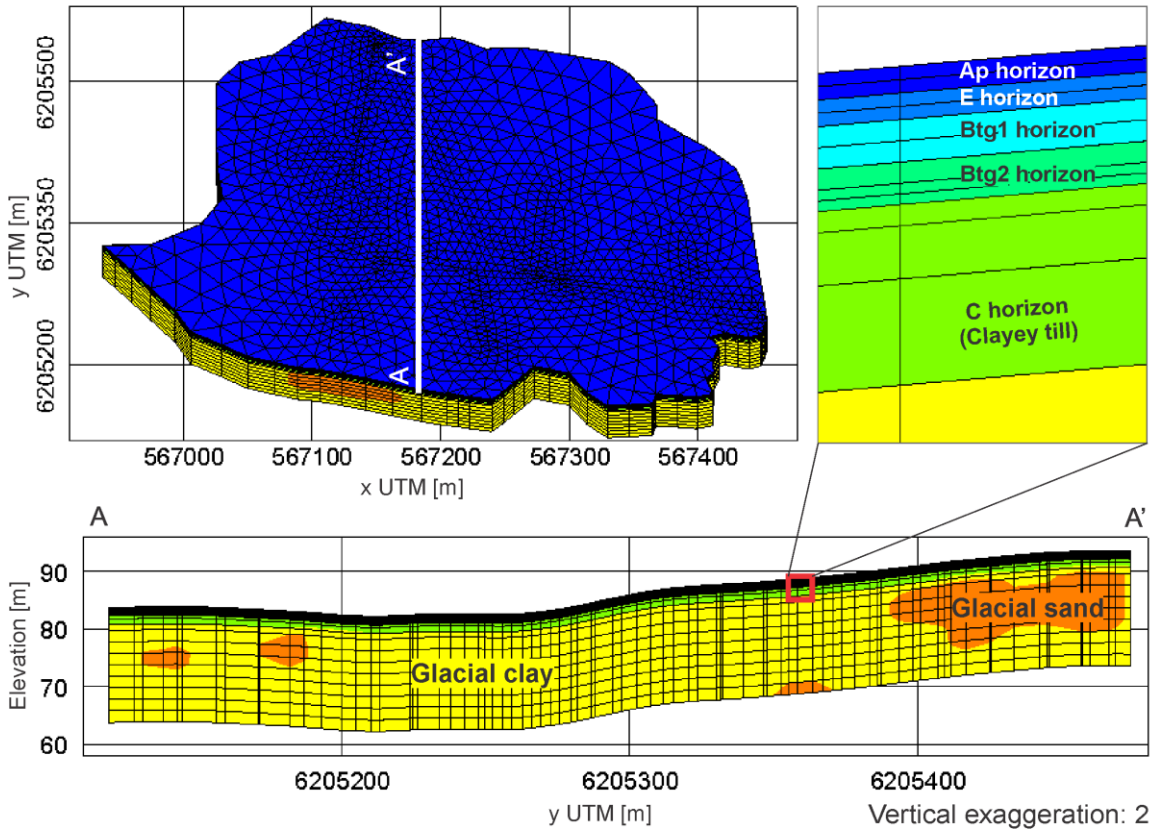

Figure 4.2 – Three-dimensional mesh and geological units of the stochastic geological realization from 3 to 20 m depth with vertical cross section AA'. Detail for the Ap, E, Btg1, Btg2, and C soil horizons in the first 3 meters depth defined by Varvaris et al. (2018) is shown as well.

4.3.3 Subsurface domain

The 3D subsurface mesh was constructed by superimposing the surface triangular mesh along the vertical direction to generate 3D triangular prism elements. The top of the 3D mesh corresponds to ground surface and a uniform vertical thickness of 20 m was assigned everywhere. A total of 21 layers of 3D triangular prism elements were generated, with each layer having a uniform thickness for the whole domain as shown in the cross-section in Figure 4.2. The upper soil horizons cover the entire study area from the surface down to a depth of 3.0 m. Those soil horizons, Ap (25 cm), E (25 cm), Btg1 (40 cm), Btg2 (40 cm) and C (170 cm), were discretized with twelve layers of 3D elements. The C horizon corresponds to a clayey till, according to the stratigraphy presented by De Schepper et al. (2017) and Varvaris et al. (2018). One element layer was defined from a depth of 3 m to 4 m and 8 layers having each a thickness of 2 m were defined from a depth of 4 m down to the bottom of the simulation domain at a depth of 20 m. The number of nodes and triangular prism elements in the 3D mesh were 32582 and 59976, respectively.

The location of the subsurface tile drains was obtained from existing maps and from consultations with local farmers. The tile drains were assumed to be located at a depth of 1.2 m (Varvaris et al., 2018). The total tile drains length is 1457 m, and the drainage density (total length per surface area) is 106 m/ha. The vertical discretization around the drains was 10 cm, which is the same value used by Mohanty et al. (1998) and Thomas et al. (2016). The tile drains were represented as seepage nodes in HydroGeoSphere with a fixed pressure of zero and without resistance to flow. Hence, tile drain flow occurs when the water table rises above the drain level. Water at the seepage nodes is instantaneously removed from the system and, therefore, water flow inside the drains towards the outlet is not numerically simulated. Outflow from all active seepage nodes is added to provide the total drainage flow rate at each time step. Typical tile drain velocities vary from 0.1 to 0.6 m/s (Szejba and Bajkowski, 2019) but can reach as much as 1.5 m/s (Sammons et al., 2005). At our study site, the longest linked drain connection is about 530 m. Using the range of values cited above, between 0.1 m/s and 1.5 m/s, the travel time in that longest drain connection could range between 350 s and 53 000 s. Considering these potential travel times with respect to the temporal scale of the discharge observations (daily) and the seasonal analysis (2 years), using the sum of drain discharge at all active seepage nodes to represent the total drain discharge was assumed to be a suitable approximation.

Coupled surface water, groundwater and tile drain flow were simulated for two different models that differ in the representation of the soil horizons in the top 1.3 m of the simulation domain. Both models use the same description of the geology for the rest of the domain, between depths of 1.3 m and 20 m, where a spatially variable distribution of Quaternary sand and clay units is assigned based on the study of He et al. (2014, Figure 4.2, Table 4.2). The two models are described below.

Table 4.2 - Hydraulic properties of the stochastic geological realization of He et al. (2014) assigned between depths of 3 m and 20 m

Soil texture	Parameter	Value
Glacial sand	Horizontal saturated hydraulic conductivity, Ks,h [m/s]	4.2E-04
	Vertical saturated hydraulic conductivity, Ks,v [m/s]	4.2E-05
	Specific storage, Ss [1/m]	5.0E-05
Glacial clay	Horizontal saturated hydraulic conductivity, Ks,h [m/s]	2.5E-08
	Vertical saturated hydraulic conductivity, Ks,v [m/s]	2.5E-09
	Specific storage, Ss [1/m]	5.0E-05

4.3.4 Reference homogeneous layered soil model

The first model, called here the reference model, assumes that each soil horizon between ground surface and a depth of 1.3 m is homogeneous. Soil properties calibrated by Varvaris et al. (2018) are assigned to horizons Ap, E, Btg1 and Btg2 (shown in Figure 4.2). For each soil horizon, the average values of soil

parameters measured on core samples collected across the field are used as input for the pedotransfer functions (PTF) developed by Iversen et al. (2011). The PTF predicted values were used for the initial parameterization of the water flow models and, afterwards, the parameters were further adjusted during calibration that used the observed tile drain discharge as the objective function. Varvaris et al. (2018) assumed that their four-layer two-dimensional models were suitable to represent the spatial variation in topography and soil hydraulic characteristics of tile-drained fields. Therefore, in this study, it is assumed that the three-dimensional homogeneous soil layers model implicitly accounts for heterogeneity since the parameterization was based on the calibrated two-dimensional models by Varvaris et al. (2018).

Varvaris et al. (2018) assumed that the clayey till underneath the soil layers, below a depth of 1.3 m, is impermeable. However, we chose to include the clayey till in the simulations, from a depth of 1.3 m to 3.0 m, and define it as a low-permeability unit corresponding to the C soil horizon (Figure 4.2). We assign to that unit hydraulic properties similar to those used by He et al. (2015), De Schepper et al. (2017) and Børgesen and Schaap (2005). A similar C horizon configuration was used by De Schepper et al. (2017) and Hansen et al. (2019a). Specific storage values from He et al. (2015) are assigned to all soil horizons. The hydraulic properties of the soil horizons for the reference model are presented in Table 4.3.

Table 4.3 - Hydraulic properties of the soil horizons (0 to 3 m depth) used in the homogeneous soil model

Parameter	Ap horizon	E horizon	Btg1 horizon	Btg2 horizon	C horizon
Depth [cm]	0 - 25	25 - 50	50 -90	90 - 130	130 - 300
Horizontal hydraulic conductivity, Kh [m/s]	4.2E-05	3.9E-05	2.8E-05	2.8E-05	8.9E-08
Vertical hydraulic conductivity, Kv [m/s]	4.2E-05	3.9E-05	2.8E-05	2.8E-05	8.9E-09
Porosity [-]	0.41	0.38	0.38	0.36	0.40
Van Genuchten, α [1/m]	1.5	1.4	1.4	1.3	1.0
Van Genuchten, n [-]	1.4	1.3	1.3	1.2	1.4
Residual saturation, Sr [-]	0.16	0.19	0.21	0.28	0.10
Specific storage, Ss [1/m]	1.0E-05	1.0E-05	1.0E-05	1.0E-05	1.0E-05

Sources: Ap, E, Btg1 and Btg2 horizons have Kh and Kv from Iversen et al. (2011) and porosity, α, n and Sr from Varvaris et al. (2018). C horizon has Kh and Kv from He et al. (2015), porosity from De Schepper (2017), α, n and Sr from Børgesen and Schaap (2005). All Ss values are from He et al. (2015)

4.3.5 Heterogeneous soil layers model

Borehole data investigation showed that the soils are stratified and spatially heterogeneous (Varvaris et al., 2018) with clay-rich soils embedded in loamy soils (coarse sandy loam and sandy clay loam). For the development of the heterogeneous layered soil model, we assume that soil properties can be inferred from EC estimates based on electromagnetic induction. Hansen et al. (2019a) also applied this approach for the delineation of soil zones in a field in the same catchment. The EC measurements indicate the presence of zones with higher EC and a probably higher clay content and lower hydraulic conductivity

in the uppermost portion of the soil, down to a depth of 1.2 m. However, no specific EC values were related to the soil texture. The delimitation of the soil heterogeneities was based on EC estimates and the texture description from boreholes. EC estimates were defined for a 20 cm depth resolution, resulting in six layers of different EC values from the ground surface to a depth of 1.2 m. The textures noted in borehole at different depths were approximated to conform with 20 cm soil layers. We defined the heterogeneous soil layers of 40 cm thickness from the ground surface to 1.2 m depth based on EC delimitation shown in Figure 4.3. Three loamy soil layers with clay-rich zones were therefore defined (Table 4.4): a coarse sandy loam soil between 0 and 40 cm depth and two sandy clay loam soils between 40 and 80 cm and 80 and 120 cm depth. The nomenclature of soil horizons defined for the homogeneous layered model (Ap, E, Btg1, Btg2 and C) was therefore not adopted and a clayey till layer was defined between 120 to 300 cm depth.

Table 4.4 - Hydraulic parameters of the soil layers from 0 to 3 m depth used in the heterogeneous soil model. Soil textures according to the USDA soil texture classification

Parameter	Coarse sandy loam	Sandy clay loam	Sandy clay loam	Clay-rich zones	Clayey till
Depth [cm]	0 to 40	40 to 80	80 to 120	0 to 120	0 to 300
Horizontal hydraulic conductivity, Kh [m/s]	5.9E-04	3.0E-04	4.0E-05	8.9E-08	8.9E-08
Vertical hydraulic conductivity, Kv [m/s]	5.9E-04	3.0E-04	4.0E-05	8.9E-06	8.9E-08
Porosity [-]	0.40	0.36	0.38	0.42	0.42
Van Genuchten, α [1/m]	19.2	8.2	14.6	1.8	1.8
Van Genuchten, n [-]	1.2	1.2	1.1	1.2	1.2
Residual saturation, Sr [-]	0.16	0.18	0.17	0.24	0.24
Specific storage, Ss [1/m]	1.0E-05	1.0E-05	1.0E-05	1.0E-05	1.0E-05

Source: The loamy soils have Kh, Kv and porosity measured from soil samples and the clayey soils have Kh and Kv from He et al. (2015) and porosity measured from soil samples. α and n are estimated with the van Genuchten-Mualem model (van Genuchten et al., 1991, Mualem et al., 1976). Sr values were estimated from the residual water contents from Varvaris et al. (2018). Ss values are from He et al. (2015).

The borehole description was used to support the clay-rich zones delineation although few clayey samples were located out of the delineated clay-rich zones (Figure 4.3). The textures noted in borehole descriptions are approximated for each 20 cm layer. For example, if most of the soil located in the 20 to 40 cm is described as loamy, then the texture for this depth interval indicates loamy soil (Figure 4.3).

van Genuchten parameters and K values obtained on samples from the nearby area (Figure 4.1b) were used for the loamy soils. The hydraulic properties of the clay-rich zones from a depth of 0 to 120 cm, were assumed invariable with depth and the van Genuchten parameters obtained from samples of the topsoil with high clay content were used. The hydraulic conductivities of the clay-rich zones were extracted from He et al. (2015). Those hydraulic properties were also applied for the clayey till between 120 to 300 cm depth. However, the vertical hydraulic conductivity (Kv) of the clay-rich zones was increased to account for the effect of the macropores and improve model performance. Drain discharge

and hydraulic heads were better simulated for Kv values 100 times higher than the horizontal hydraulic conductivities from 0 to 120 cm depth. The hydraulic properties of the soil layers for the heterogeneous soil model are presented in Table 4.4.

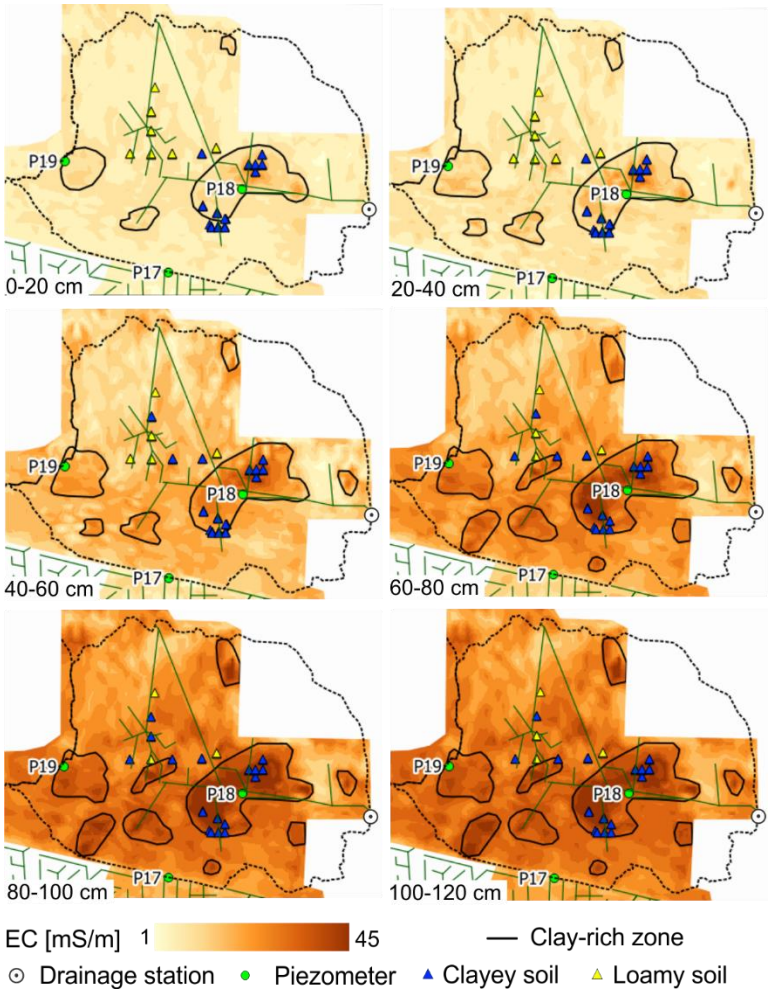

Figure 4.3 - Electrical conductivity (EC) estimates and soil textures from borehole analysis from 0 to 120 cm depth in each 20 cm thickness layer and interpreted clay-rich zones of low hydraulic conductivity into the loamy soils (coarse sandy loam and sandy clay loam).

4.3.6 Actual evapotranspiration

AET from the surface and subsurface are simulated using climatic and land use factors to define the complete soil water budget. Evapotranspiration properties of winter wheat (*Triticum aestivum L.*), listed in Table 4.5, were assigned to the top of the model. The maximum root depth was set to 1.2 m (Palosuo et al., 2011) and a canopy interception of 0.05 mm was defined based on Li et al. (2008). Values for the transpiration fitting parameters (C_1, C_2 and C_3) and the evaporation depth were those recommended by Kristensen and Jensen (1975) for Danish soils. The values of evaporation and transpiration limiting

pressure heads were adjusted for winter wheat (Varvaris et al., 2018). Leaf area index values were extracted from an 8-day composite data set from the NASA Earth Observation data (EarthData, 2015).

Table 4.5 - Evapotranspiration properties of winter wheat applied to the surface domain

Parameter	Value	Source
Root zone depth [m]	1.2	Palosuo et al. (2011)
Evaporation depth [m]	0.2	Kristensen and Jensen (1975)
Canopy interception [mm]	0.05	Li et al. (2008)
Transpiration fitting parameters		
C1 [-]	0.31	Kristensen and Jensen (1975)
C2 [-]	0.15	Kristensen and Jensen (1975)
C3 [-]	5.9	Kristensen and Jensen (1975)
Transpiration limiting pressure head		
Wilting point [m]	-160	Varvaris et al. (2018)
Field capacity [m]	-15	Varvaris et al. (2018)
Oxic limit [m]	-0.1	Varvaris et al. (2018)
Anoxic limit [m]	0	Varvaris et al. (2018)
Evaporation limiting pressure head		
Minimum [m]	-160	Varvaris et al. (2018)
Maximum [m]	-0.1	Varvaris et al. (2018)

4.3.7 Boundary conditions

The upper boundary of the model, corresponding to ground surface, is assigned daily precipitation and potential evapotranspiration fluxes. For the surface water flow domain, a critical depth boundary was assigned at the field outlet corresponding to the lowest ground surface elevation in the model, where the drainage station is located. The lateral boundaries correspond to groundwater divides and are therefore impermeable. De Schepper et al. (2017) included a downward flow component in the Fensholt catchment at a depth of 20 m. We tested the addition of this downward flow component, but it had a negligible effect for our study site. Therefore, the bottom boundary was assumed impermeable.

4.3.8 Simulation strategy and performance metrics

The simulations target a two-year period, 2014 and 2015, for which measurements of drain discharge and hydraulic head are available. A prior model spin-up was required, which is typical for coupled surface and subsurface hydrologic models (Ajami et al., 2014). For the spin-up, we ran both models for 10 years using precipitation data from 23 July 2002 to 22 July 2012. The simulated hydraulic heads at the end of this 10-year period were then used as initial hydraulic heads for the simulation period from 23 July 2012 to 1st January 2016.

The two different models were based on existing conceptual models developed for the site. Their performance in reproducing drain discharge was assessed by computing the mean absolute error (MAE), the Nash-Sutcliffe efficiency (NSE) (Nash and Sutcliffe, 1970) and the Kling-Gupta Efficiency (KGE) (Gupta et al., 2009). The reproduction of hydraulic heads was assessed with the MAE and the root mean square error (RMSE).

4.3.9 Sensitivity analysis and correlation

We calculated the composite-scaled sensitivity and the parameter correlation coefficients of the vertical and horizontal hydraulic conductivities, specific storage and porosity of all geological formations for the measured hydraulic heads and drain discharge. The observations were grouped into head and discharge groups. The same weight was applied to each group, such that they have the same contribution to the objective function, regardless of the number of measurements of heads and drain discharge available. No information on the measurement uncertainty was available for the application of weights to the individual measurements. The period of 01/08/2015 to 01/11/2015 was chosen for the sensitivity analysis. The three months period comprises low and high flow conditions and was chosen to keep simulation times manageable. The value of each parameter was varied by 10% in successive simulations, while keeping fixed values for the other parameters, to compute the Jacobian matrix with the PEST software (Doherty 2016a,b) that allows to quantify the composite-scaled sensitivity and the parameter correlation coefficients.

4.4 Results

4.4.1 Drain discharge and surface runoff

The simulated drain discharge, evapotranspiration and surface runoff for 2014 and 2015 are shown for the reference model and the heterogeneous soil model in Figures 4.4a and b, respectively. The Figures also show the observed drain discharge and the precipitation times series used as input.

For the reference model, the NSE for drain discharge is equal to 0.75 for the 2014-2015 period, which indicates an overall good performance. The model is able to represent low flow rates, lower than 1 mm/d, observed in summer. However, no drain discharge is simulated during the summer of 2014, although a few summer peaks were observed. For the summer of 2015, the simulated discharge during flow peaks is slightly higher than the observed one. Some discharge peaks are underestimated in 2014 and in January and April 2015, resulting in an underestimated cumulative drain discharge from January 2014 to mid-September 2015 (Figure 4.5).

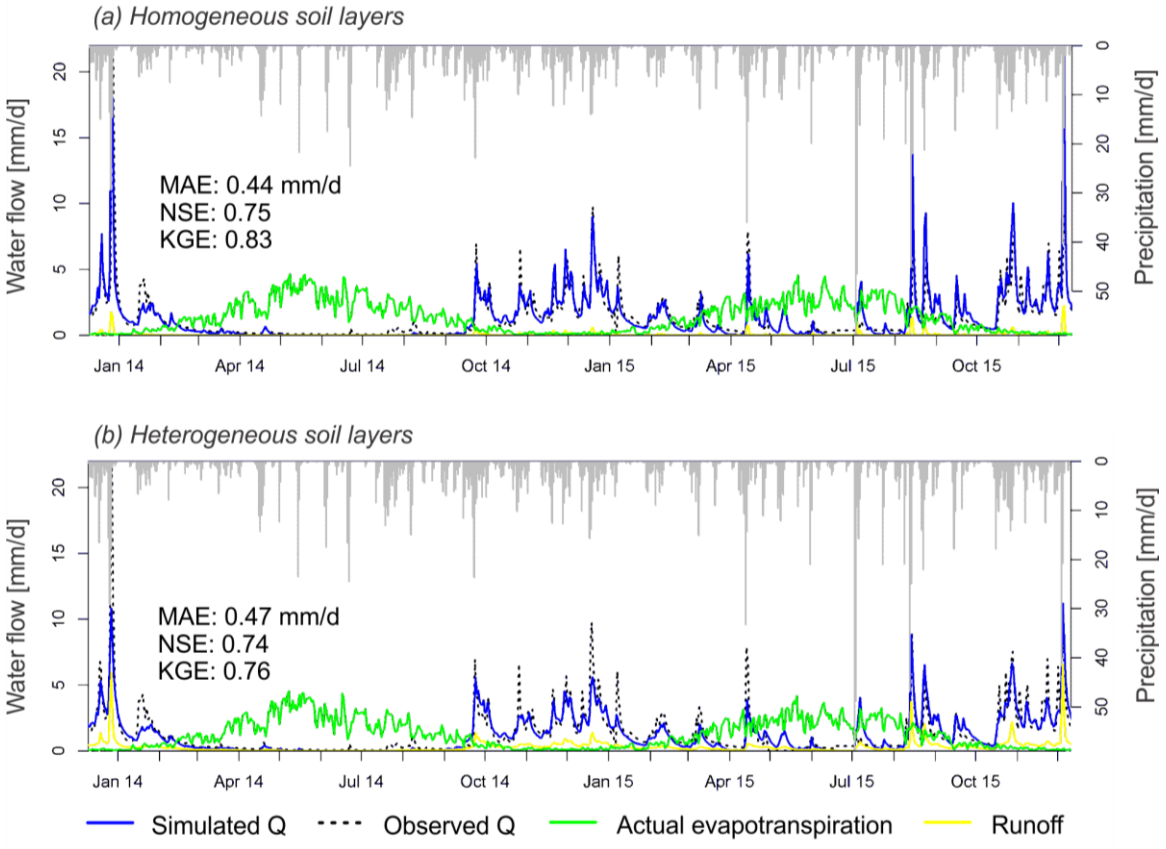

Figure 4.4 - Observed and simulated drain discharge (Q), observed precipitation, simulated evapotranspiration (ET) and surface runoff from January 2014 to January 2016 for the (a) reference model and (b) heterogeneous soil layers model. Observed data were measured at the tile drainage system outlet. MAE: Mean absolute error, NSE: Nash Sutcliffe efficiency, KGE: Kling-Gupta efficiency.

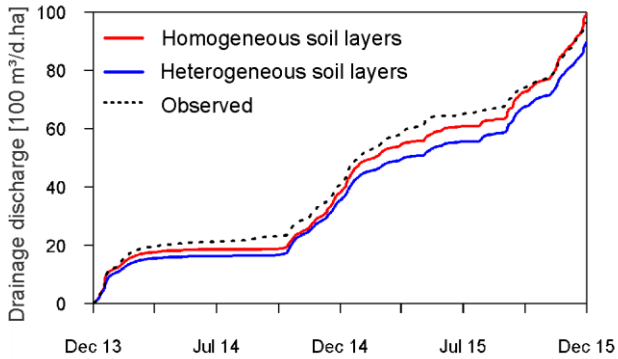

Figure 4.5 - Cumulated drain discharge for the homogeneous and heterogeneous soil layers models compared with the observations.

The global water balance for the reference model and the observed drain discharge for the years 2014 and 2015 are presented in Figures 4.6a and b, respectively. The surface runoff shown in the Figures corresponds to surface water outflow at the critical depth boundary. The actual evapotranspiration

includes canopy, surface and porous medium evaporation as well as transpiration. The simulated drainage corresponds to 42% of the total rainfall for 2014, a percentage comparable to the observed drainage, which is equal to 44% of total rainfall for the same year. For 2015, the simulated discharge corresponds to 53% of the rainfall, against 49% for the observed discharge. Evapotranspiration is the most important outflow during the summer period and it is similar in magnitude to the change in water stored during the winter period. Simulated surface runoff is not significant. The variation in water stored in the surface and the porous medium is less than 1% of the total precipitation for the yearly basis analyses.

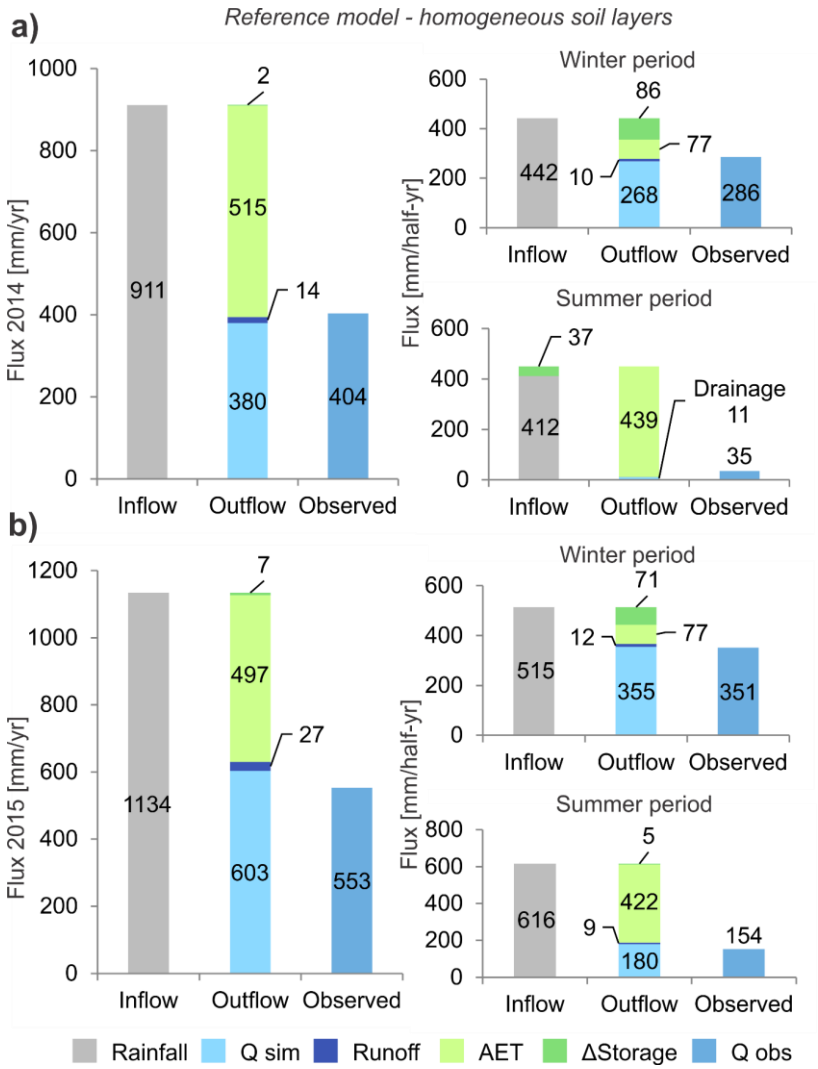

Figure 4.6 – Simulated water budget components for the reference model (homogeneous soil layers) and observed drain discharge for a) the year 2014, the winter period 1/10/2013 to 31/03/2014 and the summer period 1/04/2014 to 30/09/2014 and (b) the year 2015 and the winter period 1/10/2014 to 31/03/2015 and the summer period 1/04/2015 to 30/09/2015. Rainfall corresponds to total precipitation, Qsim and Qobs are the simulated and observed drain discharge, AET is actual evapotranspiration, and ΔStorage is the change in water stored in the drainage area.

Although more complexity is included in the heterogeneous soil layer model, potentially improving the simulation of hydrological processes, the performance of the model in reproducing drain discharge shown in Figure 4.4b (MAE = 0.47 mm/d, NSE = 0.74 and KGE = 0.76) is slightly worse compared to the reference model (MAE = 0.44 mm/d, NSE = 0.75 and KGE = 0.83). Including spatially-variable hydraulic properties of the more loamy and clayey soils therefore does not improve the model compared to the reference model that uses average values. Compared to the reference model, surface runoff increases, and the drain discharge volume decreases for the heterogeneous model. Consequently, drain discharge peaks are in general underestimated and the cumulative discharge volumes are lower than for the reference model (Figure 4.5).

The water mass balance for the heterogeneous model is presented in Figure 4.7. In 2014, the AET is the most important outflow, followed by drainage. In 2015, the drain discharge is higher than AET. The annual simulated drain discharge is 352 mm in 2014 and 536 mm in 2015. These volumes correspond to 39% and 47% of total rainfall for 2014 and 2015, respectively. Drain discharge underestimates the annual observed values of 404 mm and 553 mm for 2014 and 2015, respectively. Simulated surface runoff corresponds to 10% and 12% of the total rainfall for 2014 and 2015, larger than simulated by the reference model. At the study site, observations indicate that surface runoff mostly occurs in winter, when AET is very low relative to precipitation (see winter periods in Figure 4.7). However, the summer of 2015 presents higher simulated surface runoff (8% of rainfall) than expected for the period. The water exchange from the surface to the subsurface media at each time step represents infiltration, which can originate from precipitation, ponding of water on the soil surface and surface runoff. The cumulative simulated infiltration for 2014 and 2015 is 2116 mm, which is only 150 mm higher than the total infiltration of the reference model for the same period. However, the exfiltration from the porous medium to the surface (598 mm) is 336 mm higher than the exfiltration of the homogeneous soils model (262 mm), contributing to the higher surface runoff volumes in the heterogeneous soils model. For 2014 and 2015, the total simulated drain discharge corresponds to 50% of the infiltration (against 49% of observed discharge). Storage variations in the porous medium surface domains have little effect on annual water balances.

The surface runoff peaks simulated at the outlet coincide with the peaks of rainfall during winter, when the soil is saturated. At the end of the 2015 summer, when the rainfall intensity is high, runoff for both models is greater than at the end of the 2014 summer, when rainfall intensity is lower.

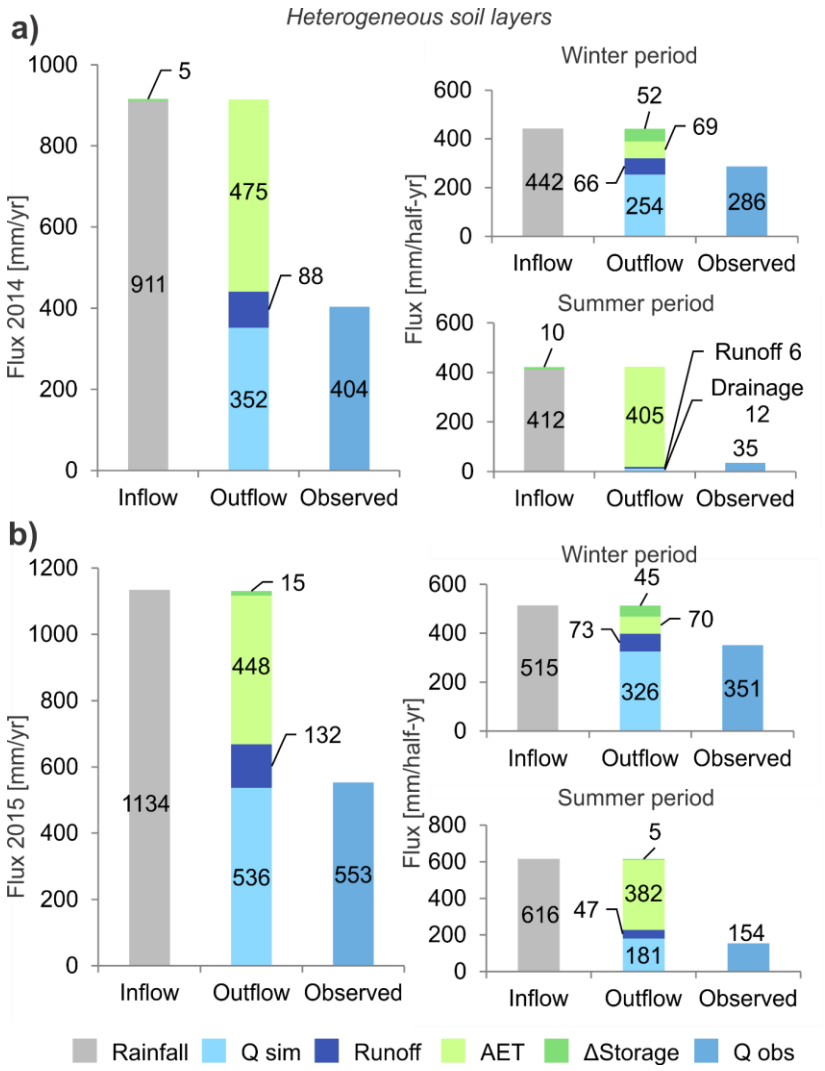

Figure 4.7 - Simulated water budget components for the heterogeneous soil model and observed drain discharge for a) the year 2014, the winter period 1/10/2013 to 31/03/2014 and the summer period 1/04/2014 to 30/09/2014 and (b) the year 2015 and the winter period 1/10/2014 to 31/03/2015 and the summer period 1/04/2015 to 30/09/2015. Rainfall corresponds to total precipitation, Qsim and Qobs are the simulated and observed drain discharge, AET is actual evapotranspiration, and ΔStorage is the change in water stored in the catchment.

4.4.2 Hydraulic head

Observed hydraulic heads in piezometer 17, which corresponds to the local water table elevation and its seasonal variation, are generally well reproduced by the reference model (Figure 4.8) except for the periods from November to December 2014 and September to November 2015 when the head is overestimated. The seasonal variation is also well simulated in piezometers 18 and 19, but the hydraulic head is underestimated by around 50 cm. The model was suitable to simulate the slow decrease of water levels in the spring and summer and the fast increase in the fall. Error statistics for the 3 piezometers are shown in Table 4.6 with average MAE and RMSE values of 0.55 m and 0.61 m.

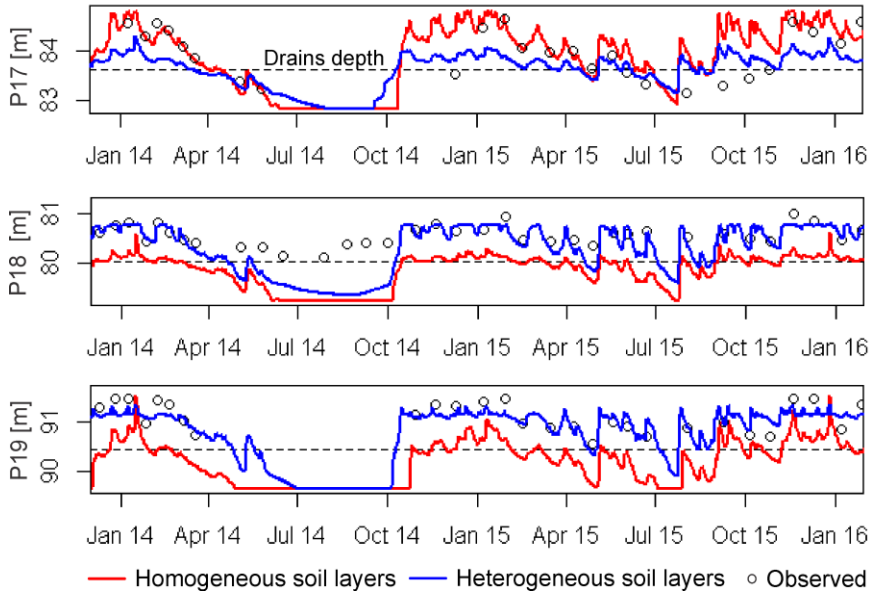

Figure 4.8 - Observed and simulated hydraulic heads in piezometers P17, P18, and P19 from January 2014 to January 2016. The location of the tile drains, estimated to be at a depth of 1.2 m below ground surface, is presented as a dashed line.

Table 4.6 – Performance metrics for hydraulic heads in piezometers P17, P18 and P19 for the homogeneous and heterogeneous soil layers models. MAE = Mean absolute error and RMSE: Root Mean Square Error

Model	MAE [m]			RMSE [m]		
	P17	P18	P19	P17	P18	P19
Homogeneous soil layers	0.30	0.68	0.68	0.42	0.71	0.70
Heterogeneous soil layers	0.38	0.28	0.17	0.43	0.40	0.20

A snapshot of the spatial distribution of the water table depth for the reference model is shown in Figure 4.9a for both winter and summer. In winter (15/01/2015), the simulated water table level is near the tile drain elevation and it rises to the soil surface in several areas located further from the drains. In summer (15/07/2015), the hydraulic heads are lower than the tile drain elevation almost everywhere.

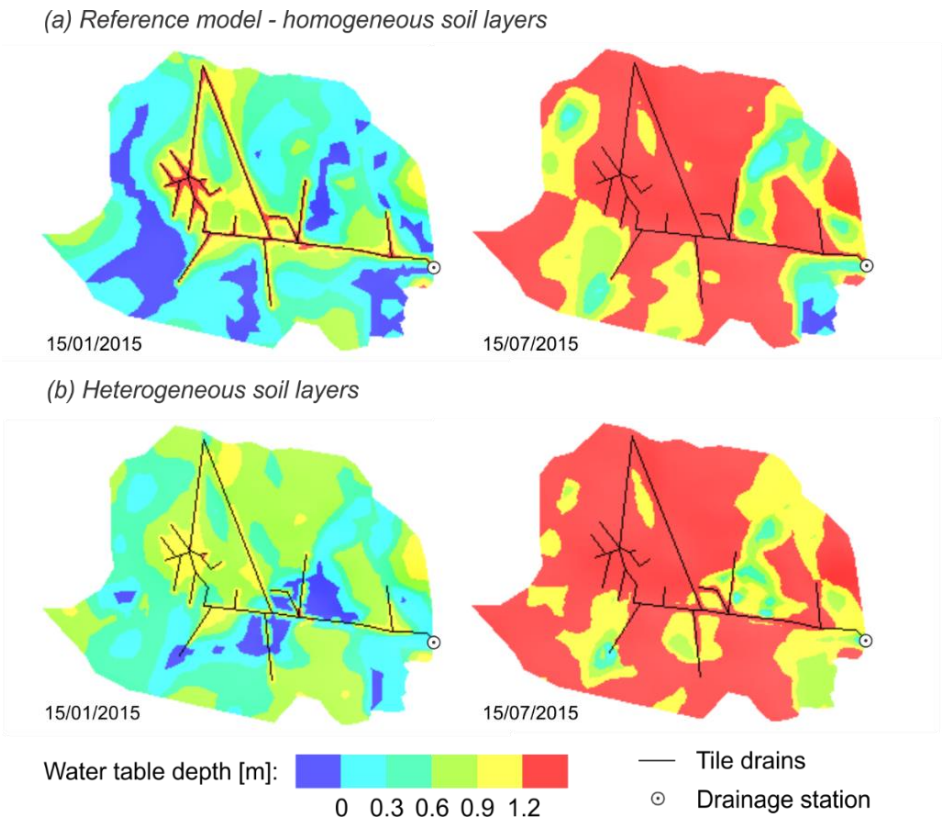

Figure 4.9 – Water table depth for the a) homogeneous and b) heterogeneous soil layers models for 15th January 2015 (wet season) and 15th July 2015 (dry season).

The heterogeneous soil model also reproduces observed hydraulic heads fairly well (Figure 4.8), especially for piezometers P18 and P19, which are located in clay-rich zones. The reproduction of hydraulic heads observed at piezometers P18 and P19 is better than for the reference model, with MAE varying from 0.68 m to 0.28 m (P18) and from 0.68 to 0.17 m (P19) and RMSE varying from 0.71 m to 0.40 m (P18) and from 0.70 m to 0.20 m (P19). The MAE for hydraulic heads observed at P17 for the heterogeneous model (0.38 m) is higher compared to that of the reference model (0.30). Simulated heads in piezometer P17 are generally lower than observed heads and heads simulated with the reference model.

The spatial distribution of the water table depth in winter (15/01/2015), shown in Figure 4.9b, is drastically different from that simulated with the homogeneous soil layers model. Simulated hydraulic heads are higher, and the depth to water table is lower in the clay-rich zones around the tile drains, mainly in the central part of the study site. In summer (15/07/2015), the simulated water table depth is almost similar for the reference and homogeneous models.

4.4.3 Sensitivity analysis and correlation

For the reference homogeneous soil layers model, one or more observations were highly sensitive to the horizontal hydraulic conductivity of the Btg1 and Btg2 horizons and the porosities of the Ap, E and Btg1 horizons. The most correlated parameters are the specific storage of the Btg2 horizon with the porosities of both the Btg2 horizon and the glacial clay, and the horizontal hydraulic conductivity of the Btg1 and Btg2 soil horizons. However, other parameters are also highly correlated as indicated in Figure 4.10a.

For the heterogeneous soil layers model, one or more observations were highly sensitive to the horizontal hydraulic conductivities of the clayey till, the sandy soil from 40 to 80 cm, and the clayey loam from 80 to 120 cm, the vertical hydraulic conductivity of the glacial clay, and the porosities of both sandy and clayey loam from 0 to 40 cm depth. In general, the sensitivity of simulated hydraulic heads with respect to the model parameters was greater for piezometers P18 and P19 than for P17 and they were also greater than for the reference model. The most correlated parameters are the specific storage of the clayey soil from 0 to 40 cm with the horizontal K for the clayey soil from 40 to 80 cm and the porosity of the sandy soil (80-120 cm) with the vertical K of the glacial sand. The parameter correlation coefficients are overall lower than for the homogeneous model (Figure 4.10b).

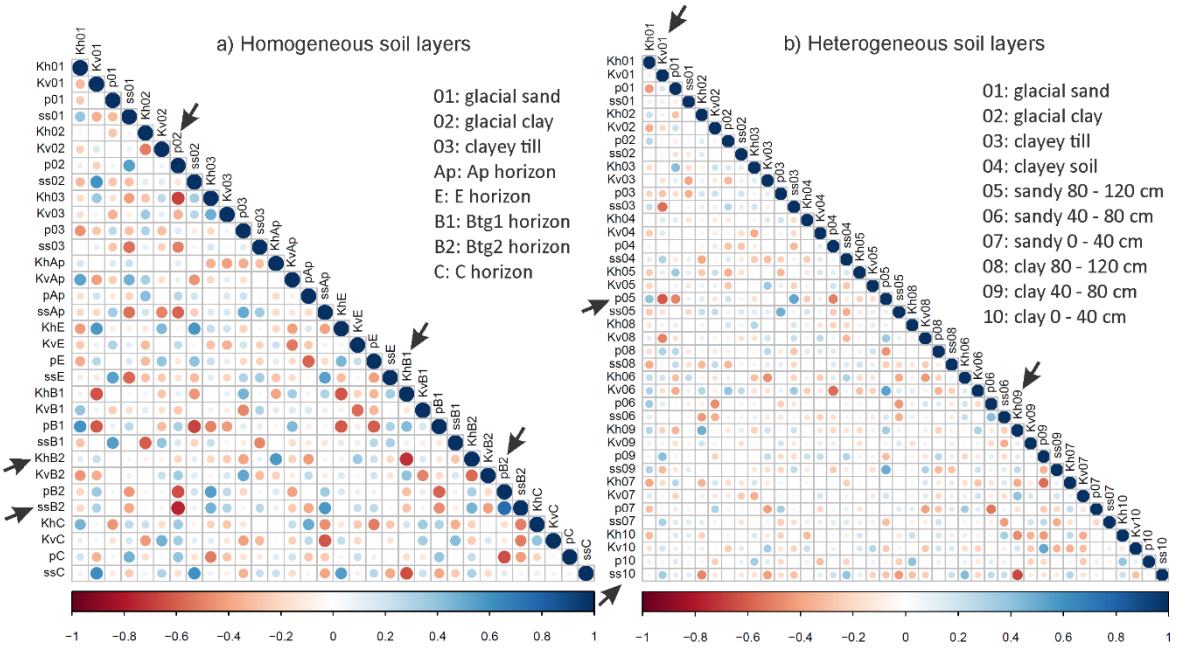

Figure 4.10 – Parameter correlation coefficients of the vertical (Kv) and horizontal (Kh) hydraulic conductivities, specific storage (ss) and porosity (p) of all geological formations for the measured hydraulic heads and drain discharge (Q) for the a) homogeneous soil layers model and the b) heterogeneous soil layers model. The most correlated parameters are highlighted by arrows.

4.5 Discussion

4.5.1 Zonation based on spatially distributed EC estimates

When creating a hydrological model, assumptions about the structure of the subsurface will inevitably be wrong, impairing the representation of critical hydrological processes (Voss, 2011). We assumed that including heterogeneity in the model would improve the simulation of hydrological processes in tile-drained fields. This assumption was based on the fact that tile drain discharge represents an important water flow path and is controlled by both large and small-scale heterogeneity.

The definition of heterogeneous soil zones based on spatially distributed EC estimates is promising due to the non-invasive measurements obtained at different depths. However, the zonation based on EC estimates remains a coarse estimation of reality. For a few boreholes, the delineated areas based on the EC estimates shown in Figure 4.3 are not consistent with the visual description available from the borehole logs.

The zonation of soil heterogeneity was suitable for the implementation in the 3D hydrological model and avoided the need to interpolate from sparse borehole data, which could result in an erroneous distribution of soil properties. The depth specific EC estimates were used as a criterion to define zones with effective parameters. These zones were easily delineated using the triangular mesh structure for the implementation of different soil properties.

In the heterogeneous soil layers model, the most significant difference between piezometers P17, P18 and P19 is that piezometers P18 and P19 are located in strongly anisotropic clay-rich soils that have a 100:1 ratio between the vertical and horizontal hydraulic, while soils in the vicinity of piezometer P17 are isotropic. The anisotropy for P18 and P19 favors flow in the vertical direction as opposed to the horizontal direction. The strong anisotropy around P18 and P19, and the lack of anisotropy around P17, may explain the contrasted response observed for the sensitivity analysis, with simulated hydraulic heads at P18 and P19 more sensitive to the model parameters than heads at piezometer P17 for the same model, and also compared to the reference model for all piezometers. The parameter correlation coefficients are lower in the heterogeneous soils model (Figures 4.4a and b), suggesting that the enhanced representation of soil heterogeneity could potentially improve the capacity of the model to assimilate the observations when compared to the reference model. Furthermore, the combination of relatively high composite-scaled sensitivity and low parameter correlation coefficients indicates a good capability of the calibration process to constrain the model parameters (Hill et al., 2016).

The delineated zones were based on sparse borehole data and EC estimates. However, the topography also plays an important role in recharge and surface runoff. A depression zone located around piezometer P18 may affect the soil properties as indicated from the soil texture from the boreholes analysis at the depth of 0 to 40 cm (Figure 4.3). Future work can focus on delineating soil zones also based on topography.

4.5.2 Subsurface drainage simulation

The reference (homogeneous) and heterogeneous soil layers models reproduce the observed tile drain discharge reasonably well, with lower tile drain flow in summer and higher in winter. The low summer drain discharge mainly results from higher evapotranspiration during the crop growing season. The transition from low flow, or almost no flow, to the initiation of drainage in autumn is reproduced by both models. Both models also capture the dynamics of the drain discharge peaks and reproduce the low/no flow behavior during the summer periods in 2014 and 2015.

The slightly worse performance of the heterogeneous soil layer model may be explained by a better representation of macropores in the reference model. In the homogeneous model, the effect of macropores is implicitly accounted for in the parameter estimation as described by Varvaris et al. (2018), while it was only considered in the vertical hydraulic conductivity of the clay-rich zones in the heterogeneous model.

The cumulative drainage from 2014 to 2015 is underestimated with the heterogeneous soil layers model during the entire period and it is underestimated from January 2014 to October 2015 with the reference homogeneous model. Using a 2D hydrological model at the same site, Varvaris et al. (2019) overestimated the cumulative drain discharge for the period 01/06/2013 to 01/06/2014. This overestimation was likely caused by the inclusion in their model of a systematic coverage of the field by tile drains, whereas tile drains are only at specific locations in the field. Our models represent the tile drain network more realistically, with lateral spreading between tile drains sufficiently large to allow some of the percolated water to bypass the tile drain system and flow deeper.

The underestimation observed in our models could be caused by the lack of lateral subsurface inflow. The cumulative drainage for 2014 and 2015 indicated that increasing the model complexity with heterogeneous soil layers does not improve the overall behavior of the drain discharge simulations in terms of volume and temporal dynamics. However, including heterogeneity results in a markedly different spatial resolution in hydraulic heads, and thus water table elevations, especially in winter (left panel in Figure 4.9). For the homogeneous model, the water table is generally low in the vicinity of the drains, but close to or at ground surface further away. For the heterogeneous model, areas with a near-surface water

table are in the clay-rich zones and the total extent of areas with high water table elevations is smaller. Although the spatial hydraulic head distribution cannot be validated from field observations, the simulated distribution for the homogeneous case may be questioned because a water table close to ground surface over such large areas is unlikely in an agricultural tile-drained field. Despite the similarity of the simulated drain discharge for both models, their marked differences in the simulated spatial variation of the water table can in turn affect a subsequent simulation of nutrient reduction and transport processes dependent on moisture content, such denitrification. One implication of these results is that head observations complement the drain discharge data for the evaluation of the model's performance.

Eastman et al. (2010) observed that the soil texture in drained fields influences the generation of outflow (drain discharge and surface runoff) from precipitation. It can be assumed from our study that the soil texture heterogeneity within a drained field also influences outflow generation.

4.5.3 Hydraulic heads and surface-subsurface water exchange

The groundwater dynamics observed in the piezometers is reproduced both with the homogeneous and heterogeneous soil layers model. The water table fluctuations are more sensitive to soil properties than the simulated drain discharge, especially for the heterogeneous soil layers model. One possible reason is that hydraulic heads represent local measurements, representative of conditions in the vicinity of a piezometer, while drain discharge provides a cumulative value for the study field. At our field site, the piezometer screens were installed from ground surface to a depth of 2 m, and the topsoil properties thus have a potentially great influence on the observed heads.

Using the homogeneous soil layers model, it was not possible to reproduce observed heads in all three piezometers simultaneously, which suggests that soil heterogeneity should be accounted for to accurately simulate observed heads. By introducing the clay-rich zones in the soil layers, the heterogeneous model resulted in an overall improvement in the fit for the three piezometers (Table 4.6). Heads in piezometer P17 (located in the sandy loam soil) are underestimated, which can be explained by the fact that the hydraulic properties for the loamy soils were estimated by water retention curves and applied directly without calibration. Moreover, the effect of hysteresis was not considered in this study since the soil water retention curves were only measured under drying conditions. Not including hysteresis may explain some of the differences between the simulated and observed hydraulic heads across the field, since several studies have identified the important role of hysteresis in water flow and solute transport modeling (Kaluarachchi and Parker, 1987; Arrey et al., 2018; Likos et al., 2014). The model results corroborate the assumptions of Hansen et al. (2013) that a better representation of local heterogeneity and the spatial variation of hydraulic conductivities can improve the spatial dynamics in hydraulic heads. Therefore, the

hypothesis that including clay-rich zones in tile-drained field improves the model performance may be true for the hydraulic heads, but we cannot conclude that it was also the case for the drain discharge.

According to Woolhiser et al. (1996), poor surface runoff simulation is expected if 1) a model structure cannot accommodate the spatial variability of saturated hydraulic conductivity or precipitation, 2) a model cannot simulate the interaction between infiltration and surface runoff after a rainfall event or 3) there is an inadequate knowledge of the soil properties. Adding spatial variability of hydraulic conductivity in the model increased the simulated surface runoff volumes from 2% to 10% in 2014 and from 2% to 12% in 2015, related to the total precipitation. As a comparison, Sloan et al. (2016) simulated the water balance components for drained soils at the edge of the study site using the DRAINMOD model and found that surface runoff represented 12% of total precipitation for clay, 7% for silt and 0.4 % for sand.

The higher volume of exfiltration water from the porous medium (saturated excess runoff) simulated for the heterogeneous models can be explained by the difference of hydraulic conductivity values between the loamy soils (coarse sandy loam and sandy clay loam) and clay-rich zones. In the more permeable loamy soil, subsurface flow is more likely to occur than in the clayey soil, where surface runoff would be generated (Sloan et al., 2016). Although surface runoff was not monitored in the study area and simulated runoff could not be compared to observed runoff, including clay-rich zones identified using EC estimates in the hydrological model resulted in more realistic runoff patterns compared to the study of Sloam et al. (2016).

Our simulations demonstrate how soil properties control runoff generation as confirmed by Hümann et al. (2011), who conducted experiments to identify the dominant runoff generation process in agricultural and forested sites. Larger values for overland flow were also obtained in the hydrological models of Merz and Bárdossy (1998), which were conceptualized with structured (or organized or deterministic) soil variability, as opposed to homogeneous and stochastic variability. Merz and Plate (1997) developed physically-based hydrological models including spatial variability of soil properties and compared a spatially homogeneous, a randomly heterogeneous and a structured heterogeneous model. They investigated a subcatchment that was composed of clay particles with a downslope position, similar to our study site. They showed that the structured heterogeneous spatial variability strongly influenced runoff. Furthermore, the effects of the spatial variability were small for very small and for large runoff events, although they only investigated summer events. In our model, larger surface runoff was generated during the large rainfall events in winter due to increased soil saturation. In the study of Merz and Plate (1997), the soil was relatively dry prior to the large rainfall event, representing the effect of infiltration excess runoff.

The flooded areas in depression zones observed around piezometer 18 dominated by clay-rich zones are better represented by the heterogeneous soil layers model (Figure 4.9). That result suggests that the simulation of groundwater–surface water exchange is spatially improved when horizontal soil heterogeneity was included using EC estimates.

4.5.4 Model resolution and computational time

The same mesh was used in both models, with maximum cell length of 10 m in the vicinity of the tile drains. A similar cell discretization configuration was adopted in the 3D hydrological model developed by Nousiainen et al. (2015). They used a grid cell diameter of 6.25 m in the control model and 12.5 m in the model realizations for an agricultural field with an area of 12 ha, which is similar to the area of our study site (14 ha). The vertical discretization was refined to match the EC data resolution (~20 cm). We also generated a triangular mesh with higher resolution by reducing the maximum element size from 10 m to 5 m in the vicinity of the tile drains, where the element areas ranged from 0.1 to 10 m^2. The number of nodes and triangular elements in the refined 2D surface mesh were 3789 and 7446, respectively. However, refining the triangular mesh near the tile drains did not have a significant effect on the simulation of the drain discharge and heads and the coarser configuration was maintained.

The horizontal mesh resolution was slightly coarser far from the tile-drains, with element size up to 30 m. A finer mesh with a maximum element length of 1 m could better represent the horizontal heterogeneity far from the tile drains, at the expense of increased simulation times. However, simulated heads at the boundaries (P17 and P19), further away from the tile drains, are less influenced by preferential flow in the tile drains. Consequently, we assume that increasing the mesh resolution near the boundary, and further away from the drains, would not improve drain flow simulations and therefore not justify the additional computational burden of a denser mesh.

The maximum 1h time step was used to ensure numerical stability, especially for the heterogeneous soil model. Daily stress periods were necessary to accommodate daily drain discharge.

Including greater soil heterogeneity considerably increased the simulation time, from 15 to 91 hours. The difference in soil properties changed the water flow paths, creating larger hydraulic gradients, which requires smaller time steps to solve the porous medium water flow and the surface-subsurface water exchange.

The location of all drains was included explicitly in the model by resolving the drain location in the mesh. If this approach were to be used for large-scale models, the number of computational nodes would

increase very significantly, leading to very large computational times that may render the simulation impractical.

4.5.5 Limitations of the conceptual model

Only one stochastic realization of the geological model developed by He et al. (2014) was used to assign hydraulic properties for model layers between the depths of 3 to 20 m. The small area of the studied field and the lack of deep piezometers do not allow a comprehensive analysis of groundwater flow below a depth of 2 m. Therefore, alternative representations of the deeper geological units were not investigated. Considering the overall good simulations of the outflow, the use of a different geological model for the deeper units would likely not improve the drain discharge simulations.

Including the soil horizontal heterogeneity in hydrological models with tile drains is relevant for the identification of flooded areas. Furthermore, the parameter correlation coefficients indicate that the soil parameters are less correlated, reducing the likelihood of non-unique parameter sets. However, the heterogeneous soil layers model required a larger number of parameters than the reference model, as each soil layer had two different soil zones. Soil heterogeneity data, such as in situ measurements of soil water content, is rarely available at other sites and at larger scales. Therefore, further calibration is necessary to overcome the lack of representation of soil hydraulic properties.

4.5.6 Limitation in modeling approach

In structured soils, macropores can be an important pathway for water flow and solute transport, as observed in some Danish glacial tills (Klint and Gravesen, 1999; Nilsson et al., 2001; Christiansen et al., 2004). In a modeling study, Haws et al. (2005) found that assuming homogeneity for a field with preferential pathways contributed to the deficiencies of their tile drain water and solute discharge simulations. Vogel et al. (2000) showed that including spatial variability in the hydraulic properties using the dual-permeability approach improved the simulation of water and solute movement in naturally heterogeneous field soils. In the clayey areas at our study site, the soil may exhibit strong structures and possibly a high content of macropores (Iversen et al., 2004).

The drainage network at the site is represented explicitly by resolving the network in the computational mesh and defining seepage nodes for the exchange of water. The amount of water drained is assumed to be controlled by the hydraulic gradient that develops between the subsurface and the drain, which depends on the drain elevation, and the hydraulic conductivity of the porous media, while the drain pipes themselves are assumed not to pose a resistance to water flow. In reality, the tile drain walls, and possible clogging of drains will increase resistance to flow, which can only be estimated through model calibration.

Improved model performance is therefore likely to be obtained through model calibration. However, both models provided results that are in good agreement with observed head and drain discharge in terms of absolute values and temporal dynamics. It was thus assumed that the performances of the models were adequate for assessing the impact on local scale heterogeneity.

For the study site, it was possible to represent the drainage network explicitly in the computational mesh. For large scale modeling, this will not be computationally efficient. Furthermore, the location of drains is commonly unavailable and the tile drainage system outlets are rarely documented. This lack of data makes the explicit representation of drains in large scale model very uncertain and ways to represent the effect of drainage from agricultural fields need to be developed.

4.5.7 Equifinality in tile drain discharge modeling

Uncertainty associated with the structure of a model, the correlation between parameters, the accuracy of the numerical solution, the scarcity of data, and the scale of representation leads to inherently non-unique model solutions, whereby different model configurations might adequately reproduce historical observations and honour expert knowledge (Refsgaard et al 2012; Zhou et al., 2014; Hill et al., 2016; Delottier et al., 2017; Aster et al., 2018). This concept, referred to as equifinality (Beven, 2006; Beven and Freer, 2001), was systematically studied by Klaus and Zehe (2010) for the simulation of physically-based preferential flow in a tile-drained field. Among the large number of model configurations tested, they showed that a smaller group of models performed equally well during calibration, leading to equifinality, which in turn affects the predictive uncertainty for their preferential flow simulations.

We investigated how the inclusion of heterogeneity, consisting of clay-rich zones, can influence simulation results for the tile-drained field, provided that the model inputs, observations and tile-drain network are identical. Representation of heterogeneity was based on EC estimates but there is uncertainty associated with the delineation the clay-rich zones and their hydraulic properties. Even if the inclusion of clay-rich zones using EC estimates in the model closely represented the soil structure and their properties were accurately defined, the model would still be subject to equifinality due to errors in prior model assumptions, boundary conditions and field measurements.

In our study, using average soil properties for the homogeneous soil layers resulted in simulated drain discharge that reproduce observations as well as the heterogeneous soil layer model. This is probably due to the cumulative hydrological processes occurring at the field that affect the discharge simulation at the outlet. These results reveal equifinality for our simulations, as shown also by Klaus and Zehe (2010). Incorporating soil heterogeneity to simulate drain discharge at our field site is probably not warranted because the homogeneous model performs equally well and it reduces computational times and facilitates

model refutability and transparency (Hill, 2006). Furthermore, data at most sites will likely be scarcer than for our well monitored field site such that increasing the inverse problem dimensionality, by introducing more parameters, could favour equifinality and increase uncertainty for simulated drain discharge.

4.6 Conclusion

This study demonstrated that spatially distributed depth specific electrical conductivity (EC) estimates can be used with borehole data for mapping soil heterogeneities in clayey till soils, improving hydrological simulations in a tile-drained field. The effect of heterogeneous soil properties on drain discharge and the water table fluctuation were investigated using 3D integrated hydrological models conceptualized with homogeneous and heterogeneous topsoil layers, respectively. Heterogeneous soil zones were identified using depth specific EC estimates derived from the apparent electrical conductivity data measured using an electromagnetic induction instrument. Hydraulic parameters for the loamy soils were estimated from soil water retention measurements in the laboratory. The vertical hydraulic conductivity of the clay-rich soils in the heterogeneous soil model was manually calibrated. All other parameters for both models were obtained from previous hydrological assessments at the site and the models were therefore not calibrated.

Simulations with the heterogeneous soil layers model showed that including clay-rich zones in predominately loamy soils (coarse sandy loam and sandy clay loam) affected the spatial distribution on shallow groundwater heads and drain discharge, together with a change in surface runoff, actual evapotranspiration, and storage. Including the topsoil heterogeneity generally improved the match to observed shallow groundwater levels, particularly where clay-rich zones had been identified. Although the drain discharge simulated by the two models was comparable, the homogeneous soil layers model resulted in better agreement between simulated and observed drain discharge. This improvement is probably due to the implicit representation of preferential water flow through macropores in defining hydraulic properties, while only the vertical hydraulic conductivities were adjusted in the heterogeneous case.

The good reproduction of drain flow by the homogeneous soil layers model implies that including average soil hydraulic properties in 3D hydrological models is suitable to simulate tile drain discharge even for complex heterogeneous subsurface properties. However, the homogeneous model demonstrated coarse agreement with the observed spatial distribution of hydraulic heads within the field, which is important when simulating nutrient reduction and transport processes dependent on water table elevation and moisture content.

Chapter 5

3D surface-subsurface modeling of a bromide tracer test in a macroporous tile-drained field: improvements and limitations

Modélisation hydrologique 3D d'un essai de traceur de bromure dans un champ drainé contenant des macropores : avancées et limitations

V. F. Boico, R. Therrien
Department of Geology and Geological Engineering, Université Laval. Quebec City, Canada.

J. H. Fleckenstein, G. Nogueira
Department of Hydrogeology, Helmholtz Centre for Environmental Research, UFZ. Leipzig, Germany.

B. V. Iversen, R. J. Petersen
Department of Agroecology, Aarhus University. Tjele, Denmark.

Résumé

L'évaluation et la prévision des pertes de nutriments dans les zones agricoles drainées reposent souvent sur des modèles basés sur la physique. Cependant, l'application des macropores et des drains souterrains dans les modèles hydrologiques et de transport de solutés est limitée en raison du grand nombre de paramètres. L'objectif de ce chapitre est d'examiner l'efficacité d'un modèle tridimensionnel pour simuler un essai de traceur de bromure (Br) en utilisant la condition limite *seepage nodes* pour représenter explicitement les drains souterrains, et le concept de porosité unique avec zone immobile pour représenter l'écoulement préférentiel à travers les macropores. Le modèle a bien fonctionné pour simuler les débits de drainage et le transport de Br vers les drains. Cependant, la plupart des pics de Br et la masse de Br tardive déchargée à la sortie du système de drainage ont été sous-estimés. L'imprécision du modèle a probablement été causée par la représentation incomplète de l'hétérogénéité du sol, des macropores et la dispersion numérique.

Abstract

The assessment and forecasting of nutrient losses in tile-drained agricultural areas often rely on physically based models with adequate representation of macropores and tile drains. However, the implementation of macropores and tile drains in hydrological and solute transport models is limited due to the large number of parameters. The purpose of this chapter is to investigate the efficiency of a three-dimensional model to simulate a bromide (Br) tracer test using the seepage nodes boundary condition to explicitly represent tile drains, and applying the single porosity with an immobile zone concept to represent preferential flow through macropores. The model performed well in simulating drain discharge and the transport of Br to tile drains. However, most of the Br peaks and the late-time Br mass in the drain outflow were underestimated. The model inaccuracy was likely caused by the misrepresentation of the soil heterogeneity, macropores and dispersion processes.

5.1 Introduction

Although tile drains that are installed in rural catchments can increase crop yield by improving soil moisture conditions, they simultaneously create preferential flow paths that rapidly transport agrochemicals and nutrients to surface water bodies (Brown and van Beinum, 2009; Reichenberger et al., 2007; Zehe et al., 2001; Gramlich et al., 2018; Stamm et al., 1998). This is particularly problematic for nitrate contamination, as tile drains carry nitrate to surface water bodies before it can be denitrified in the subsurface of the soil. Hydrological and solute transport models that are developed to estimate tile drain discharge and nutrient concentrations in drainage water can be used to forecast water contamination and the effect of mitigation measures such as norms for fertilizer application, cover crops, engineering restoration and spatially differentiated regulation for lowering N-loads (Refsgaard et al., 2019). The usability of the model, however, depends on its simplicity and its reliability to reproduce the main processes that govern water flow and nutrient transport.

Tile drainage has been implemented in many physically-based hydrological models in one, two and three dimensions. Examples of one-dimensional models include RZWQM (Ma et al., 2007; Walker et al., 2000) and DRAINMOD (Sammons et al., 2005; Wang et al., 2006). Models that are two-dimensional include MHYDAS-DRAIN (Tiemeyer et al., 2007), CATFLOW (Klaus and Zehe, 2011; Maurer, 1997) and ANTHROPOG (Carluer and De Marsily, 2004). Finally, three-dimensional models include MIKE-SHE (Hansen et al., 2013), CATCHY (Muma et al., 2014; Muma et al., 2016), FLUSH (Nousiainen et al., 2015; Salo et al., 2017; Turunen et al., 2013) and HydroGeoSphere (Amado et al., 2017; De Schepper et al., 2015, De Schepper et al., 2017, Frey et al., 2016; Rozemeijer et al., 2010, Thomas et al., 2016). Some 3D modeling studies have considered tile drains as a uniform high conductivity layer (Rozemeijer et al., 2010; Carluer and Marsily, 2004, De Schepper et al., 2015; Thomas et al., 2016), as a head-dependent sink in all grid cells in the model (Hansen et al., 2013), as discrete 1D lines (De Schepper et al., 2015), or as nodal sinks (seepage nodes) at tile drain locations (De Schepper et al., 2017, Hansen et al., 2019; Boico et al., 2022b). Other studies used seepage nodes to reduce long computational times from those required for the discrete lines approach (De Schepper et al., 2017, Boico et al., 2022a) simulating the flow and transport dynamics around the drains, as well as the drain discharge and concentration.

Macropores are large, structured pores that have high continuity and low tortuosity (Jarvis 2020) and can be formed by root and earthworm channels (biopores) as well as fissures and cracks. These features promote non-equilibrium transport, where rapidly-infiltrating, nutrient-rich water in the macropores does not equilibrate with the slow-flowing water within the bulk of the soil matrix (Jarvis et al., 1998). Previous work has shown that macropores present in clayey till soils create a hydraulic connection (preferential flow) between the surface and the drainage systems (Williams et al., 2016; Radcliffe et al., 2015). The

presence of both the preferential flow from macropores and tile drains can create drain discharge events that have high levels and concentrations of solutes, increasing the risk of surface water contamination (Akay and Fox, 2007; Frey et al., 2016; Júnior et al., 2004; Rosenbom et al., 2015; Stamm et al., 1998, 2002). For instance, Holbak et al. (2021) observed that the inclusion of biopore macroporosity in the Daisy hydrological model (Abrahamsen and Hansen, 2000) increased the tracer discharge peak and leaching to deeper soil layers and drainpipes. Other physically-based modeling studies using APEX (Ford et al., 2015; Francesconi et al., 2014), EPIC (Wang et al., 2018), SWAT (Boles et al., 2015) and HydroGeoSphere (De Schepper et al., 2017) that incorporated tile drains without accounting for macroporosity could have been improved if macropores were considered, with some showing deficiencies in solute transport simulations.

The concepts of dual porosity and dual permeability are commonly used to simulate non-equilibrium transport. The dual porosity model (also known as the mobile-immobile model; van Genuchten and Wierenga, 1976; Köhne et al., 2004) allows water flow and solute transport to occur only in the macroporous domain (mobile porosity), while water in the matrix domain is considered immobile. In the dual permeability model (Gerke and van Genuchten 1993), both macroporous and matrix domains allow water flow and solute transport. The dual porosity and dual permeability concepts have been widely tested in 2D hydrological models of tile-drained soils (e.g., Varvaris et al., 2018; 2019, Bishop et al., 2015; Abbaspour et al., 2001; Frey et al., 2012; 2016, Klaus and Zehe, 2011, Gärdenäs et al., 2006). Christiansen et al. (2004) implemented the dual permeability concept using the coupled MIKE-SHE/Daisy code in a tile-drained catchment to simulate stream discharge and hydraulic heads. However, drain discharge and solute concentration simulations in 3D models using a dual continuum concept is limited to the plot-scale (Salo et al., 2017, Warsta et al., 2013, Turunen et al., 2013) due to the large number of parameters that are rarely available and the long computational times.

Using a 2D solute transport model, Varvaris et al. (2021b) simulated a tracer test in a tile-drained catchment. They represented macroporous soils with different conceptual models, including single porosity, single porosity with an immobile zone, dual porosity and dual permeability. All the conceptual models that were tested underestimated the tracer concentration at the drain outlet, revealing deficiencies in the 2D model for solute transport simulation. They suggested improvements by including deeper soil layers in the model and developing a 3D hydrological and solute transport model.

The objective of our study is to simulate the tracer test investigated by Varvaris et al. (2021b) using a 3D model, according to their suggestion, to improve the representation of the tracer concentration at the drain discharge location. Using the HydroGeoSphere model allowed us to simultaneously simulate the 2D surface water flow and the 3D groundwater flow, as well as accurately represent the locations of the

tile drains in the densely tile-drained field. The observed drain discharge, tracer mass at the drain outlet, and hydraulic heads at three shallow piezometers were tracked with the model. We hypothesize that modeling tile drains with seepage nodes can be used to reproduce a Br tracer test breakthrough curve. Contrary to Varvaris et al. (2021b), we also hypothesize that a single porosity model with immobile zone is suitable for the simulation of tracer mass peaks at the drain outlet as well as the late-time tracer mass. When single porosity with immobile zone concept is applied, the total porosity is divided into two components: mobile and immobile. However, differently than the dual porosity concept, the water content in the immobile domain (micropores) is constant and only solute can move in and out of this domain. This requires the use of only two more parameters than the single porosity approach alone. Those parameters are the immobile porosity and the mass transfer coefficient. Therefore, unlike the dual porosity and dual permeability models, the single porosity with immobile zone approach allows 3D models to be used without requiring too many additional parameters and complex formulations. The simulations presented here, to our knowledge, are the first attempts at modeling solute transport using seepage nodes to represent tile drains and using the single porosity with immobile zone approach to represent macroporosity in a fully coupled 3D model.

5.2 Method and data

5.2.1 Site description

Our study site covers an area of 7.6 ha, located about 20 km south of the city of Aarhus, Denmark (55°59'7"N 10°4'3"E, Figure 5.1). The site drains into a small headwater stream within the larger Fensholt subcatchment (6 km^2), ultimately draining into the Kattegat Sea to the east. The local climate is humid, characterized by mild winters, cool summers, and frequent rainfall (He et al., 2015). The average annual precipitation in the Fensholt catchment for the 1990–2017 period was 856 mm, with annual values ranging from 601 to 1137 mm. The landscape consists of rolling hilly terrain with ground elevation ranging from 61 to 87 m above mean sea level. The study site is densely tile-drained with all drains merging into a single drain outlet (Figure 5.1c). The tile drain outlet terminates where the hillslope meets the riparian lowland and discharges onto the soil surface as overland flow. The study site is mainly used for winter wheat crops.

The geology of the area is mainly composed of Quaternary glacial clay from the Weichselian glacial age (Hansen et al., 2014; He et al., 2014; Prinds et al., 2020). The vertical hydraulic conductivity (Kz) of this geological unit is relatively low, at Kz = 1.0E-09 m/s (De Schepper et al., 2017), and it was assumed to be essentially impermeable for our study. A low-permeability clayey till unit overlying the glacial clay was defined by De Schepper et al. (2017), corresponding to the C horizon in the study by Varvaris et al.

(2018). Varvaris et al. (2021a) collected a total of 24 undisturbed soil samples to produce a macroscopic description of the soil texture and to determine the soil water retention (SWR) curves of the Ap (0–25 cm), E (25–55 cm), Btg1 (55–90 cm) and Btg2 (90–120 cm) horizons. These soils were classified as sandy loam, according to the USDA soil texture classification. The saturated hydraulic conductivity (isotropic) was measured at different depths using the constant-head method (Klute and Dirksen, 1986). Varvaris et al. (2021b) showed that including macropores in 2D hydrological models improved the simulations of bromide concentrations in tile drains, suggesting that macropores can play a dominant role in water and solute transport at the study site. Varvaris et al. (2021b) provided additional information on soil sampling and laboratory experiments.

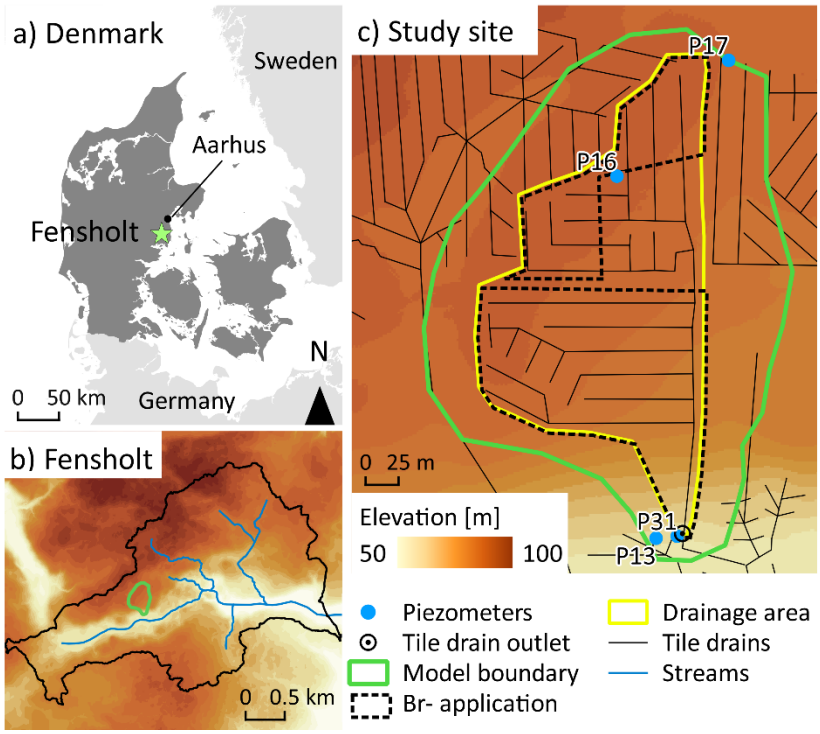

Figure 5.1 – (a) Location of the Fensholt catchment in Denmark (55°59' N, 10°5' E), (b) location of the studied drainage area and stream system within the Fensholt catchment and (c) mapped tile drains within the study site, as well as the location of piezometers, the gauging station at the tile drain outlet and the bromide application area. The ground surface elevation, based on a 1.6-m digital elevation model, is shown in the backgrounds of (b) and (c).

5.2.2 Hydrologic data

Precipitation data were obtained from a meteorological station situated 3 km southwest of the study area. Potential evapotranspiration (PET) was estimated with the Penman-Monteith equation using data from a meteorological station in Foulum, Denmark (56°29'N 9°35'E), 62.5 km from the study area. Total precipitation and PET for the studied period, from 1 August 2017 to 16 April 2018, were 594 mm and

216 mm, respectively. Daily tile drain discharge at the outlet (Figure 5.1c) was measured by an electromagnetic flow meter (KROHNE Optiflux 3070 flow meter, Krohne Messtechnik GmbH, Duisburg, Germany). Measured precipitation, calculated PET and observed drain discharge at the drain outlet are presented in Figure 5.2. The water table in the Fensholt catchment is shallow (De Schepper et al., 2017; Hansen et al., 2019; He et al., 2014) and three piezometers (P13, P16 and P17 shown in Figure 5.1c), screened from the ground surface to a depth of 2 m, were installed to manually measure water table levels twice a month. Piezometers were already installed at the field site prior to our study, as part of the iDRÆN project from Aarhus University (see more at www.idraen.dk). A third piezometer (P31, in Figure 5.1c), at a depth of 3 m and screened from 2 to 3 m below the surface of the ground, was installed for the Petersen et al. (2020) study. Daily water levels in P31 were measured from 3 February 2017 to 19 February 2018 using a mini-Diver (van Essen Instruments) adjusted to compensate for barometric pressure (Petersen et al., 2020).

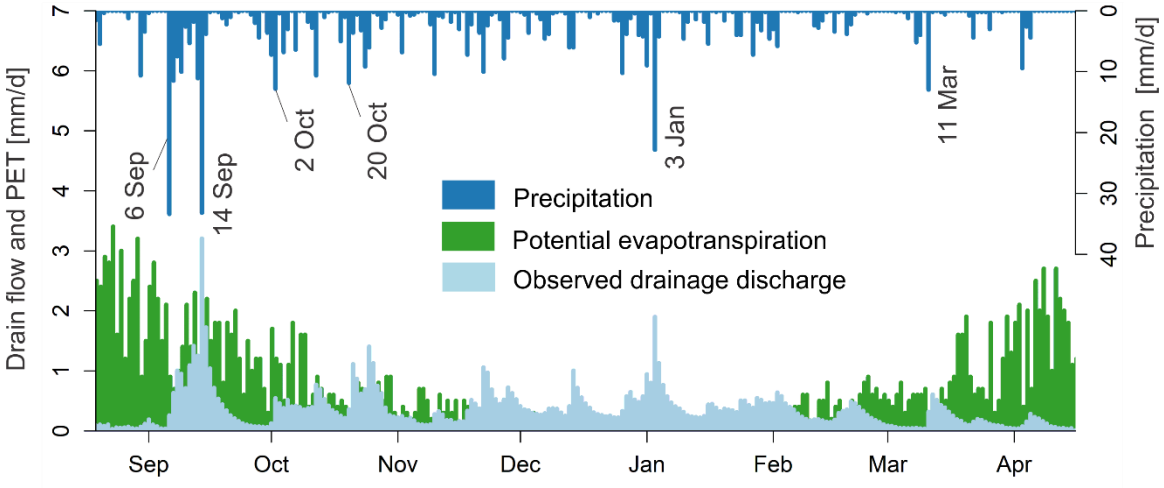

Figure 5.2 – Measured precipitation, calculated potential evapotranspiration (PET), and observed drain discharge at the drain outlet during the monitoring period from 19 August 2017 to 16 April 2018

5.2.3 Bromide tracer application and monitoring

Bromide (Br) tracer field experiments were carried out at the study site as part of the study by Varvaris et al. (2021b). The Br tracer was applied on 23 August 2017 using a tractor- mounted sprayer and the Br concentration at the drain outlet was monitored from 19 August 2017 to 1 January 2019. The Br tracer was evenly applied over 3.2 ha of the 3.8-ha tile drainage system area that contributes to the monitored outlet station (Figure 5.1c). A total of 60 kg of Br/ha was dissolved in 300 L/ha of water, corresponding to a total of 187 kg (and a solution concentration of 200 g/L) that was applied to the agricultural area after the harvest period and before plowing. For Br analysis, drainage water samples were collected by an automated sampler (ISCO 3700 Portable Sampler) located a few centimeters into the tile drain outlet to

ensure that flowing drainage water was sampled, as described in Varvaris et al. (2021b). By 16 April 2018, a cumulative amount of 140 kg of Br had been collected at the outlet, representing 75% of the total Br applied. The remaining 47 kg were likely stored in the soil or transported out of the tile drainage area through runoff or groundwater, given that Br exhibits little sorption and degradation.

5.3 Model application

The hydrological models were set up using the coupled surface–subsurface model HydroGeoSphere (HGS; Aquanty Inc., 2017; Therrien et al., 2010) for transient 3D variably-saturated flow and bromide transport. The simulations were run for the 1 January 2017 to 16 April 2018 period. The time between 1 January 2017 to 1 August 2017 was used as a spin-up period for the model and the 1 August 2017 to 16 April 2018 period was used for model calibration.

5.3.1 Numerical model

HydroGeoSphere is a 3D numerical model that simulates coupled variably-saturated groundwater flow and overland flow, as well as solute transport in the subsurface and surface domains. Variably saturated flow in the subsurface is described by Richards' equation and surface flow is described by the diffusion wave approximation of the Saint-Venant Equations. Interception and actual evapotranspiration (AET) are simulated as mechanistic processes as described in Panday and Huyakorn (2004). Relative permeability and the relationship between saturation and pressure heads in the porous media can be described by the van Genuchten relationships (van Genuchten, 1980) and are entered in tabular form in the HydroGeoSphere model. Three-dimensional solute transport in variably-saturated porous media is described by the advection-dispersion equation. Therrien et al. (2010) and Aquanty Inc. (2017) provides a comprehensive description of the governing equations and their implementation in HGS.

5.3.2 Numerical discretization

A 2D triangular mesh was generated with the AlgoMesh software (Merrick and Merrick, 2015) to discretize the surface domain. Surface topography was represented by interpolating a 1.6-m resolution digital elevation model onto the surface mesh. Mesh lines were defined along drains and mesh nodes were set at the location of the piezometers. A minimum internal angle of 20° and a maximum edge length of 20 m were applied for the triangular elements during mesh generation. In areas with steep slopes and tile drains, we constrained the mesh cell length to less than 7 m and 10 m, respectively, to ensure accurate simulations of surface runoff and surface water–groundwater interactions. The final 2D mesh contained 2247 nodes and 4378 triangular elements.

5.3.3 Surface domain

The entire surface domain was parameterized with winter wheat properties, provided in Boico et al. (2022b). The rill storage height (H_R) and obstruction storage height (H_O) were applied in HGS to implicitly represent the micro-topography of the soil surface. The value for H_R was manually calibrated to 0.02 m, consistent with the values specified for hillslopes by Ala-Aho et al. (2017). The coupling length (L_C) represents the thickness of the interface between the surface and the subsurface domains. Values for HO and LC were set to 0.03 m and 0.001 m, respectively. The Manning coefficient was manually calibrated to 0.06 s/m1/3, which is within the range of values reported in Li and Zhang (2001). Snowmelt and accumulation were not included in the models due to mild winter conditions with average temperatures above freezing (Danish Meteorological Institute, DMI).

5.3.4 Subsurface domain

The soil horizons covered the entire study area, from the surface to a depth of 3.0 m. Depths for the Ap, E, Btg1, Btg2 and C horizons were defined as being from 0 to 0.25 m, 0.25 to 0.55 m, 0.55 to 0.90 m, 0.90 to 1.20 m and 1.20 to 3.00 m, respectively. The base of the model domain is at a depth of 3 m, at the point where the soil layers come into contact with Quaternary glacial clay, as indicated by De Schepper et al. (2017). The 3D subsurface mesh was generated by superimposing the 2D surface triangular mesh from the ground surface to a depth of 3 m. The soil formations were discretized using 14 finite element layers of 3D triangular prisms with a refined thickness of 0.1 m around the tile drain elevations (Figure 5.3).

We initially assigned the hydraulic properties defined by Varvaris et al. (2021b) to the soil horizons and proceeded with the model calibration as described in section 5.3.9. The initial and calibrated parameters of the soil units are presented in Table 5.1. Horizontal and vertical transverse dispersivities have the same value and are referred to as transverse dispersivity in Table 5.1.

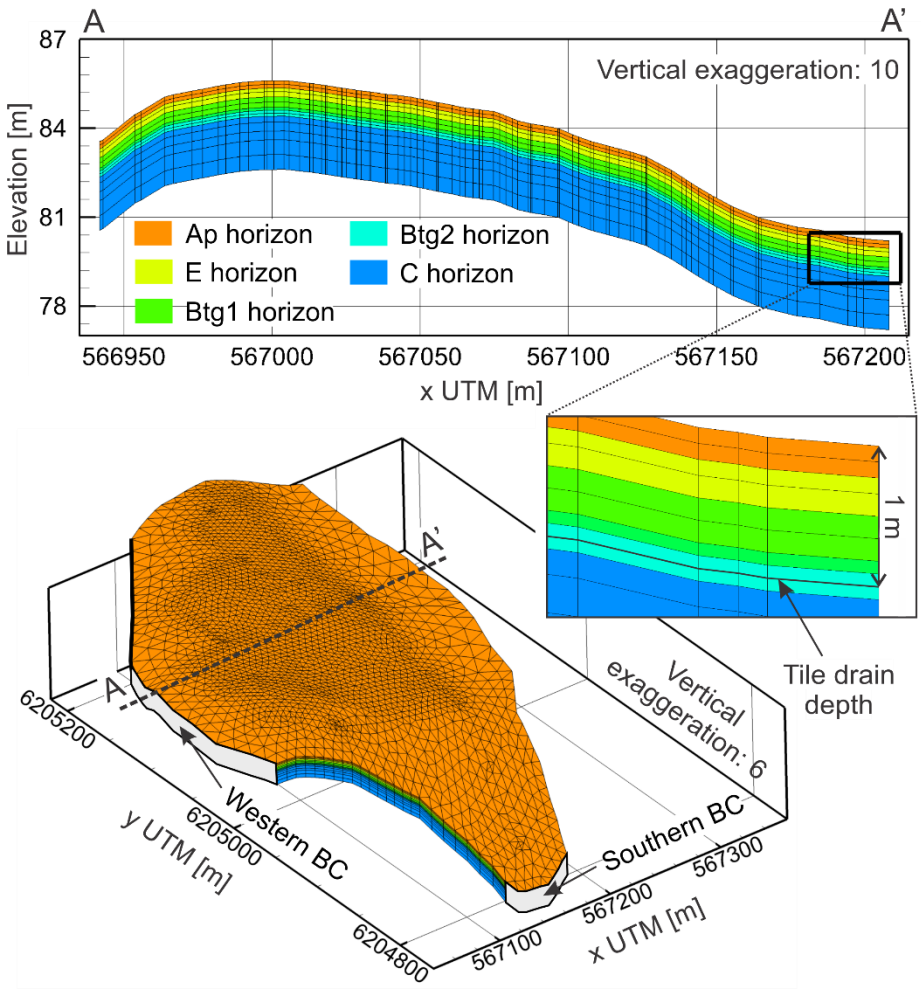

Figure 5.3 – View of the three-dimensional mesh and location of the 3rd type flow boundary conditions (BC) in the western (inflow) and southern (outflow) parts of the study site. The vertical cross-section A-A' shows the soil horizons extending from the surface to a depth of 3 m. A close-up shows the Ap, E, Btg1 and Btg2 soil horizons and the tile drain depth.

Table 5.1 – Initial and calibrated values of the hydraulic properties of the soil horizons (0 to 300 cm depth)

Parameter	Ap horizon	E horizon	Btg1 horizon	Btg2 horizon	C horizon
Depth from ground surface [cm]	0 - 25	25 - 50	50 -90	90 - 130	130 - 300
Initial values taken from the literature					
Horizontal hydraulic conductivity, Kx [m/s]	4.1E-4	1.3E-4	8.9E-5	6.9E-6	8.9E-8
Horizontal hydraulic conductivity, Ky [m/s]	4.1E-4	1.3E-4	8.9E-5	6.9E-6	8.9E-8
Vertical hydraulic conductivity, Kz [m/s]	4.1E-4	1.3E-4	8.9E-5	6.9E-6	8.9E-9
Immobile/mobile water content θim [m]/ θm [m]	0.18/0.24	0.18/0.18	0.21/0.16	0.21/0.17	0.21/0.17
Longitudinal/transverse dispersivity, λL [m]/λT [m]	0.2/0.02	0.2/0.02	0.2/0.02	0.2/0.02	0.2/0.02
Mass transfer coefficient α [1/s]	9.7E-6	5.6E-6	2.8E-6	2.8E-6	2.8E-6
Van Genuchten, α* [1/m]	2.40	2.10	1.59	1.12	1.12
Van Genuchten, n [-]	1.84	1.61	0.32	0.025	0.025
Calibrated values					
Horizontal hydraulic conductivity, Kx [m/s]	2.4E-5	7.7E-5	5.8E-6	8.3E-7	3.0E-7
Horizontal hydraulic conductivity, Ky [m/s]	4.9E-6	1.1E-6	1.7E-6	1.7E-6	8.9E-7
Vertical hydraulic conductivity, Kz [m/s]	7.6E-5	8.0E-4	2.0E-5	8.7E-6	1.6E-8
Immobile/mobile water content θim [m]/ θm [m]	0.36/0.06	0.26/0.10	0.27/0.10	0.30/0.08	0/0.42
Longitudinal/transverse dispersivity, λL [m]/λT [m]	0.05/0.005	0.05/0.005	0.05/0.005	0.05/0.005	0.05/0.005
Mass transfer coefficient α [1/s]	1.0E-10	1.0E-10	1.0E-10	1.0E-10	-

Data sources for the initial values: Ap, E, Btg1 and Btg2 horizon hydraulic conductivity, mobile and immobile water content, dispersivity, mass transfer coefficient and van Genuchten parameters are calibrated effective parameters for the matrix taken from Varvaris et al. (2021a,b). C horizon hydraulic conductivity derived from He et al. (2015) and water content and dispersivity are equal to those of the Btg2 horizon.

5.3.5 Anisotropy

Many studies in clayey till agricultural soils have detected the anisotropy of saturated hydraulic conductivity due to biological macropores and compaction from tillage (Frey et al., 2016, Nilsson et al., 2001, Petersen et al., 2008). On average, hydraulic conductivity may vary up to 3 orders of magnitude after tillage, particularly in the top 40 cm of soil (Petersen et al., 2008) where the Ap and E horizons were defined in our model. Petersen et al. (2008) investigated soil samples of glacial till soils in Denmark and revealed that both horizontal and vertical hydraulic conductivity decreased over time after tillage. However, these changes were not uniform and resulted in relatively higher permeability in the vertical direction. One possible explanation is the development of desiccation cracks and root channels during soil settlement, which are predominately vertically oriented (Dörner and Horn, 2006). In our study site, hydraulic conductivity along the y axis (K_y, north-south) may be lower than that along the x axis (K_x, east-west) due to tractors running east-west. The downslope redistribution of finer sediments can also contribute to soil anisotropy (Kokulan et al., 2018). The calibrated parameters conformed with the expected anisotropy patterns in our study site, with lower hydraulic conductivities in the north-south direction in the first 90 cm below the ground surface (Table 5.1).

5.3.6 Flow boundary conditions

For the transient flow simulation, daily precipitation and potential evapotranspiration fluxes were assigned to the upper boundary of the model, which corresponds to the ground surface. A critical depth boundary condition was assigned to the surface nodes located at the model boundaries to allow surface water to leave the domain as overland flow.

The lateral boundaries were extended to allow a buffer distance of 10 to 65 m outside the boundaries of the drainage area (Figure 5.1c). The model boundary was based on elevation contours to conform with the water divide wherever possible. Adding this buffer area was necessary to avoid numerical convergence issues that may arise from the imprecise boundaries that were based only on the tile drainage system (Figure 5.1c).

Variable hydraulic heads at the lateral subsurface boundaries of the study site were initially set to be equal to the heads from a larger scale transient model for the Fensholt catchment (Boico et al., 2022a), since the study site is not delineated by the water divide and does not have symmetric boundary conditions. However, the larger catchment-scale model does not as refined around the study area and was unable to reproduce lateral flow conditions for our model. Therefore, a variable flux based on a fixed hydraulic head located away from the study site (3rd type boundary condition or general head boundary) was defined in the western and southern lateral parts of the subsurface domain (Figure 5.3) to represent regional inflow and outflow, respectively.

We tested the inclusion of geological layers at depths from 3 to 20 m, as defined by Boico et al. (2022a) and De Schepper et al. (2017). However, they had a negligible effect on the simulated heads at the piezometers and tile drain discharge and were thus not retained. Instead, we added a downward flux component at the bottom of the domain at a depth of 3 m (Table 5.2) to represent a low flow underneath the glacial clay, which was not simulated by the shallow subsurface domain. A similar outflow component was also included at the bottom of previous hydrological models developed for the same area (Vavaris et al., 2021a, 2021b, De Schepper et al., 2017, Boico et al., 2022a).

Table 5.2 - Initial and calibrated values for the boundary conditions

Boundary conditions	Parameter	Initial value	Calibrated value
Western lateral flow 3rd type BC	Hydraulic conductivity, Ksw [m/s]	1E-05	2E-6
	Fixed hydraulic head, hw [m]	91.0	
	Distance from the field, dw [m]	200	
Southern lateral flow 3rd type BC	Hydraulic conductivity, Kss [m/s]	5E-05	6E-5
	Fixed hydraulic head, hs [m]	58.5	
	Distance from the field, ds [m]	100	
Bottom flow	Fixed flux [m/s]	-7E-08	-1E-07
Tile drains (seepage nodes)	Equivalent conductance [m²/s]	1E-05	4E-06
	Depth [m]	1.0	

Initial bottom flux from De Schepper et al. (2017)

All tile drain paths in the drainage area were explicitly represented in the model as seepage nodes set to the elevation of the drain node (see Figure 5.1c). The seepage nodes function as a specified hydraulic head (1st type boundary condition) in saturated conditions, when the water table is above the drain nodes. It is inactivated in unsaturated conditions. For a given seepage node i, the drain flow rate is given by:

$$Q_i = C(h_i - h_d) \qquad h_i > \mathrm{h_d} \tag{5.1}$$

$$Q_i = 0 \qquad h_i \leq \mathrm{h_d} \tag{5.2}$$

where C is an equivalent conductance [$L^2\,T^{-1}$] for the seepage node (Table 5.2), h_i [L] is the hydraulic head at the node and h_d [L] is the elevation of the drain.

5.3.7 Solute transport modeling

To simulate the tracer test, the Br tracer was applied to the top layer of the porous medium by specifying a 3rd type boundary condition for transport, where the inflowing water is assigned a specified Br concentration. To reproduce the approximate conditions for the application of the 187 kg of Br tracer in the field, a specified fluid flux of 1.7E-9 m/s was assigned to the application area (Figure 5.1c). The Br was applied for a period of 5 h on 23 August 2017 with a Br solute concentration of 200 g/L (section 5.2.3). The initial concentration of Br was zero everywhere in the domain and there were no other sources of Br. We assumed Br transport in the model to be conservative, with negligible adsorption and desorption and no decay.

Macropores create preferential flow paths for water and nutrients, especially during dry periods (Kazemi et al., 2008). They also play a dominant role in solute transport processes in loamy structured, tile-drained fields (Varvaris et al., 2021b). To account for the influence of macropores, total porosity was divided into mobile and immobile fractions, corresponding to the single porosity with immobile zone conceptual model as defined in HYDRUS-2D (S□imu□nek et al., 2008; 2016). This conceptualization ensures

physical nonequilibrium solute transport while maintaining uniform water flow. Transport between the mobile and immobile domains was simulated with a first-order reaction (Sudicky, 1990). It is therefore assumed that there is no flow in the immobile domain. The solute mass balance for that domain is given by:

$$\frac{\partial(\theta_{Imm} C_{Imm})}{\partial t} = \alpha_{Imm}(C_m - C_{Imm}) \tag{5.3}$$

where C_{Imm} [M L^{-3}] is the solute concentration in the immobile zone, θ_{Imm} [-] is the porosity of the immobile zone, C_m [M L^{-3}] is the solute concentration in the mobile zone, and α_{Imm} [T^{-1}] is a first-order mass transfer coefficient between the mobile and immobile zones.

5.3.8 Simulation strategy and performance metrics

The simulations target an eight-month period from August 2017 to April 2018, for which data for hydraulic head measurements in three piezometers, drain discharge, and Br concentrations at the drain outlet are available. A prior model spin-up is recommended for coupled surface and subsurface hydrologic models (Ajami et al., 2014). For our spin-up process, we simulated an eight-month period from January to August 2017, using daily precipitation data. The simulated hydraulic heads and surface water depths at the end of the spin-up period were then used as the initial values for the simulation period that started on 1 August 2017. Time steps were limited to a maximum of 1 hour with a maximum saturation variation of 0.02 between successive time steps to ensure numerical stability. The mesh was refined around the tile drains to reduce excessive numerical dispersion. However, the cell dimensions were larger in some areas to reduce computational times.

The model performance was assessed by the mean absolute error (MAE), the root mean square error (RMSE) and the Nash-Sutcliffe efficiency (NSE; Nash and Sutcliffe, 1970). The water and solute mass balance errors were also monitored.

5.3.9 Model parameterization and calibration

The goal of this modeling study was to gain a better understanding of the processes that control the movement of the Br tracer in a tile-drained fields using the mobile and immobile water content concept. By explicitly representing tile drain locations, it also aimed to understand the influence of tile drains on the observed hydrological and solute transport processes. Automated model calibration was conducted using PEST (Doherty, 1994, 2018), a model-independent program often used in parameter estimations and uncertainty analyses for hydrological numerical models (Burrows and Doherty, 2015; Munz et al., 2017; Nogueira et al., 2021; Nolan et al., 2015; Wang et al., 2020). PEST reduces discrepancies between model outputs and field-observed values by iteratively adjusting model parameters in order to minimize

a weighted multivariate objective function. During calibration, different weights were applied to each set of observations (heads, drain discharge and Br concentration) in order to ensure equal contributions to the objective function regardless of the number of measurements available. In this study, the model was calibrated in two steps. First, parameters of the flow model were calibrated to hydrological observations. Then, both the flow and transport models were simultaneously calibrated to hydrological and Br concentration observations.

The hydrological parameters were first calibrated against hydraulic heads in the piezometers and water discharge at the outlet of the tile drainage system. The initial parameters were taken from Varvaris et al. (2021b) and thereafter used for automated calibration for an eight-month period starting in August 2017 (when the Br tracer was applied in the field). This step was taken to improve the goodness of fit for the hydraulic heads and drain discharge. Then, we added solute transport parameters into the simulation for the same period, for further calibration. We did not use the previously calibrated hydrological parameters since the results from the initial model were still not reasonable for the tracer test period. Thus, in this second step, values of hydraulic conductivity, mobile and immobile water content, dispersivity and mass transfer coefficient were calibrated against all observation types (hydraulic heads, drain discharge and Br mass). By doing this, we could also assess the effects of additional unconventional observations on overall results, such as solute concentrations. Assimilating solute concentrations was found to improve the simulations of a stochastic inverse model (Xu and Gómez-Hernández, 2016). In a review study, Schilling et al. (2019) found that the inclusion of observations of concentration in the calibration of integrated surface water and groundwater numerical models substantially improved model parameterization. However, Haws et al. (2005) found that additional concentration data did not improve the modeling results. The failure of their simulations was attributable to factors such as non-unique parameters and problems with representing heterogeneity.

5.3.10 Sensitivity analysis and correlation

We calculated the composite-scaled sensitivity and the parameter correlation coefficients of both the model parameters and the observations. The composite-scaled sensitivities were calculated using PEST, for overall observations and also separately for the Br mass, drain discharge, and the hydraulic heads of piezometers P13, P16, P17 and P31. The sensitivity analysis was performed for the whole simulation period. Each parameter was varied by 10% in successive simulations, while fixed values were maintained for the other parameters to compute the Jacobian matrix in PEST.

5.4 Results and discussion

5.4.1 Sensitivity analysis and correlation

Sensitivities indicate the relevance of observations compared to the estimated parameter values (Hill and Tiedeman, 2007). Overall, the sensitivity analysis indicated that simulations were highly sensitive to the conductance of the drains (C, Figure 5.4). Drain Br masses were also relatively sensitive to the mobile porosity in the Ap horizon, suggesting that velocities in the topsoil layer influence the Br mass transport simulations. The drain discharge was equally sensitive to the rill storage and the Kx of the E horizon. Rill storage may influence the infiltration rates, and consequently, the generation of drain discharge. Hydraulic heads in P7 were also sensitive to KxE, rill_s and C, as well as the specific storage of the C horizon and the Ky of the C horizon. Hydraulic heads in P17 were highly sensitive to the bottom flux boundary condition. The higher sensitivities for P17 can be explained by its location at the boundary of the model where the water table depth varies considerably.

The simulated hydraulic heads at P13, P16 and P31 were only slightly sensitive to most of the model parameters, indicating that those observations alone do not contain enough information to support satisfactory parameter estimation. On the other hand, the simulated drain discharge was highly sensitive to most parameters and therefore observed drain discharge probably better informs model calibration.

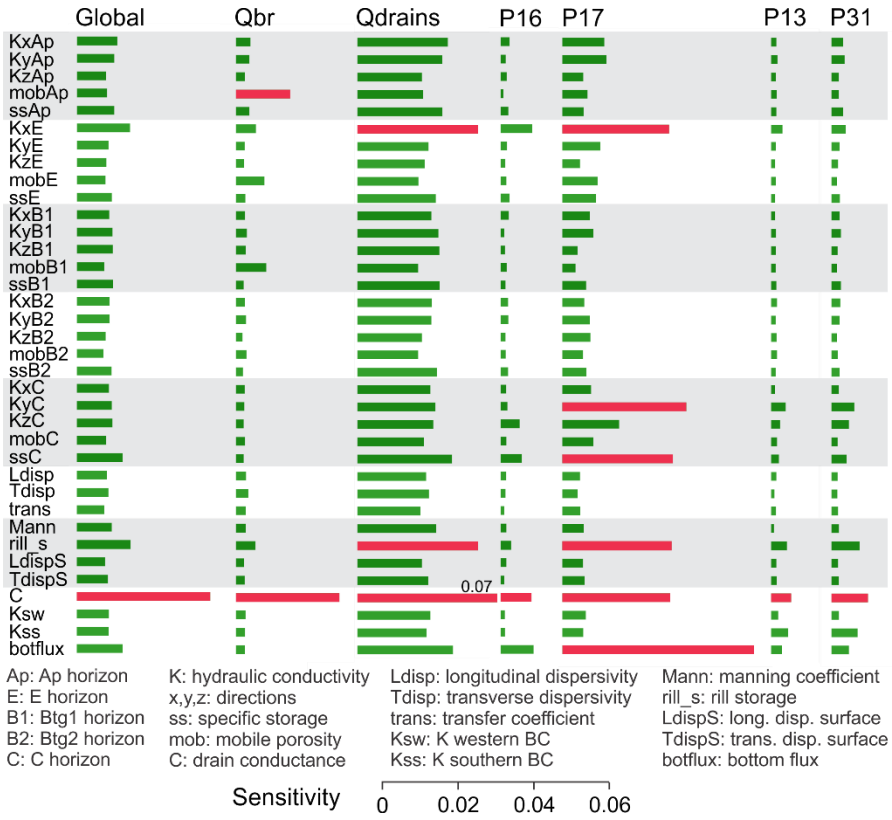

Figure 5.4 – Composite-scaled sensitivities. Sensitivities were calculated with PEST, for all observations globally (Global) and separately for the Br mass discharge (Qbr), drain discharge (Qdrains), and the hydraulic heads of piezometers P13, P16, P17 and P31. Parameters discussed in the text are highlighted in red.

The parameter correlation coefficients of the calibrated model were generally low (Figure 5.5). The most highly correlated parameters were the horizontal hydraulic conductivities of the Ap and E horizons (KxAp and KxE), the longitudinal and transverse dispersivities (Ldisp and Tdisp), the mobile porosity of the Btg1 horizon and the vertical hydraulic conductivity of the Btg2 horizon (mobB1 and KzB2), the horizontal hydraulic conductivity and the specific storage of the Ap horizon (KyAp and ssAp), and the horizontal hydraulic conductivity of the E horizon and the bottom flux (KxE and botflux). High sensitivities combined with low correlations suggest good identifiability of the model parameters, which in turn indicates robust model parameterization (Doherty and Hunt, 2009; Hill et al., 2016).

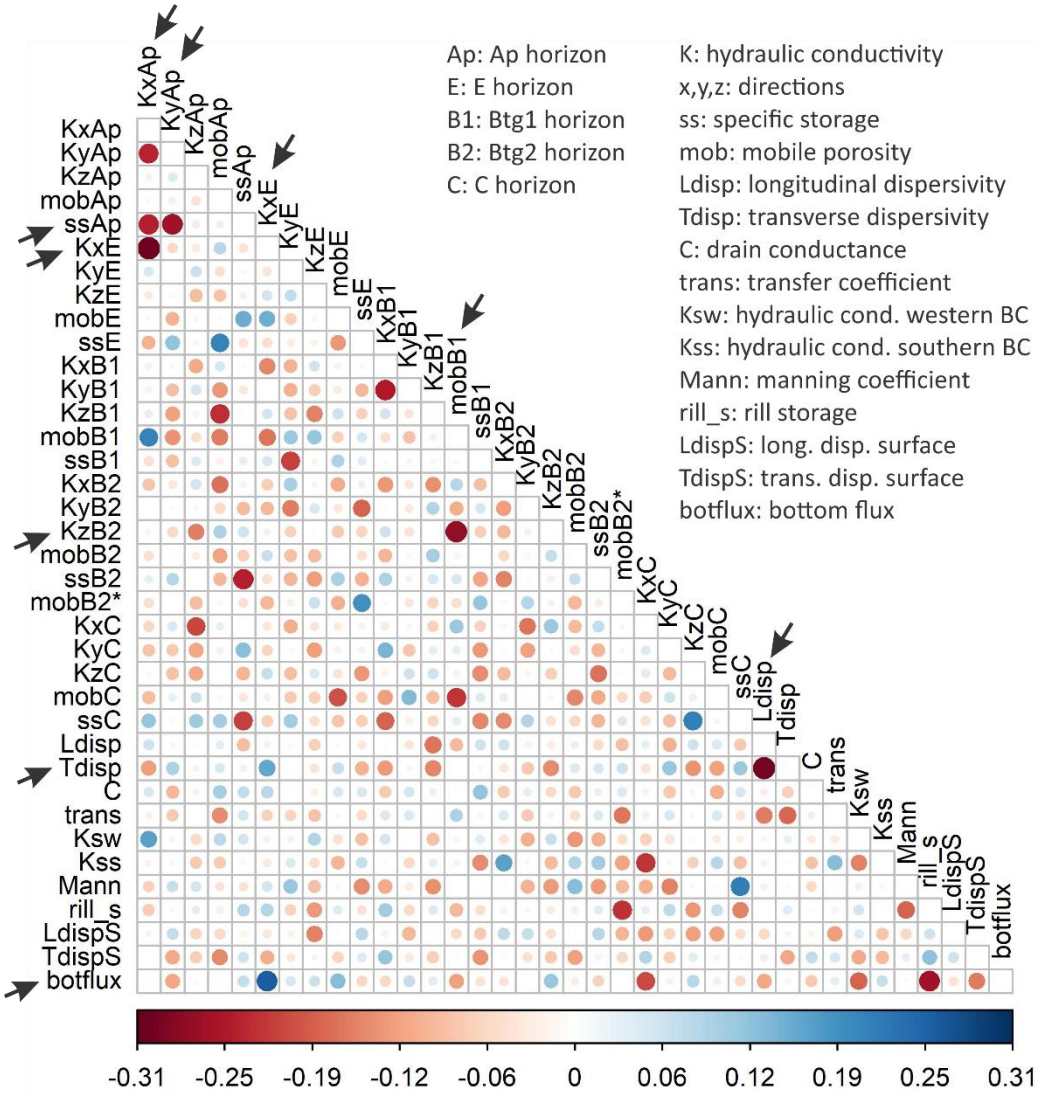

Figure 5.5 - Parameter correlation coefficients. The most highly correlated parameters are indicated by arrows.

5.4.2 Water balance

Expressed in equivalent heights for the study site, Table 5.3 shows total volumes of the water input (rainfall and lateral inflow at the western boundary), output (tile drain discharge, runoff, actual evapotranspiration, lateral outflow at the southern boundary, bottom outflow) and storage variation during the simulation period. The storage variation was negative and is indicated in the output in Table 5.3. The simulated drain discharge for the area was 101 mm, while the measured drain discharge for the same period is 90 mm. The combined equivalent height of surface runoff (197 mm), AET (135 mm) and drain discharge from the drainage area (101 mm) represent 70% of the cumulated rainfall (594 mm).

Table 5.3 – Simulated water balance components for the eight-month tracer test period. Rainfall represents total precipitation, AET is actual evapotranspiration, and ΔStorage is the change in water stored at the study site. Lateral inflow and outflow were included as 3rd type boundary conditions.

Water balance component	Equivalent height [mm]	Percentage of total input
Input		
Rainfall	594	
Lateral inflow (Western BC)	20	
Output		
Drainage system*	101	16
Drains outside drainage system	60	10
Overland	197	32
AET	135	22
Lateral outflow (Southern BC)	38	6
Bottom outflow	65	11
ΔStorage	18	3

*Observed = 90 mm (15% of total input)

5.4.3 Drain discharge and flow peaks simulation

The simulated and observed drain discharge results are presented in Figure 5.6. The MAE and NSE are 0.18 mm/d and 0.40, respectively. Compared to the NSE of 0.75 from a 3D model by Boico et al. (2022b) that simulated tile drainage in a field within the same catchment, our simulated drain discharge performed more poorly. The tile-drained system modeled by Boico et al. (2022b) contains fewer and more widely spaced tile drains compared to our study. The NSE from our study is comparable to the NSE calculated for the tile drainage simulations from Nousiainen et al. (2015), which were 0.52 in 2010 and 0.37 in 2011. The NSE from our study is also comparable to that of the catchment-scale modeling studies from Boico et al. (2022a), which was approximately 0.31 for the same drainage area. Our NSE value is better than the study by Hansen et al. (2013) where the NSE varied from negative values to 0.15 for different drainage areas.

We expected intense rainfall events (Figure 5.2) to produce large values for tile drain discharge in the simulations. This was modeled by Williams et al. (2016), where storm water bypassed the soil matrix and was rapidly transported to tile drains. However, our simulations underestimated the highest drain discharge peak on 14 September 2017 and the second highest peak on 3 January 2018 (Figure 5.6). In contrast, the drain discharge was overestimated at the beginning of October and November 2017 and after the second highest discharge peak in January 2018. The drain discharge is highly sensitive to the tile drain conductance, as shown by the composite-scaled sensitivities (Figure 5.4). The calibration process decreased the value for drain conductance and its lower value is likely responsible for the underestimated peaks in Sepfigurtember 2017 and January 2018. Greater conductance, however, resulted in an

overestimation of the total drain discharge and poorer model performance. Another undesired effect of reducing the drain conductance was the generation of more flooding conditions in the winter (see section 5.4.5). The misrepresentation of high flow peaks indicates that the conceptual model is not able to represent preferential flow paths that rapidly deliver water to tile drains following the most intense rainfall events.

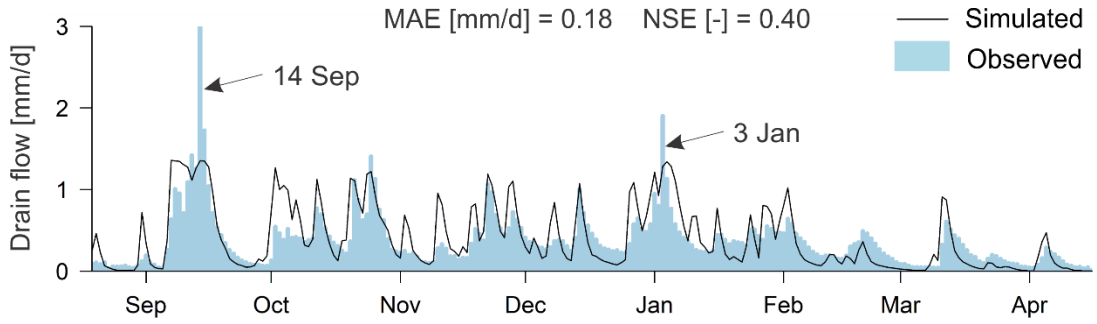

Figure 5.6 - Observed and simulated drain discharge at the outlet from August 2017 to April 2018. MAE: Mean absolute error, NSE: Nash Sutcliffe efficiency.

5.4.4 Hydraulic heads

The hydraulic heads measured in piezometer P16 remained nearly static around the depth of the tile drains (at 1 m below the ground surface) from October 2017 throughout the rest of the measurement period (Figure 5.7a). In the preceding periods in August and September 2017, the piezometer was dry during measurements, indicating that the hydraulic head was below 84 m. Simulated hydraulic heads varied between 84 m or below (completely dry piezometer) and 85.5 m (around 50 cm below ground surface). Although few measurements are available for comparison, the results show that the model was unable to simulate the relatively stable hydraulic head conditions, especially from October 2017 to the end of the simulation period. During the first few months of the simulation, the model overestimated hydraulic heads in piezometer P17 (Figure 5.7b), located at the northern boundary of the study site, outside the drainage area. One possible reason for the overestimation is the inaccurate representation of the heterogeneity in the vicinity of the piezometer where the screens were installed (from the ground surface to a depth of 2 m), as observed by Boico et al. (2022b). The model, however, simulated a good match with the observed hydraulic heads from December 2017 to the end of the simulation period. The MAE for the simulated hydraulic heads in piezometer P13 (0.43 m) was better than for P16 (0.62 m) and P17 (0.61 m). Finally, in piezometer P31 located near the outlet of the drainage system, hydraulic heads were well simulated with an MAE equal to 0.30 m, despite slight underestimations. Based on these results, we conclude that the simulated shallow hydraulic heads were better in the lower part of the field. We attribute the discrepancy between simulated and observed heads in the upper part (P16 and P17) to

limitations in the conceptual model (see section 5.4.7). Moreover, the lack of high-frequency hydraulic head data does not allow for further conclusions about the performance of the model at the temporal scale in our study. Such data could enhance model performance and parameterization if they were available.

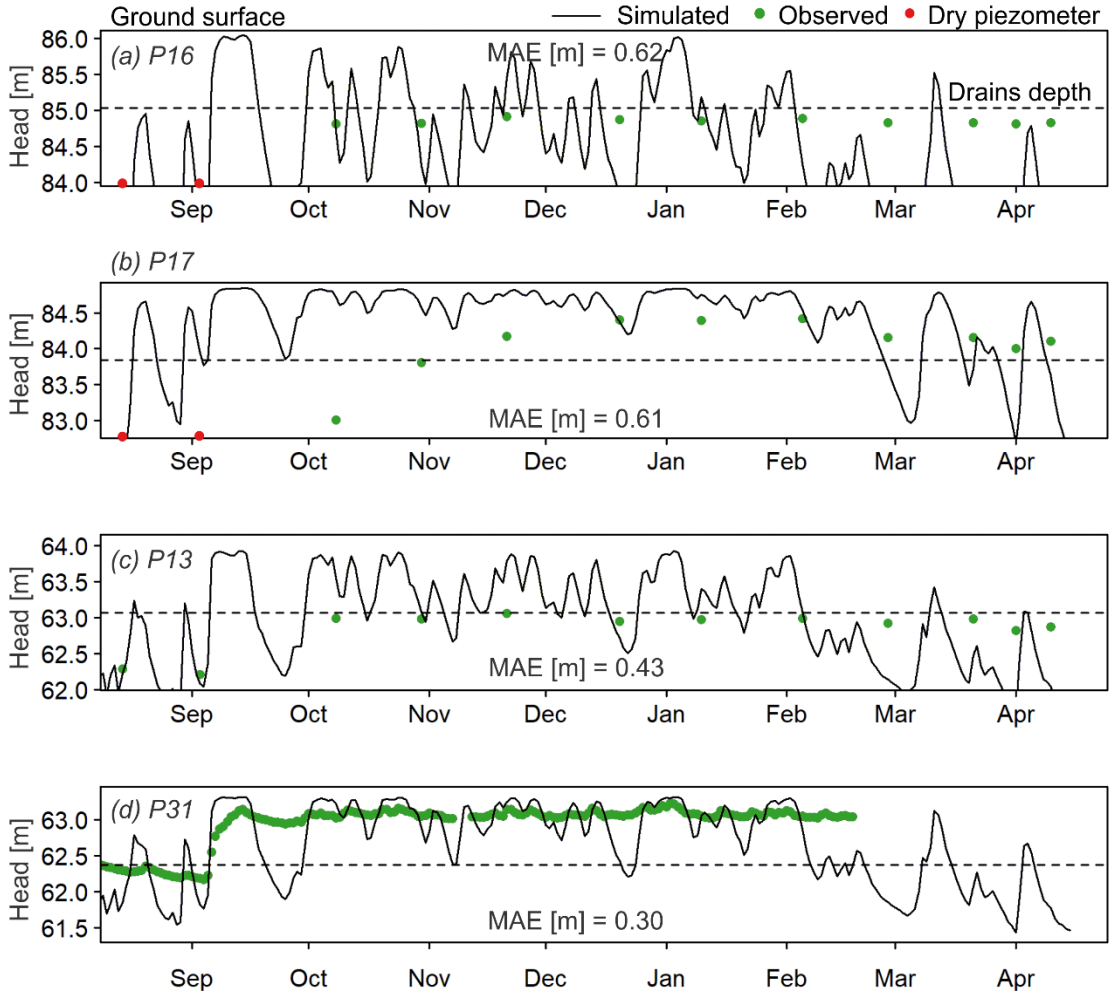

Figure 5.7 - Observed and simulated hydraulic heads in piezometers a) P16, b) P17, c) P13 and d) P31 during the monitoring period from 19 August 2017 to 16 April 2018. The ground surface coincides with the top of each plot. The location of the tile drains, estimated to be at a depth of 1 m below ground surface, is indicated by the dashed lines. The first day of each month is labeled in the horizontal axis. MAE: mean absolute error.

5.4.5 Surface water

The model simulated realistic surface water flow patterns during most of the simulation period, without the tile-drained field getting submerged by ponding water. However, after high-intensity rainfall (e.g., on 6 and 14 September, 2 and 20 October, 3 January and 11 March; Figure 5.2) the subsurface became almost fully saturated, which generated surface water flow in most parts of the study site. Figure 5.8 shows the simulated surface water depths at five days before the rainfall event on 2 October (13 mm)

and at one and five days after the event. Most of the surface water flows out through the eastern and southern boundaries of the model, as indicated by velocity vectors in Figures 5.8b and c. The southern and eastern parts of the model showed higher surface water depths after the rainfall event. The western boundary was relatively wetter than the rest of the domain, representing saturated subsurface conditions due to lateral inflow. Of the total cumulated surface runoff of 197 mm (Table 5.3), only 19 mm flows out of the southern boundary. Figure 5.8b shows that, in the tile drainage area, the surface water depth one day after the rainfall event is generally below 0.02 m. This is lower than the rill storage height and therefore lateral surface flow is prevented from occurring.

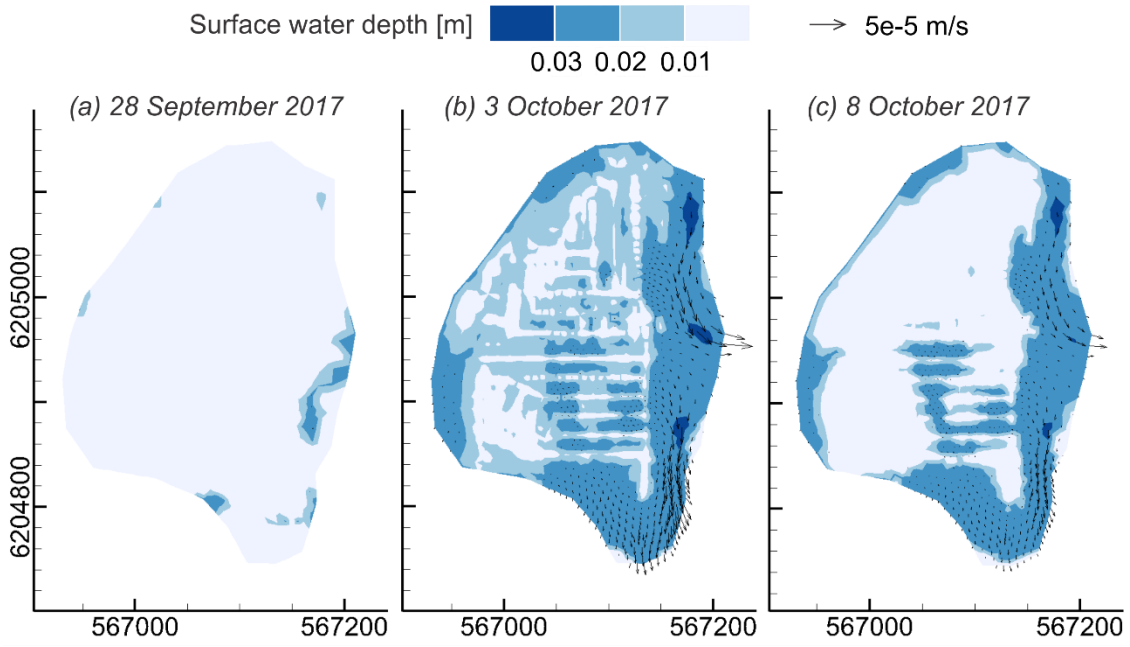

Figure 5.8 – Surface water depths 5 days before, and 1 and 5 days after the rainfall event on 2 October (13 mm). Black arrows indicate the direction of water flow, with larger vectors indicating relatively higher water velocities.

5.4.6 Bromide simulations

During calibration, the hydraulic and transport parameters were adjusted to improve the agreement between the observed and measured daily Br mass at the drain outlet. The mobile porosity of the Ap, Btg1 and Btg2 horizons were reduced from their initial values, leading to an increase in velocities and a decrease in the residence time of Br in the soil. The rill storage height was increased, which in turn increased water accumulation at the surface and reduced Br runoff. Anisotropy (which resulted from the automated calibration) reduced the north-south hydraulic conductivity, which led to higher subsurface saturation and Br storage in the upper part of the study site. The conductivity of the drains, when decreased from initial values, allowed for less Br to be leached from the soil during the first few rainfall

events and more Br leaching later in the simulation. The NSE for the daily Br mass after calibration was 0.36, which is similar to the model performance when simulating drain discharge (0.40).

Our results suggest that when we applied the model with mobile and immobile zones, it was well-suited for the simulation of the rapid Br transport to tile drain that occurred during the first few months. The underestimation of the Br mass peak on 14 September 2017 and the overestimation in early October 2017 (Figure 5.9) are associated with, and likely caused by, discrepancies in the drain discharge simulation (Figure 5.6). However, the model underestimates some of the Br mass peaks and the late-time Br masses from December 2017 to April 2018. During the first 2 months (September and October), the simulated Br mass that was lost to tile drainage was 73 kg, while the measured Br mass lost was 68 kg. For the following months (November to April), the simulated Br mass that was lost to tile drainage was 18 kg while the observed mass lost was around 53 kg. Throughout the whole simulation period, August to April, the simulated Br mass that was lost to tile drainage was 91 kg, which is 48% of the total applied mass. The observed mass loss was 140 kg, corresponding to 74% of the applied mass (Table 5.4). A large fraction of the tracer mass (28%) remained in the soil at the end of the simulation period (mid-April). This mass, stored in the subsurface, may be released into tile drains over time. It seems, however, that this stored amount was overestimated by our model as the amount of Br mass that was lost through tile drains was underestimated. The low values for the dispersivities may have generated excessive numerical dispersion, contributing to a large stored amount of Br. Part of the Br mass that is leaving the model through overland flow, and eventually captured by tile drains outside the drainage area, may also contribute to the underestimation of Br mass at the drain outlet. A better representation of rapid preferential flows in the model would improve the Br mass and storage simulations (see section 5.4.7.3). Furthermore, a more reliable spatial representation of soil structure and hydraulic properties would change subsurface saturation and the generation of surface water flow, possibly increasing the Br mass captured by tile drains.

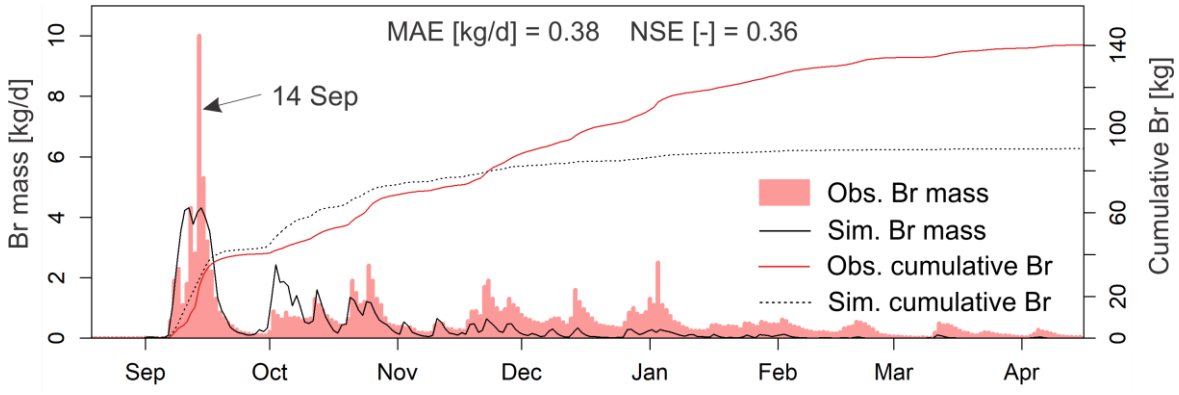

Figure 5.9 - Observed and simulated daily Br mass and the cumulative Br mass at the drain outlet from 19 August 2017 to 16 April 2018. MAE: Mean absolute error, NSE: Nash Sutcliffe efficiency

Table 5.4 - Simulated mass balance components for the eight-month tracer test period. The total input is the total Br applied on the surface. The total output is the Br mass that leaves the model through tile drain discharge from the drainage area, outside the drainage area, overland flow and lateral and bottom boundaries. ΔStorage is the change in bromide mass stored in the model.

Bromide mass component	Total mass [kg]	Percentage of total input
Input		
Application	189.8	
Output		
Drainage system*	90.6	48
Drains outside drainage system	10.1	5
Overland	30.1	16
Lateral and bottom BC	6.1	3
ΔStorage	52.9	28

*Observed = 140.2 kg (74% of total input)

Concentrations of Br at the drain outlet were successfully simulated for the first two months (September and October), but they were underestimated for the remainder of the simulation, until April 2018 (Figure 5.10). Varvaris et al. (2021b) produced similar results, with simulated concentrations being lower than observed ones after the first two months of the tracer test. Varvaris et al. (2021b) stated that one reason Br concentrations were underestimated was because the water and Br solute that bypassed the tile drainage network was overestimated. This water would have left the model through the bottom of the domain, which was at a depth of 1.2 m in their study, and recharged the subjacent aquifer. In our study, the model indicated that of the total applied Br mass, 28% was stored in the upper 3 m of the subsurface, with significant Br mass loss through surface runoff, at 16% (Table 5.4).

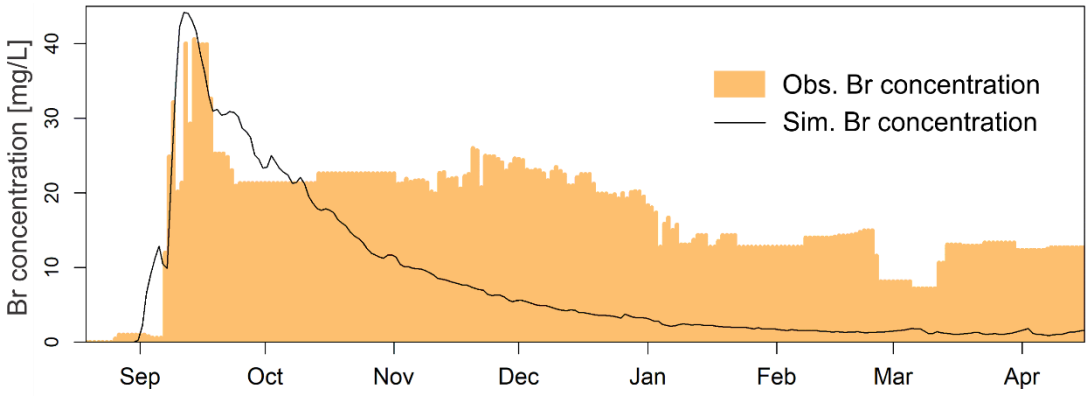

Figure 5.10 - Observed and simulated daily Br concentration at the drain outlet from 19 August 2017 to 16 April 2018.

Figure 5.11 shows the spatial distribution of simulated Br concentrations on the day of application (23 August 2017), two weeks after application (8 September 2017) and on 2 December 2017. On 8 September, two weeks after application, the Br concentration increased near the model boundaries,

especially in the southern part, and it decreased close to the tile drains (Figure 5.11b). After the intense rainfall events on 6 and 14 September, simulation results showed overestimated hydraulic heads (Figure 5.7) and high surface water depths over almost the entire study site. The day after the second rain event, the amount of Br transported out of the study site through surface runoff (4.6 kg) was greater than the amount discharged by tile drains (4.2 kg). Fully saturated conditions that generate surface runoff are unlikely to occur in a tile-drained field, suggesting that the simulation overestimated the amount of Br loss through surface runoff. As expected, in December, three months after the Br application, the Br concentration at the model surface was low (below 1 mg/L, Figure 5.11c) and most of the Br applied on the surface had already infiltrated into the soil or migrated along with surface runoff.

Figures 5.11d, e and f show Br concentrations along an east-west vertical cross-section on the day of application, on 8 September and on 2 December 2017. Higher Br concentrations were initially simulated in the top soil (Ap horizon), with low Br concentrations (<0.1 mg/L) reaching the tile drains. On 8 September, there were higher concentrations of Br between the ground surface and the tile drains (Figure 5.11e). The color contours in the close-up in Figure 5.11e show Br migration towards the drain, with higher Br concentrations converging at the drain nodes. After four months, in December, the highest Br concentrations occur between the tile drains (Figure 5.11f). During the simulation period, the Br concentration in the C horizon near the bottom of the model remains very low (<0.1 mg/L). These low Br concentrations may be caused by the lower hydraulic conductivity and higher mobile porosity values in the C horizon compared to the soils above. The Br concentrations follow a pattern that is plausible for tile-drained soils, with Br migrating towards the tile drains (Figure 5.11b, e and f). This reaffirms that there is good representation of the main Br transport process from soil surface to tile drains when they are explicitly represented in the model domain.

The pattern for simulated daily Br mass was similar to the pattern for drain discharge during the first few months of the simulation. However, unlike drain discharge, Br mass was underestimated from mid-November, when Br concentrations were also underestimated (Figure 5.10).

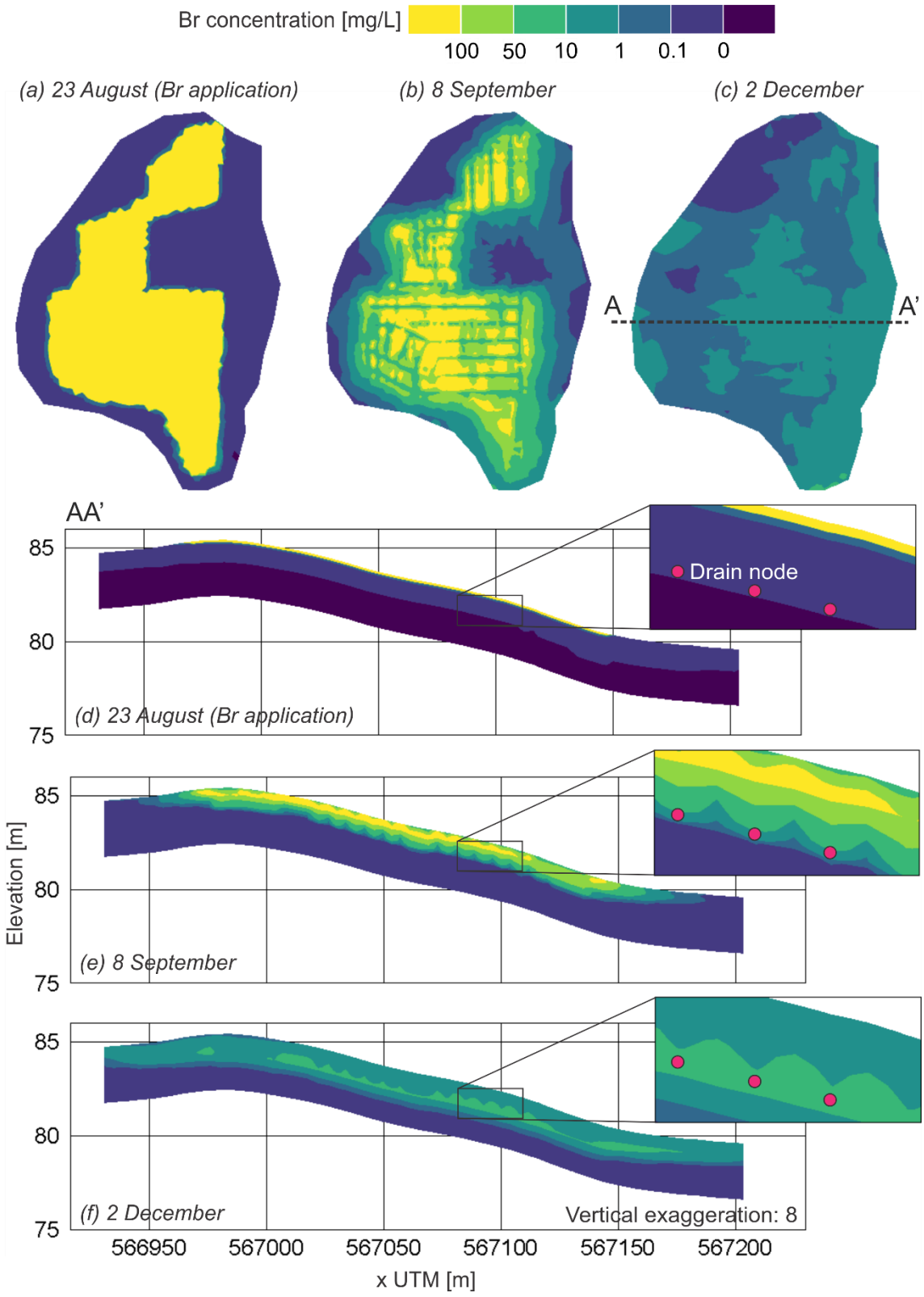

Figure 5.11 – Bromide concentrations at the soil surface and vertical cross-section AA' in the same direction as a tile drain. Insets show details on Br transport to tile drains.

5.4.7 Improvements for and limitations of conceptual model

5.4.7.1 Three-dimensional coupled surface-subsurface model

The Br tracer test for this study area was simulated by Varvaris et al. (2021b) using a 2D variably-saturated subsurface flow model. Their conceptual model had a width of 20 m and a depth of 1.2 m. A constant downward flux was set at the bottom of the domain and the lateral boundaries were impermeable. A seepage node representing the tile drain was set at 1 m below the ground surface. Br concentrations were simulated using five models with different porosity approaches: single porosity, single porosity with immobile zone, dual porosity, dual permeability and dual permeability with immobile zone. All models underestimated the cumulative Br at the tile drain outlet. The highest accuracy was obtained using the single porosity with immobile zone approach, which we adopted in our model. We expanded on the modeling approach from Varvaris et al. (2021b) to more accurately describe the spatial variability of the soil as well as the volume of water and solute masses that bypass the tile-drainage system. We used a 3D coupled surface and subsurface flow and solute transport model to simulate surface runoff and surface–subsurface water and solute exchange. Our study site comprised an area of 7.6 ha that included the outline of the entire tile drainage system and four piezometers to evaluate the performance of the hydraulic head simulation. Lateral inflow and outflow were also simulated. Furthermore, the soil horizons were represented from the ground surface to a depth of 3 m, incorporating an additional 1.8 m compared to the conceptual model developed by Varvaris et al. (2021b). The arrival time of Br was accurately simulated in our model. However, after the first two months, Br concentrations were underestimated resulting in a lower cumulative Br mass than that observed, similar to Varvaris et al (2021b). Improvements in the 3D conceptual model with respect to soil heterogeneity and microporosity, as well as mesh refinement, may be necessary for proper Br transport simulation. These topics are discussed in the following sections.

5.4.7.2 Heterogeneity

Effective porosity, dispersivities and hydraulic conductivities are critical parameters for successful solute transport modeling and are dependent on geological heterogeneity (Konikow et al., 2011). Therefore, the representation of Br concentrations in tile drainage could be improved by a detailed representation of soil heterogeneity in the conceptual model. To account for the spatial variation in hydrological and solute transport parameters, a detailed characterization of the site may be required and implemented in the conceptual model. In our study, we assumed homogeneous soil horizons with a sandy loam texture (Ap, E, Btg1 and Btg2) over the entire subsurface domain of the model. However, clayey soils and peat located near the tile drain system outlet (Petersen et al., 2020, Prinds et al., 2020) can reduce soil permeability when compared to our conceptual model, introducing uncertainty into the Br transport simulation. To

overcome this uncertainty, we recommend the application of geostatistical approaches combined with field data to generate stochastic realizations of more heterogeneous hydrofacies and soil horizons (such as in Fleckenstein et al. (2006) and Labolle and Fogg (2001)). For example, geostatistical software such as T-PROGS could be used to achieve this (Carle, 1999).

5.4.7.3 Macroporosity

The underestimated Br mass that reached the drain outlet from December 2017 to the end of the simulation period may be attributed to an imprecise representation of the immobile zone in the model. The calibrated mass transfer coefficient in our model is low compared to other studies (Bishop et al., 2015; Frey et al., 2016; S imu nek et al., 2003; Varvaris et al., 2021b; Vervloet et al., 2018), resulting in low mass transfer to the immobile domain. Simulations that were attempted with higher mass transfer coefficients, however, increased the Br mass stored in the immobile zone and reduced the amount of Br that leached through tile drains, resulting in a low Br mass being discharged at the outlet. Due to low mass transfer coefficient, the single porosity with immobile zone concept that we defined in our study functions as a single porosity model with low soil porosity. Furthermore, the mobile and immobile porosities were uniformly distributed in the horizontal soil layers throughout the simulation period, which corresponds to a uniform distribution of macropores. We acknowledge the dynamic nature of macropore size distribution and continuity due to soil structure being heavily affected through exposure to temporal variations in climate, biological activity, seasonal root growth and agricultural management, such as tillage (Jarvis et al., 2020; Williams et al., 2016). Due to the inherently dynamic nature of macropores, calibrating a model with a static macropore structure can be challenging and can introduce uncertainties.

Better representation of matrix diffusion and macropore advective transport may be possible using a dual permeability approach (De Schepper et al., 2015). For instance, Frey et al. (2012) have shown that a dual permeability representation of the subsurface is required to simulate nitrate transport in low-permeability macroporous soils. Applying a dual permeability approach, however, increases the number of model parameters and can significantly increase simulation times.

Similar to soil hydraulic properties, the way that macropores are arranged in the field may vary within the hillslope, changing the residence time of the water in the system. For instance, in a physically-based modeling study, a larger density of macropores at the foot of a hillslope relative to the respective density upslope resulted in overall longer residence times. A larger density of macropores upslope had the opposite effect (Klaus and Zehe, 2011). Future studies should account for the spatial variation of macropore density in the field.

5.4.7.4 Mesh refinement in sloping terrains

The southern part of the study site has a steep slope with a grade that reaches 23%. Sloping terrains may produce fast overland flow and subsurface lateral flow (Tang et al., 2012). Vertical infiltration may decrease as the slope increases, especially for sandy loam soils (Morbidelli et al., 2018). The accuracy of simulated hillslope hydrological processes has been shown to improve with refined spatial resolution (Camporese et al., 2019; Sulis et al., 2011). In our study, we used a relatively coarse mesh to reduce computational times, which may have reduced the accuracy of drain discharge and hydraulic head simulations in the southern part of the model.

5.4.7.5 Equifinality

Uncertainties in model structure, scaling, parameter correlation, accuracy of the numerical solution and the scarcity of data leads to inherently non-unique model outcomes. As a result, different model setups might simulate an adequate fit with the observations and honour expert knowledge (Refsgaard et al., 2012, Zhou et al., 2014, Hill et al., 2016, Delottier et al., 2017, Aster et al., 2018). This concept is referred to as equifinality (Beven, 2006, Beven and Freer, 2001). Therefore, several structural model setups may reproduce the observed tile-drain flow equally well. Klaus and Zehe (2011) found considerable equifinality in a 2D model setup when explicitly representing macropores. Other research found similar drain discharge in hydrological models when using different concepts to represent macroporosity (Varvaris et al. 2018, 2021a), different conceptualizations of tile drains (De Schepper et al., 2015) and with a model using either homogeneous or heterogeneous soil layers (Boico et al., 2022b).

Simpler models can be chosen to reduce model equifinality. However, they may be unable to simulate important processes and hydrological interactions in complex systems, which prevents their use for specific applications (Ebel and Loague, 2006). Furthermore, complex hydrological models are useful for concept development, such as process identification and characterization, for complex hillslope or catchment-scale models (Ebel and Loague, 2006). In complex models, equifinality can be reduced by including more measured data in the calibration process. In this study, we included measured data in the model through the lateral boundaries (3rd type) that used average values for hydraulic heads and stream levels, improving the simulation of hydraulic heads. Similarly, the inclusion of non-conventional observations, such as Br concentrations, aids model parameterization by providing extra information during calibration (Schilling et al., 2019; Xu and Gómez-Hernández, 2016). PEST was used to carry out a linear predictive uncertainty reduction and data worth analyses and revealed that adding Br observations decreased the variance in the uncertainty of drain conductance value predictions (a relevant parameter in our simulation; see section 5.4.1 and Figure 4.4). The variance decreased by 30% when using Br

observations, in comparison to 42% from using solely drain discharge observations (data not shown). This reinforces the use of multiple data sets for the parameterization of numerical models to reduce the equifinality problem (Nogueira et al., 2021; Schilling et al., 2019).

The sensitivity and correlation analyses showed that the parameters are weakly correlated, but the sensitivities of some observations are low. This indicates that the model parameters are not well constrained by some observations and that improving the simulations may require more data or a different model structure.

5.4.8 Implications for nutrient transport

Nitrate is one of the most studied agricultural nutrients due to significant nitrate contamination in agricultural catchments (Chae et al., 2004; Kaown et al., 2009; Kim et al., 2009; Lasserre et al., 1999; Molénat and Gascuel-Odoux, 2002; Seidenfaden et al., 2022; Refsgaard et al., 2019). Soil nitrogen models simulate the nitrogen cycle, including nitrogen input, mineralization, nitrification, denitrification, nitrogen uptake, and nitrate leaching (Almasri and Kaluarachchi, 2007). However, these have limitations in simulating the fate of nitrate in the subsurface and must be linked with models that simulate variably saturated groundwater flow and solute transport in porous media (Bonton et al., 2012). As a non-absorbing inert solute, the simulation of a Br tracer is useful to parameterize advective–dispersive transport in hydrological–nitrate transport models. Such parameters can be used, for instance, as the initial values for the calibration of a nutrient transport model. Furthermore, in our study, we were able to capture transport behavior around the location of tile drains at field scale by explicitly representing tile drains using seepage nodes in the numerical model. Such representation allows for the simple implementation of tile drains and fast computational times, presenting an improvement in the modelling of tile-drained agricultural systems.

5.5 Conclusion

We applied relatively simple numerical modeling approaches to simulate preferential flow through both tile drains and macropores using a 3D surface–subsurface physically-based model (HydroGeoSphere). Drain discharge, Br concentration and hydraulic heads were simulated at an acceptable computational cost. This type of model can be used as a learning tool to identify the controlling factors that govern water flow and solute transport in tile-drained fields compared to simple empirical models.

Our simulation results indicated that explicitly representing tile drains with seepage nodes allows for a physically-based, yet computationally-efficient representation of bromide transport behavior around the location of tile drains at field scale. However, we cannot confirm the hypothesis that a single porosity

model with immobile zone is suitable for simulating Br peaks at the drain outlet and late-time Br mass. A better representation of soil heterogeneity and the spatial variation of the macropore density at the scale of the study could improve the hydrological and solute transport simulations. These improvements may require a more robust dual continuum approach, such as a dual permeability model. However, increasing model complexity without including more measured data in the calibration process may prevent a thorough understanding of the hydrological processes in tile-drained systems due to equifinality.

Chapter 6

Comparing alternative conceptual models for tile drains and soil heterogeneity for the simulation of tile drainage in agricultural catchments

Comparaison de modèles conceptuels alternatifs de drains souterrains et d'hétérogénéité du sol pour la simulation du drainage souterrain dans les bassins versants agricoles

V. F. Boico, R. Therrien, N. L. Young
Department of Geology and Geological Engineering, Université Laval. Quebec City, Canada.

A. L. Højberg
Department of water resources, Ramboll. Copenhagen, Denmark.

H. Delottier
Centre for Hydrogeology and Geothermics. Neuchâtel, Switzerland.

Reference:

Boico, V. F., Therrien, R., Delottier, H., Young, N. L., Højberg, A. L. (2022). Comparing alternative conceptual models for tile drains and soil heterogeneity for the simulation of tile drainage in agricultural catchments. Journal of Hydrology, 612(Part A). doi:10.1016/j.jhydrol.2022.128120

Résumé

Les drains souterrains sont des voies d'écoulement importants dans les bassins versants agricoles et doivent être inclus dans les modèles hydrologiques. L'objectif de ce chapitre est d'évaluer différents modèles conceptuels de drains souterrains et d'hétérogénéité du sol pour la simulation numérique de l'écoulement d'eau dans un bassin versant agricole drainé au Danemark. Trois modèles conceptuels ont été développés avec des *seepage nodes* pour représenter les drains et un modèle conceptuel avec une couche de perméabilité élevée pour représenter implicitement les drains. Lorsque l'emplacement des drains souterrains n'est pas connu, l'utilisation des *seepage nodes* pour représenter les drains dans les zones agricoles peut simuler de manière satisfaisante les débits des cours d'eau et des drains à l'échelle du bassin versant. L'écoulement des drains était plus sensible à l'hétérogénéité du sol que la conceptualisation des systèmes de drainage, ce qui suggère que les propriétés spécifiques du sol sont pertinentes pour simuler les débits de drainage.

Abstract

Tile drains are important water flow paths in agricultural catchments and must be included in hydrological models. The goal of this chapter is to assess different conceptual models for tile drains and soil heterogeneity for the numerical simulation of tile drainage in an agricultural catchment in Denmark. Three conceptual models for tile drains were developed using seepage nodes to represent tile drains and one conceptual model implicitly represents tile drains as a high-permeability layer. Whenever the location of tile drains is unavailable, using seepage nodes to represent drains in agricultural areas may satisfactorily simulate catchment-scale stream and drain discharge. Ddrain discharge dynamics were more sensitive to the soil heterogeneity than the tile drainage conceptualization, suggesting that specific soil properties are relevant to simulate drain discharge.

6.1 Introduction

The degree of saturation in fine-textured agricultural soils is often controlled by subsurface drainage systems, consisting of tile drains, to improve root development and crop yield. By controlling the elevation of the water table, tile drains alter both the hydrologic flow pathways in agricultural catchments (Hansen et al., 2013; King et al., 2014; Thomas et al., 2016, Werner et al., 2016) and the rates of nutrient transport from croplands to surface water bodies (Amado et al., 2017; Radcliffe et al., 2015; Rozemeijer et al., 2010b; Stamm et al., 2002). The inclusion of tile drainage in numerical models is therefore necessary for the proper simulation of hydrological processes in highly managed agricultural areas. For example, Kiesel et al. (2010) found that the incorporation of tile drains improved the ability of a hydrologic model to simulate summer rainfall events, winter flows and the hydrograph recession for a catchment in northern Germany. To evaluate the response of changes in agricultural practices on water quality in aquatic receptors, reliable estimates on travel times from the fields to the surface water system is essential (Vervloet et al., 2018; Meals et al., 2010). As drains provide a fast flow pathway between the agricultural fields and downstream recipients, it is thus crucial that hydrological models can describe fast drain flow with sufficient accuracy. An adequate simulation of tile drainage dynamics is also necessary to establish regulations for nitrogen applications to reduce groundwater and surface water contamination (Refsgaard et al., 2014). Artificial drainage must also be considered in modeling studies to provide a more complete understanding of the mechanisms that affect runoff generation (O'Connell et al., 2007).

A variety of numerical models have been used to model tile drains ranging from one-dimensional (1D) models such as RZWQM (Ma et al., 2007; Walker et al., 2000) and DRAINMOD (Sammons et al., 2005; Wang et al., 2006) , to two-dimensional (2D) models such as MHYDAS-DRAIN (Tiemeyer et al., 2007), CATFLOW (Klaus and Zehe, 2011; Maurer, 1997) and ANTHROPOG (Carluer and De Marsily, 2004) and to three-dimensional (3D) models such as MIKE-SHE (Hansen et al., 2013), CATCHY (Muma et al., 2014; Muma et al., 2016), FLUSH (Nousiainen et al., 2015; Salo et al., 2017; Turunen et al., 2013) and HydroGeoSphere (Amado et al., 2017; De Schepper et al., 2015, De Schepper et al., 2017, Frey et al., 2016; Rozemeijer et al., 2010a, Thomas et al., 2016). Tile drainage was also modelled using SWAT-MODFLOW (Frederiksen et al., 2019; Molina-Navarro et al., 2019) and SWAT+ (Bieger et al., 2017), which was modified to include tile drainage flow (Bailey et al., 2022). Modeling tile drains at the catchment scale using 3D hydrological models is challenging. Specifically, the exact location of tile drains is generally unknown and difficult to estimate with satellite imagery and geophysical methods, particularly at the catchment scale (De Schepper et al., 2015; Hansen et al., 2013; Prinds et al., 2019; Schilling et al., 2019). Furthermore, when information on drain locations is available, mesh refinement around individual drains is necessary for accurate drain discharge simulations which increases the mesh size and the computational

burden. As a result, there is a need to adapt and improve current methodologies for including agricultural tile drains in numerical models such that they can be used in large-scale applications when data on tile drain properties and locations are incomplete or absent.

While there are several methods currently used for including tile drains in catchment-scale models, these methods all possess limitations regarding their usefulness when extensive data on tile properties and locations are not available. One of the most widely-used methods represents tile drains as a high-permeability (high-K) layer, also called equivalent medium, allowing for the simulation of lateral preferential flow from tile-drained catchments without explicitly representing the drains (Rozemeijer et al., 2010a; Carluer and Marsily, 2004, De Schepper et al., 2015 and Thomas et al., 2016). The high-K layer approach allows for a simple discretization of the domain because of the absence of internal boundary conditions on the drainage pipes (Carlier et al., 2007). De Schepper et al. (2015) and Thomas et al. (2016) obtained consistent simulated drain discharge for a 5 km² catchment in Denmark and a 42 km² catchment in the USA, respectively, when applying the high-K layer concept. However, the approach used in these previous studies has three distinct limitations: i) drainage water cannot be routed to the drainage system outlet at the surface of the domain, ii) the simulation output does not clearly distinguish discharge from the individual drain networks present within the catchment, and iii) there is no clear distinction between groundwater and drainage water. Together, these limitations compromise the spatial distribution of simulated hydraulic heads and saturation, and a specific location for the outlet discharge cannot be specified. Alternatively, some studies implemented head-dependent sinks in specific grid cells at the drain level to simulate tile drainage at the catchment scale (Bailey et al., 2022; Hansen et al., 2013; Frederiksen et al., 2019; Molina-Navarro et al., 2019). In their model, drainage water is routed either to the drainage outlet, the stream or the boundary of the domain. Both high-K layer and head-dependent sink concepts can be applied when the location of the tile drains is not available. However, neglecting the tile drain location can affect the simulation of local water flow and solute transport in catchments with large non-drained areas.

Explicitly representing tile drains in 3D models as 1D lines is prone to convergence issues in hilly terrains (De Schepper et al., 2017) and is often too complex and time consuming to be used at large scales. De Schepper et al. (2015) evaluated different configurations of tile drains using discrete line elements to represent 1D water flow. They showed that by representing the main collector drains in a model, the drainage system can be simplified for large-scale simulations and drain discharge is simulated correctly once the model is calibrated. In a following study, De Schepper et al. (2017) represented tile drains as seepage nodes to reduce computational times. The seepage nodes were used for the main collector drains in two drained fields (28 and 34 ha) within the Fensholt catchment (6 km²) in Denmark. Results of this study indicated that the seepage nodes were able to successfully recreate drain discharge and the flow

dynamics around the drains. This conceptualization of drains, however, was only applied to two drainage areas with similar sizes and there was no attempt to represent an entire tile drainage system in a catchment-scale model. Hydrological models in the same catchment were developed with one single conceptual model for tile drains, focusing on the effect of seasonal variations, topography, deep geology and specific hydrological models (HydroGeoSphere and MIKE-SHE) on simulated tile drainage (De Schepper et al., 2017; Hansen et al. 2019a, 2019b). Furthermore, only one soil model was evaluated, despite the uncertainty on the soil structure and hydraulic properties.

The goal of the present study is to compare four conceptual representations, or models, of tile drains for the numerical simulation of tile drainage in agricultural catchments. The first model (the Main Drain Model) uses seepage nodes to explicitly represent only the main collector drain paths, expanding the tile drainage representation from the two fields considered in De Schepper et al. (2017) to all tile drained fields in the Fensholt catchment. In the second model, the Distributed Model, seepage nodes are regularly distributed within all agricultural areas at the drain depth, without considering the locations of specific tile drains. This second model represents a refinement of that presented in Hansen et al. (2013), by considering that only agricultural areas are subject to tile drainage, such as done in Molina et al. (2017, 2019) and Thodsen et al. (2015), and should thus allow for a better representation of local groundwater flow outside the managed agricultural zones. The third model, the High-K Layer Model, replaces drains by a high-permeability layer that implicitly simulates the fast flow in the tile drainage systems. The Distributed Model and the High-K Layer Models can reduce the mesh complexity and computational times since they do not require the representation of the exact location of all tile drains of the drainage system. All three models listed above were compared to a fourth more complex model, labelled the Benchmark Model, that explicitly represents all mapped tile drains with seepage nodes. The models were compared in terms of error performance, data availability, mesh refinement and simulation times. A secondary objective of this study was to evaluate the effect of soil heterogeneity on the simulations. A homogeneous soil model, a homogeneous soil layers model and two heterogeneous soil models were implemented using the four conceptual models for tile drains.

The drain discharge, stream generation and heads were simulated with the 3D fully-coupled surface water and groundwater flow model HydroGeoSphere (HGS). HGS has been used for the simulation of complex surface water-groundwater (SW-GW) systems at the catchment scale (e.g., Schilling et al. 2017, Ala-Aho et al., 2017; Chow et al., 2016). Tile drains significantly affect the SW-GW exchange flux patterns reducing surface runoff, lowering the water table level and shortening periods of surface ponding (Konyha et al., 1992; Skaggs et al., 1994, Carluer and De Marsily, 2004), which justifies the choice of a fully integrated surface-subsurface model. Recent 3D hydrological models including tile drainage using

HGS were published by De Schepper et al. (2015), Thomas et al. (2016), De Schepper et al. (2017) and Hwang et al. (2019).

The simulations presented here are, to the author's knowledge, the first attempt to compare conceptual models based on seepage nodes to represent all tile drainage areas within a catchment with a coupled surface-subsurface hydrological model. The methods presented here also expand on the work from De Schepper et al. (2017) by allowing the water removed from a drainage system using seepage nodes to be routed to the surface water flow domain, instead of removing it from the model completely, thereby improving the representation of surface water-groundwater interaction.

6.2 Method and data

6.2.1 Site description

The Fensholt catchment covers a 6 km^2 area located about 15 km south of the city of Aarhus in the eastern part of the Jutland peninsula, Denmark (Figure 6.1a). Land use in the catchment is dominated by intensive agriculture (around 78% of the total area, Figure 6.1b), with the main crop types being winter wheat and spring barley. The climate is temperate and humid, with average temperatures ranging from 0°C in winter to 16°C in the summer with considerable variation (Danish Meteorological Institute, DMI). The average annual precipitation in the Fensholt catchment for the 1990–2015 period was 856 mm, with annual values ranging from 601 to 1137 mm.

The surficial geology consists of a 20-50 m thick cover of Quaternary glacial deposits overlain by 2-3 m of post-glacial freshwater peat in some areas around the main stream valley. Neogene and Paleogene marine sediments underlie the Quaternary cover. The Neogene layers are composed of a clayey formation from the Miocene with interbedded sandy units, while the Paleogene layers are largely composed of impermeable marl and clay. The groundwater system in the Quaternary cover is unconfined and the water table is generally close to the ground surface. The geology and hydrogeology of the Fensholt catchment have been extensively characterized and conceptualized by He et al. (2014), De Schepper et al. (2017), Varvaris et al. (2018) and Hansen et al. (2019a).

The surficial material within the catchment is predominantly composed of poorly-drained clayey till soils with a clay content of 12–35% (Hansen et al., 2019a). Due to the poor natural drainage of the soils, the agricultural areas within the catchment are intensively drained, as shown by the mapped tile drainage systems (Figure 6.1b). Information about the actual location of tile drains is typically hard, and sometimes almost impossible, to obtain. Although in Denmark information about the location of subsurface drained fields must be entered into a national database by contractors, some records are lost and drain maps are

often incorrect. Therefore, knowledge of the spatial distribution of tile drains at the local scale is often uncertain (Frederiksen et al., 2021, Møller et al., 2018). The tile drain spacing in the catchment is typically around 20 m, though spacing of less than 10 m has been observed within some fields. The outlets of the drainage systems discharge in the riparian lowlands or into tributaries of the main river, the Stampemølle Bæk, whose flow predominantly consists of tile drainage effluent. A comparison of stream flow rate and drain discharge suggested that about 74% of the Fensholt catchment discharge originates from tile drains (De Schepper et al., 2017).

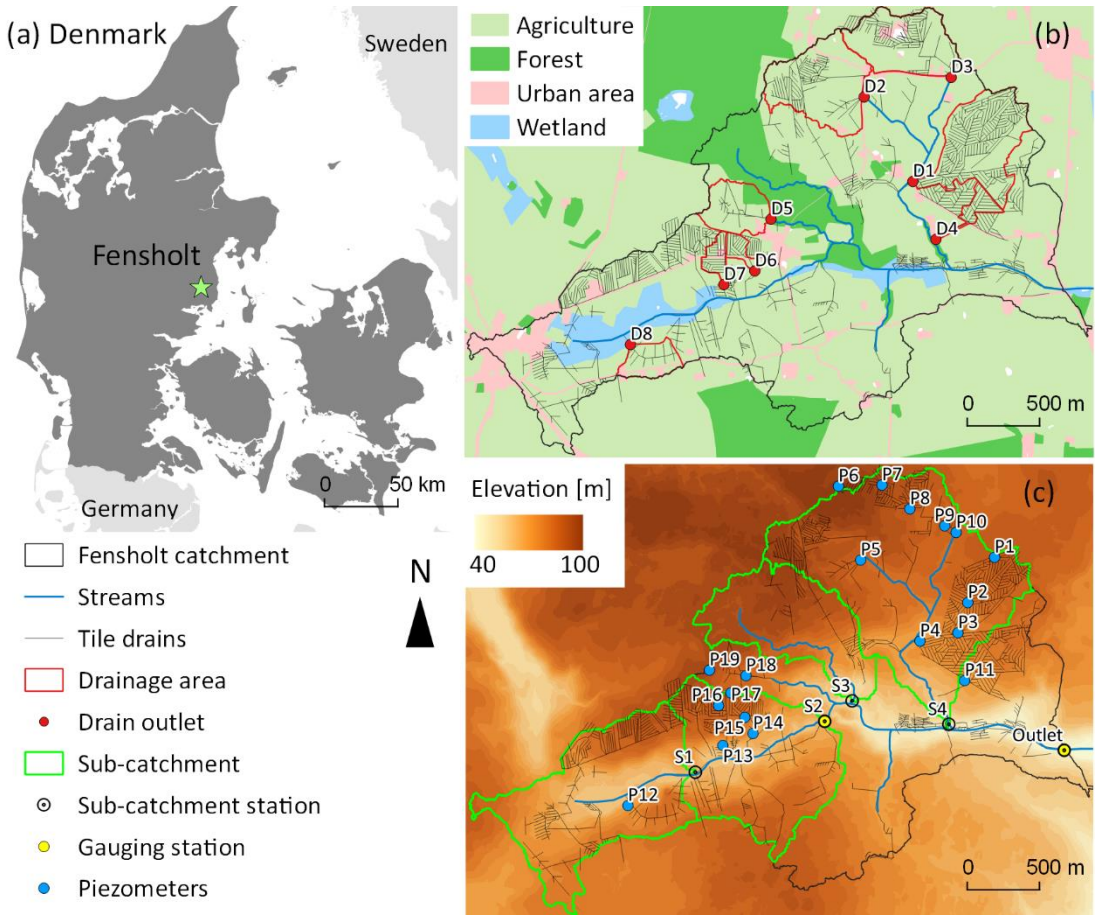

Figure 6.1 - Location of (a) the Fensholt catchment in Denmark, (b) the Fensholt catchment showing land use, tile drains, drainage areas and the drain discharge measurement stations (D1 to D8), and (c) the topography (1.6 m digital elevation model), piezometers, subcatchments delineated for investigation of stream discharge with the correspondent outlet stations (S1, S2, S3 and S4) and gauging stations at the outlet and in the center of the catchment (S2).

For this study, the catchment was subdivided into four subcatchments (Figure 6.1c, S1 to S4) to evaluate the stream discharge generated 1) downstream from a large wetland (S1), 2) in the central part of the catchment where a subcatchment station is located (S2), 3) from a tributary stream located near the forested area (S3), and 4) from a tributary stream located near tile-drained agricultural areas (S4). Subcatchments S1, S3 and S4 have not been monitored and are herein denominated "artificial stations".

6.2.2 Hydrologic data

The models presented in the next section are forced with daily precipitation and potential evapotranspiration for a 12-year period starting in January 2004. Precipitation data for the period of January 2004 to December 2013 was extracted from 10 km gridded data sets provided by the Danish Meteorological Institute (DMI). Precipitation data from January 2014 to December 2015 were taken from the precipitation station Fillerup (55°57'N, 10°5'E, around 2 km south from Fensholt catchment). Potential evapotranspiration was estimated with the Penman-Monteith equation using data from a meteorological station in Foulum, Denmark (56°29'N 9°35'E), around 62 km from the study area.

Discharge from eight tile drainage areas (Figure 6.1b, D1 to D8), the subcatchment and the catchment outlets (Figure 6.1c, S2 and Outlet) were monitored daily as part of the iDRÆN project of Aarhus University (www.idraen.dk). Drain discharge was measured with an electromagnetic flowmeter (KHRONE Optiflux 3070 flow meter, Khrone Messtechnik GmbH, Duisburg, Germany). Continuous stream discharge data was obtained from the two gauging stations (Figure 6.1c) by using water level loggers (OTT Orpheus Mini Water Level Logger, OTT Hydromet GmbH, Kempten, Germany) and a stable stage-discharge (h-Q) relation was computed from 2 years of biweekly discharge measurements using an OTT C2 current meter (Ovesen and Poulsen, 2016). Additionally, water levels were manually measured once or twice a month in two-meter-deep piezometers (Figure 6.1c, P1 to P19). Precipitation, potential evapotranspiration (PET) and measured stream discharge during the 2-year period of 2014 – 2015 are presented in Figure 6.2. Over that period, the cumulative volumes of precipitation, PET and the catchment and the subcatchment outlet discharge were 2048 mm, 1171 mm, 836 mm and 658 mm, respectively. These values are expressed as equivalent height over the contributing area.

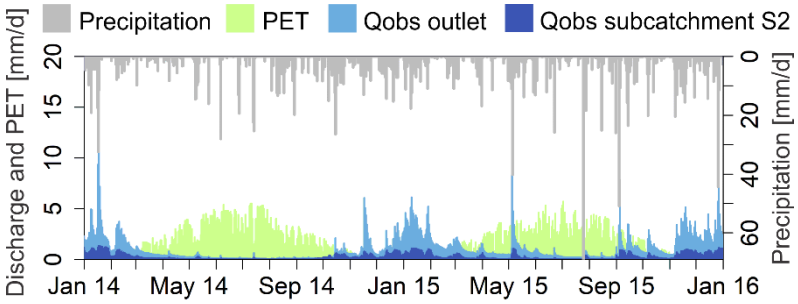

Figure 6.2 - Precipitation, potential evapotranspiration and measured stream water discharge for the simulation analysis period of 2014 – 2015 in the Fensholt catchment, Denmark.

6.3 Model application

6.3.1 Numerical model

The Fensholt basin hydrological models were developed with the hydrologic modeling software HydroGeoSphere (HGS; Aquanty Inc, 2017; Therrien et al., 2010). HGS is a finite element control volume model that simulates fully coupled 3D variably-saturated groundwater flow and 2D overland flow. The primary model input is precipitation, which is then partitioned into other components of the water cycle, such as overland flow, evapotranspiration and infiltration. In the subsurface domain, hydraulic heads and saturations are calculated for every node in the model mesh. In the surface domain, the water flux and depth are calculated for each node in the 2D mesh. Interception and actual evapotranspiration (AET) are simulated as mechanistic processes as described in Panday and Huyakorn (2004) and Aquanty Inc. (2017). Table 6.1 shows the evapotranspiration properties of winter wheat used in the models. HGS uses the Richards' equation to solve variably saturated flow in porous media, the van Genuchten parameterization to represent unsaturated flow properties of the subsurface, and the diffuse-wave approximation of the Saint Venant equations to calculate surface water flow. The Newton-Raphson technique is used to solve non-linear equations. The reader is referred to Aquanty Inc. (2017) and Therrien et al. (2010) for more information on the model and equations.

Table 6.1 - Evapotranspiration properties of winter wheat applied to the surface domain

Parameter	Value	Source
Root zone depth [m]	1.2	Varvaris et al. (2019)
Evaporation depth [m]	0.2	Kristensen and Jensen (1975)
Transpiration fitting parameters		
C1 [-]	0.31	Kristensen and Jensen (1975)
C2 [-]	0.15	Kristensen and Jensen (1975)
C3 [-]	5.9	Kristensen and Jensen (1975)
Transpiration limiting pressure head		
Wilting point [m]	-160	Varvaris et al. (2019)
Field capacity [m]	-15	Varvaris et al. (2019)
Oxic limit [m]	-0.1	Varvaris et al. (2019)
Anoxic limit [m]	0.9	Varvaris et al. (2019)
Evaporation limiting pressure head		
Minimum [m]	-160	Varvaris et al. (2019)
Maximum [m]	-0.1	Varvaris et al. (2019)

6.3.2 Soil and geological model

We used the same geological and soil structure as De Schepper et al. (2017), who developed a 3D hydrological model using HydroGeoSphere for the Fensholt catchment based on a stochastic geological realization from He et al. (2014), as shown in Figure 6.3. Three soil horizons and a clayey till layer overly the geological units in the entire model area. The A, B and C horizons and the clayey till layer were defined for depths equal to 0 to 0.3 m, 0.3 to 0.7 m, 0.7 to 1.5 m and 1.5 to 3.0 m, respectively. The geological units correspond to the Miocene and Quaternary deposits, where the Quaternary units are divided in two groups of glacial and tectonic origin. Four different conceptualizations of the A, B and C soil horizons were also considered. The first one represents the soil horizons as three distinct homogeneous soil layers, the second one represents them as a single homogeneous soil layer. The third and fourth conceptualizations represent each soil layer as being heterogeneous, with the hydraulic conductivity field generated based on geostatistical properties. More detail is given later.

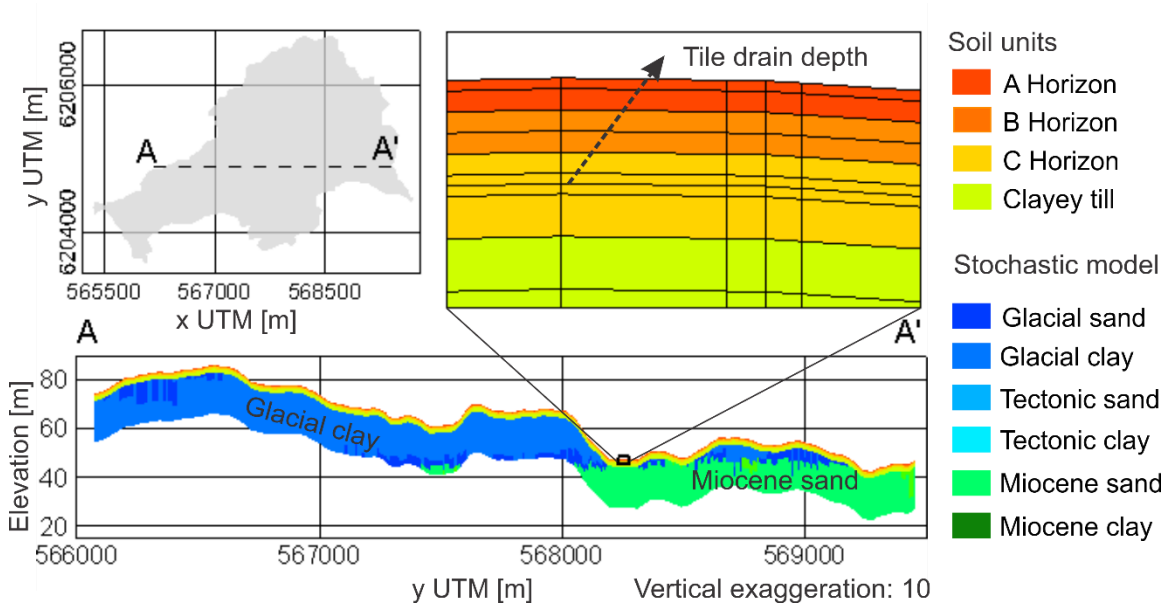

Figure 6.3 - Geological units from 3 to 20 m depth along vertical cross section AA'. Details for the A, B and C soil horizons in the first 1.5 meters below ground surface, defined by De Schepper et al. (2017), are shown as well.

6.3.3 Surface domain

The overland flow properties were assigned to the surface domain to represent the predominant agricultural use of the Fensholt catchment (Table 6.2). The rill storage height is applied at the surface of the model to reproduce the effect of the micro-topography on hydrological processes that cannot be represented at the catchment-scale in a physically-based model (Frei and Fleckeinstein, 2014). Values for the rill and obstruction storage height and the coupling length (Lc) between the surface and the subsurface domains are equal to values used by Hwang et al. (2019). Because winters are mild with average temperatures above freezing, snowmelt and accumulation were not included in the models.

Table 6.2 – Initial and calibrated overland flow parameters assigned to the surface domain

Parameter	Initial value*	Calibrated
Manning roughness coefficient, n_M [$s/m^{1/3}$]	0.2	0.5
Rill storage height, H_R [m]	0.005	-
Obstruction storage height, H_O [m]	0.01	-
Coupling length, L_C [m]	0.01	-

*Initial values of n_M from Li et al. (2018) and of H_R, H_O and L_C from Hwang et al. (2019).

6.3.4 Numerical discretization

The two-dimensional unstructured finite element meshes were created using the software AlgoMesh (Merrick and Merrick, 2015). The triangular meshes conform to the catchment boundary, stream centerlines, main collector drains and piezometer locations. A maximum edge length for triangles equal to 100 m was specified when generating the meshes. The maximum edge length was reduced to 35 m in highly steep terrain, wetlands and near streams, to improve the simulation of runoff and surface water-groundwater interactions at those locations. The 2D mesh developed for three of the four models contains 5685 nodes and 11049 triangular elements. The 2D mesh of the Benchmark Model contains 8175 nodes and 15986 triangular elements.

The 3D subsurface mesh was constructed by superimposing the 2D surface triangular mesh from the soil surface downward to a depth of 20 m to generate 3D triangular prism elements. The top of the 3D mesh therefore corresponds to ground surface and a uniform vertical thickness of 20 m was used. A total of 19 layers of 3D triangular prism elements with uniform thickness for the whole domain were generated. The upper soil horizons cover the entire catchment from the surface down to a depth of 3.0 m (Figure 6.3). This top 3 m was discretized using 10 layers with a thickness of 0.05 m above the tile drain level and 0.1 m below (Figure 6.3). Subsurface geological formations were discretized using 9 finite element layers between depths of 3 m to 20 m.

6.3.5 Boundary conditions

Daily rainfall and potential evapotranspiration were evenly applied on the surface domain of the model for the transient flow simulations. The surface nodes corresponding to the catchment outlet were assigned a critical depth boundary condition. The catchment water divide was delineated based on topography and the lateral boundaries are assumed impermeable. A constant outflow flux of 9.8×10^{-10} m/s was assigned to the bottom of the subsurface domain. This flux value corresponds to the average of 16 years simulation results (2000-2015) from a MIKE-SHE hydrological model (Hansen et al., 2014).

6.3.6 Tile drains represented as seepage nodes

The seepage nodes function as a specified hydraulic head (Dirichlet boundary condition) set to the elevation of the node. However, unlike a specified head boundary condition, this head remains in effect only if the groundwater level is above the elevation of the node. For a given seepage node *i*, the drain flow rate Q [L^3 T^{-1}] is given by $Q_i = C(h_i - h_d)$ when $h_i > h_d$, and $Q_i = 0$ when $h_i \leq h_d$, where C [L^2 T^{-1}] is an equivalent conductance for the seepage node, h_i [L] is the hydraulic head at the node and h_d [L] is the drain specified hydraulic head. In HGS, C is set to a large value to constrain the specified hydraulic head at the elevation of the node as soon as the head rises above the drain position. In the model developed by De Schepper et al. (2017) for the Fensholt catchment, the water extracted from seepage nodes was not routed to streams but summed up for comparison to observed drainage. In the present study, the extracted water from seepage nodes was injected to the outlet of the drainage systems using a boundary condition linking scheme (Hwang et al., 2019). The drain nodes represent sinks installed at 1 m below the ground while the linked nodes represent sources of water to the streams or the riparian lowland (Figure 6.4). The linked nodes are located at the drainage system outlets or at the closest position to the streams. The water flow at each discharge node was specified as the sum of the water extracted from the seepage nodes within the contributing drained areas. Because of convergence problems when developing the mesh, some drains were removed from the models, such as those too close to each other or those located near the streams or the catchment boundary. Removing drains reduced the mesh resolution and size, thus allowing faster simulation times.

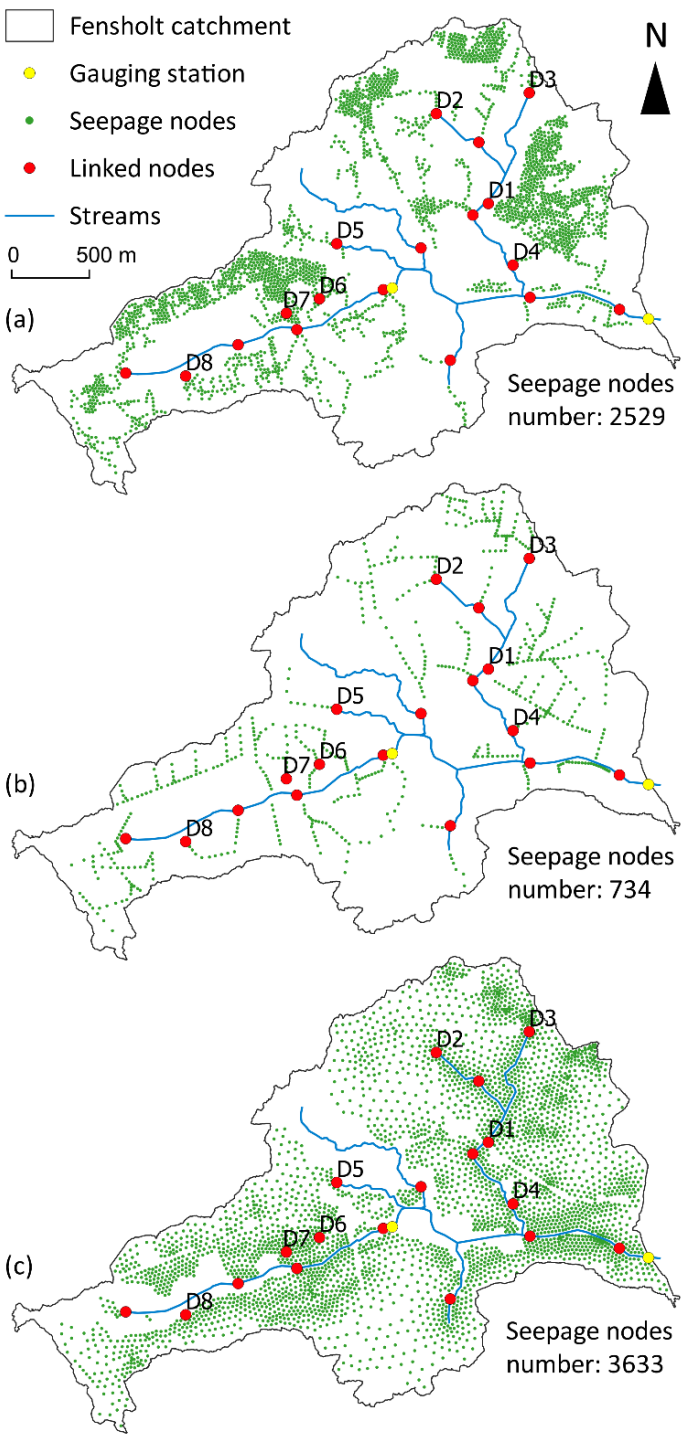

Figure 6.4 – Location of seepage nodes for the (a) Benchmark, (b) Main Drain, and (c) Distributed Models. The seepage nodes act as sinks extracting water from the subsurface and returning it to the surface at the drainage outlet (linked nodes). The drainage outlets D1 to D8 are labeled in the Figures. The location of the other outlets are estimated.

Three models were developed using the seepage node concept to represent tile drains: the Benchmark, the Main Drain and the Distributed Models. The Benchmark Model was developed to explicitly represent as many tile drains as possible in the hydrological model (Figure 6.4a). Therefore, we assume that the Benchmark Model is the best-suited conceptual model for simulating the water flow in tile-drained catchments. In the Benchmark Model, the mesh was refined to explicitly incorporate the main and lateral drains, so the mesh was refined in drainage areas to a maximum cell length of 30 m, contrary to 100 m for the other models (Figure 6.5). To avoid mesh element lengths smaller than 5 m, the design of some tile drainage networks was simplified if the individual drains were located too close together in the resulting mesh.

In the Main Drain Model, the geometry of the drainage networks in the Fensholt catchment was simplified by only considering the main collector drains and neglecting most of the lateral drains. Seepage nodes were applied along the path of the main collector drains of all tile drainage networks within the catchment (Figure 6.4b), thereby expanding the tile drainage representation in the two fields studied by De Schepper et al. (2017). This conceptualization was applied to reduce computational times (De Schepper et al., 2017) and is considered suitable for the application at the catchment scale (De Schepper et al., 2015).

In the Distributed Model, we assumed the tile drains are distributed over all agricultural areas in the Fensholt catchment. All nodes beneath the agricultural areas located at 1 m below ground surface were set as seepage nodes, without consideration of the exact drain locations (Figure 6.4c). Although a coarser mesh could be applied since the drain locations are not represented directly, the same mesh resolution as that of the Main Drain model was applied.

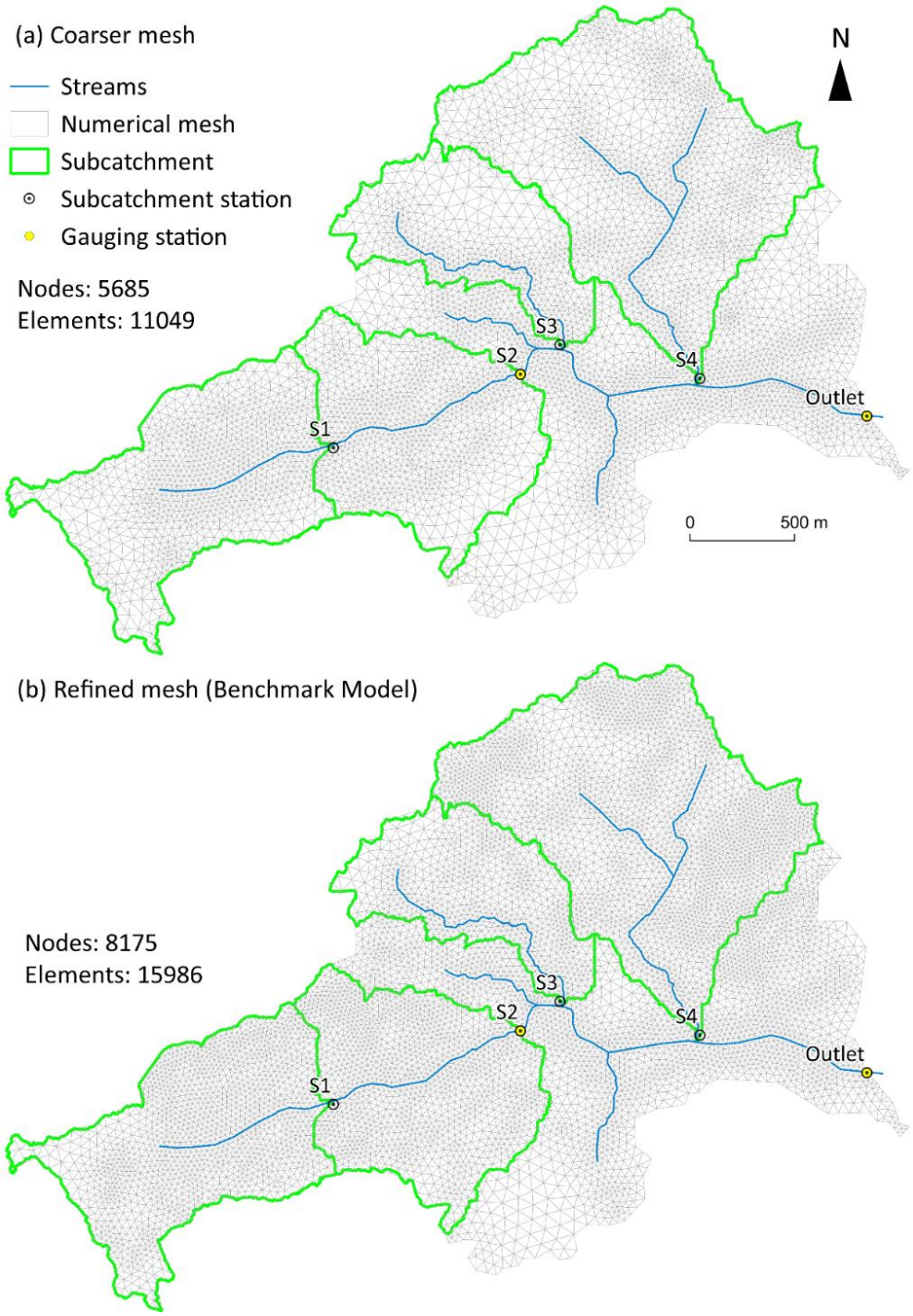

Figure 6.5 - Numerical mesh of (a) the Main Drain, Distributed and High-K Layer Models and (b) the Benchmark Model. The mesh of the Benchmark Model was refined to accommodate all tile drains in the Fensholt catchment.

6.3.7 Tile drains represented as an equivalent high-permeability layer

In the High-K Layer Model, the tile drainage is implicitly simulated as a high-permeability layer located at the average depth of the drains over the entire catchment. With this conceptual model, the distinction between groundwater and drainage water can be only roughly estimated. The high-permeability layer was isotropic and homogeneous, with the hydraulic conductivity defined by the tile drains density according to the method developed by Thomas et al. (2016). Other hydraulic parameters were equal to those used for the C horizon (Table 6.3).

Table 6.3 – Hydraulic properties of the geological model assigned between depths of 3 m and 20 m based on De Schepper et al. (2017)

Parameter	Glacial sand	Glacial clay	Tectonic sand	Tectonic clay	Miocene sand	Miocene clay
Horizontal hydraulic conductivity, Kh [m/s]	4.2E-04	2.5E-08	7.2E-06	4.6E-07	3.3E-04	5.4E-08
Vertical hydraulic conductivity, Kz [m/s]	4.2E-05	2.5E-09	7.2E-07	4.6E-08	3.3E-05	5.4E-09
Specific storage, Ss [1/m]	1.0E-03	1.0E-03	1.0E-03	1.0E-03	1.0E-03	1.0E-03

*Ss values were manually calibrated. Initial Ss values were 5.0E-05 (De Schepper et al., 2017).

The representation of tile drains using a high-permeability layer also allows for a simple discretization of the domain because there are no internal boundary conditions and there is no need to refine the mesh around the tile drain paths. Nonetheless, for the High-K Layer model we used the same mesh as used for the Main Drain and Distributed Models to allow for a more direct comparison of the effects of the alternative representations of drains.

6.3.8 Simulation strategy and performance metrics

The simulations target a two-year period, 2014 and 2015, for which measurements of stream discharge, drain discharge and hydraulic head are available. A prior model spin-up is recommended for coupled surface and subsurface hydrologic models (Ajami et al., 2014). For the spin-up, we simulated a 10-year transient model by using daily precipitation data from January 2004 to December 2013. The simulated hydraulic heads and surface water depths at the end of this 10-year period were then used as initial hydraulic heads and water depths for the simulation period from 1st January 2014 to 1st January 2016. The dual node approach was used for surface-subsurface flow coupling. A maximum saturation variation of 0.05 between successive time steps was specified for the variable time stepping procedure in HydroGeoSphere (Aquanty Inc., 2017) and time steps were limited to a maximum of 1 day.

The ability of the models to reproduce observed stream discharge was assessed by computing the mean absolute error (MAE), the Nash-Sutcliffe efficiency (NSE; Nash and Sutcliffe, 1970) and the Kling-Gupta Efficiency (KGE; Gupta et al., 2009). The NSE is highly sensitive to discharge peaks as it is calculated from squared differences between observed and simulated data (Krause et al., 2005). The metric was therefore calculated from weekly averaged discharge values. The KGE metric is based on NSE components and was also calculated on a weekly basis. The reproduction of depths to water table was assessed with the MAE and the root mean square error (RMSE). The simulated drain discharge was evaluated using the MAE, NSE and KGE. Refer to Knoben et al. (2019) for a comprehensive analysis of the NSE and KGE scores on modeling water discharge.

Models were run on a 32.0 Gb RAM computer with 4 CPU cores at 3.70 GHz without a parallel computational framework. Simulation times for the Distributed and Main Drain Models were 1.7 and 2.1 days, respectively, for the 2-year simulation period of 2014-2015. The High-K Layer and Benchmark Models had longer simulation times, equal to 2.9 and 3.1 days, respectively, for the same period.

6.3.9 Parameter estimation

We initially attributed hydraulic properties to the soil and geological units defined by De Schepper et al. (2017) and He et al. (2015) for all models. Using these properties resulted in conditions that are too dry in summer, without stream generation, and too wet in winter. One reason for this unsuccessful history matching is that De Schepper et al. (2017) only included tile drains from two drainage areas in their model, while we included all tile drains in Fensholt. The Main Drain Model was then chosen for manual calibration because of its simplicity and shorter simulation times than the Benchmark Model. Hydraulic conductivities, specific storage and Manning coefficient were calibrated against daily stream discharge for the 2014-2015 period and the NSE, MAE and KGE were evaluated.

The initial and calibrated values of the geological and soil units are presented in Tables 6.3 and 6.4, respectively. The Manning coefficient was calibrated to 0.05 $s/m^{1/3}$, which is within the range of values reported in Hwang et al. (2019) and Li and Zhang (2001). The hydraulic conductivity of the high permeability layer representing tile drainage in the High-K Layer Model was varied from the value calculated with the method of Thomas et al. (2016) without considerably improving the model, so the calculated values were maintained.

6.3.10 Alternative soil models

As mentioned previously, four alternative conceptualizations, or models, of the soils were developed to evaluate the effect of the heterogeneity in hydraulic conductivity from the ground surface down to 1.5 m, which corresponds to soil horizons A, B and C. Below a depth of 1.5 m, the hydraulic properties were similar for all models. The four soil models were implemented to the four conceptual models for tile drains, resulting in 16 model configurations. The first soil model represents each soil horizon as a distinct geological unit with uniform hydraulic conductivity, with values taken from De Schepper et al. (2017). In the second model, all three soil horizons are lumped into a single homogeneous soil unit. The third and fourth soil models assume that the soil is heterogeneous and 3D hydraulic conductivity fields for the soil were generated with the FGEN package (Robin et al., 1993). FGEN produces cross-correlated three-dimensional random fields on a regular grid based on dimensions and geostatistical parameters. The geostatistical properties were inferred from soil hydraulic conductivity values obtained from other studies in the Fensholt catchment (Boico et al., 2022b; Hansen et al., 2019a; He et al., 2015, Petersen et al., 2020). The mean and variance of the hydraulic conductivity values were 6.3E-05 m/s and 2.3E-08 m^2/s^2, respectively. The hydraulic conductivity of the homogeneous soil model was set to the mean of the hydraulic conductivity values and other hydraulic parameters were equal to the calibrated values for the C horizon (Table 6.4). The mean and variance were used to generate the heterogeneous soil models. The random hydraulic conductivity fields were generated assuming a lognormal distribution of the hydraulic conductivity, a correlation length of 0.1, and then mapped onto the 3D mesh elements.

6.4 Results

The same precipitation and potential evapotranspiration data sets were applied to all models during the simulated period (1 January 2014 to 31 December 2015) (Figure 6.2). Calibration of the Main Drain Model improved the simulation of the observed outlet stream discharge, generated reasonable water saturation at the streambed and wetlands and reproduced shallow hydraulic heads within 2 m depth of the piezometers. We applied the parameters calibrated for the Main Drain Model (Table 6.4) to the other models and obtained a comparable fit to the observations. Therefore, the Distributed, High-K Layer and Benchmark Models were not calibrated.

Table 6.4 - Initial and calibrated hydraulic properties of the soil A, B and C horizons, clayey till and the high-K layer assigned between depths of 0 m and 3 m

	Parameter	A horizon	B horizon	C horizon	High-K layer	Clayey till
	Depth [cm]	0-30	30-70	70-150	100-110	150-300
Initial value	Horizontal hydraulic conductivity, Kh [m/s]	1.0E-05	1.0E-05	3.2E-06	4.4E-04	8.9E-08
	Vertical hydraulic conductivity, Kz [m/s]	1.0E-06	1.0E-06	3.2E-07	4.4E-04	8.9E-09
	Porosity [-]	0.41	0.38	0.36	0.36	0.39
	Van Genuchten, α [1/m]	1.5	1.4	1.3	1.3	1.0
	Van Genuchten, n [-]	1.4	1.3	1.2	1.2	1.4
	Residual saturation, Sr [-]	0.16	0.21	0.28	0.28	0.10
	Specific storage, Ss [1/m]	1.0E-05	1.0E-05	1.0E-05	1.0E-05	1.0E-05
Calibrated value	Horizontal hydraulic conductivity, Kh [m/s]	4.2E-05	2.8E-05	2.8E-05	-	2.0E-07
	Vertical hydraulic conductivity, Kz [m/s]	4.2E-05	2.8E-05	2.8E-05	-	2.0E-08
	Specific storage, Ss [1/m]	1.0E-03	1.0E-03	1.0E-03	1.0E-03	1.0E-03

Sources of initial values: A, B and C horizons have Kh and Kz from De Schepper et al. (2017) and porosity, α, n and Sr from Varvaris et al. (2018). Clayey till has Kh and Kv from He et al. (2015), porosity from De Schepper et al. (2017) and α, n and Sr from Børgesen and Schaap (2005). All Ss values are from Hansen et al. (2019a). High-K layer has Kh and Kz from the equation developed from Thomas et al. (2016) and the other hydraulic parameters identical to the C horizon.

The water balance input (rainfall) and output (stream discharge at the outlet, actual evapotranspiration and storage variation) during the simulation period are presented in Figure 6.6. The cumulative volumes (in equivalent depth for the Fensholt catchment) of the simulated stream discharge are similar for all models, ranging from 988 mm in the Benchmark to 1030 in the High-K Layer Model. Those values are, however, from 18 to 23% above the measured stream discharge volume of 836 mm for the same period. This overestimation may be caused by the misrepresentation of the boundary conditions, such as lateral boundaries that are impermeable and do not allow for water to exit the model as subsurface flow. NSE for the outlet stream discharge for the four conceptual model for tile drains were between 0.51 and 0.82 indicating satisfactory to very good results (Koch et al., 2013; Moriasi et al., 2007). Therefore, we considered the hydrological models suitable for analysis of stream and drain discharge, depth to water table below ground and surface water depth using the different conceptual models for tile drains.

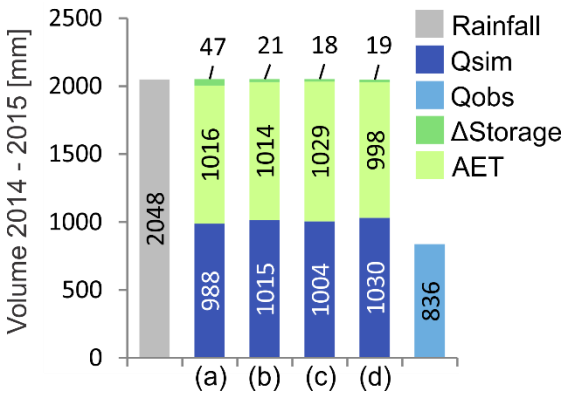

Figure 6.6 – Water balance components for the 2014-2015 period computed with the (a) Benchmark, (b) Main Drain, (c) Distributed, and (d) High-K Layer Models. Rainfall corresponds to cumulative precipitation, Qsim and Qobs are the simulated and observed stream discharge at the outlet, AET is actual evapotranspiration, and ΔStorage is the change in water stored in the catchment.

6.4.1 Stream discharge

The stream discharge dynamics at the outlet were well simulated for all models, reproducing the transition between low and high discharges (Figure 6.7). However, all models overestimated most of the discharge peaks at the outlet when compared to measured data, particularly in the second half of 2015 (Figure 6.7). The lowest MAE (0.45 mm/d) was obtained with the Benchmark Model and the highest (0.66 mm/d) with the Distributed Model. The NSE and KGE were best for the Benchmark Model, 0.82 and 0.83, respectively, followed by the Main Drain Model (0.61 and 0.71), the High-K model (0.61 and 0.71), and finally the Distributed Model (0.51 and 0.64). The overall good NSE for the Main Drain Model was expected, since the model was calibrated against outlet stream discharge.

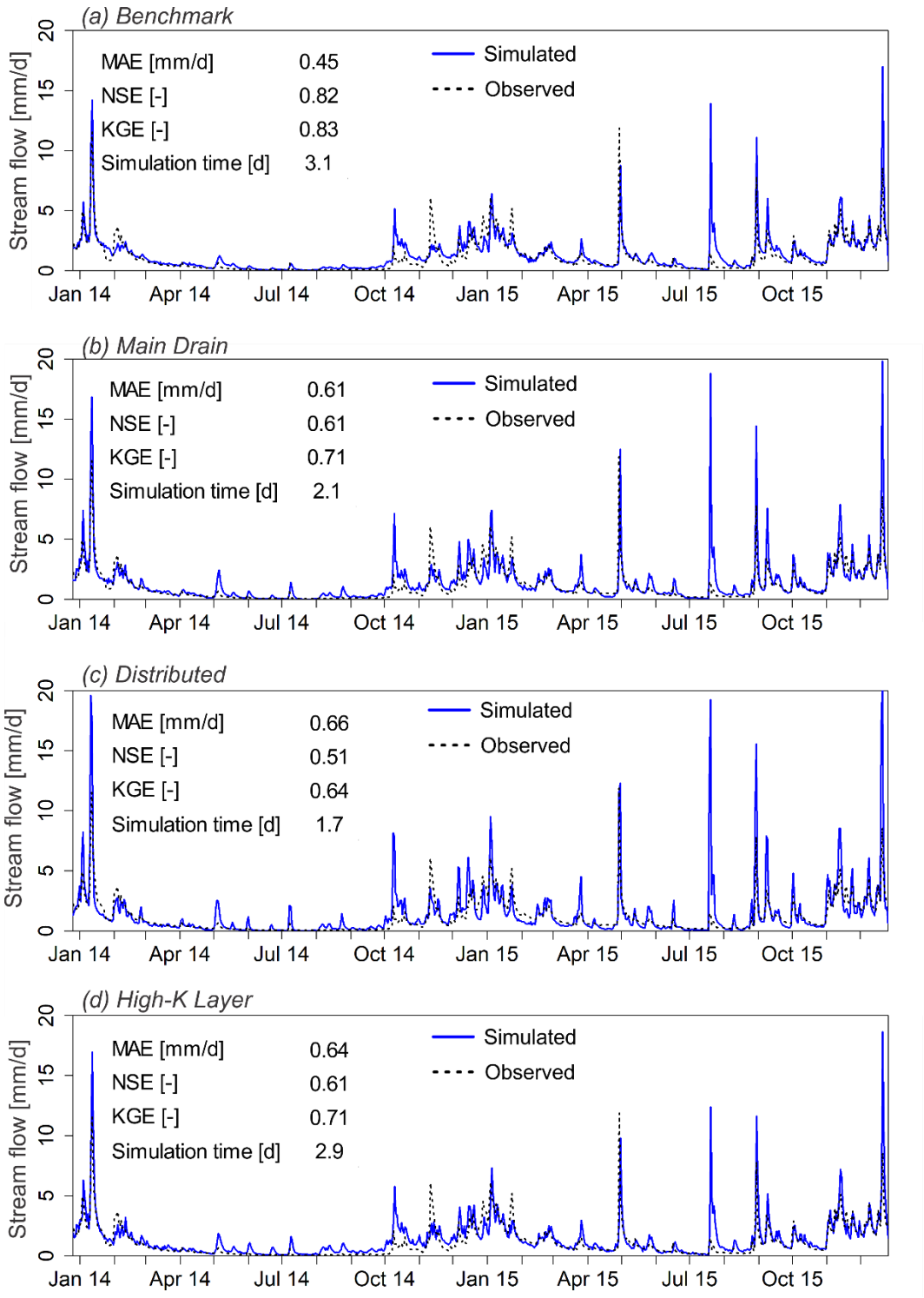

Figure 6.7 - Observed and simulated outlet stream discharge from January 2014 to January 2016 for the (a) Benchmark, (b) Main Drain, (c) Distributed, and (d) High-K Layer Models. Observed discharge is at the catchment outlet. MAE: Mean absolute error, NSE: Nash Sutcliffe efficiency, KGE: Kling-Gupta efficiency. MAE is calculated from daily discharges and NSE and KGE from weekly discharges.

The same overall good behavior of the Benchmark Model was not observed in the subcatchment station S2, where the stream discharge was overestimated during the two years of simulation, with MAE = 0.62 mm/d, NSE = 0.16 and KGE = 0.11 (Figure 6.8 and Table 6.5). The Main Drain and High-K Layer Models showed less variation than the Benchmark Model at station S2. For the former models, low stream discharge is rarely reproduced, and the peaks were less overestimated (Figure 6.8). Although the Main Drain and High-K Layer Models overestimated subcatchment low stream discharge, they showed better performance than the other models with NSE and KGE varying from 0.62 to 0.72 (Table 6.5). The Distributed Model simulated low stream discharge close to the measurements at station S2 (Figure 6.8). However, the peaks were also overestimated at S2, resulting in poor performance for NSE and KGE compared to the Main Drain and High-K Layer Models (Table 6.5).

Table 6.5 - Error statistics of catchment outlet stream discharge, subcatchment stream discharge (station 2), drain discharge and depth to water table for the 2014-2015 period. The errors are presented for the Benchmark (B), Main Drain (MD), Distributed (D) and High-K layer (HK) models using the reference soil layers model and the alternative soil models (homogeneous soil, heterogeneous soil 1 and heterogeneous soil 2).

Criterion	Soil layers				Homogeneous soil				Heterogeneous soil 1				Heterogeneous soil 2			
	B	MD	D	HK	B	MD	D	HK	B	MD	D	HK	B	MD	D	HK
Outlet stream discharge																
MAE [mm/d]	0.45	0.61	0.66	0.64	0.42	0.57	0.59	0.64	0.40	0.55	0.57	0.58	0.38	0.58	0.64	0.64
NSE [-]	0.82	0.61	0.51	0.61	0.83	0.66	0.65	0.63	0.83	0.71	0.71	0.70	0.87	0.67	0.61	0.56
KGE [-]	0.83	0.71	0.64	0.71	0.85	0.79	0.76	0.72	0.83	0.83	0.82	0.80	0.85	0.79	0.72	0.68
Subcatchment stream discharge (station 2)																
MAE [mm/d]	0.62	0.46	0.51	0.47	0.56	0.43	0.45	0.49	0.50	0.38	0.43	0.42	0.45	0.43	0.48	0.43
NSE [-]	0.16	0.71	0.34	0.72	0.17	0.71	0.51	0.69	0.20	0.80	0.58	0.79	0.60	0.75	0.51	0.74
KGE [-]	0.11	0.63	0.44	0.62	0.14	0.65	0.54	0.58	0.19	0.72	0.59	0.72	0.45	0.76	0.58	0.69
Drain discharge (average from 8 drainage stations)																
MAE [mm/d]	1.09	1.04	1.14	-	1.15	1.09	1.17	-	1.20	1.14	1.18	-	1.08	1.03	1.14	-
NSE [-]	0.27	0.30	0.11	-	0.09	0.14	0.03	-	-0.04	0.04	-0.02	-	0.32	0.35	0.16	-
KGE [-]	0.34	0.36	0.28	-	0.18	0.21	0.16	-	0.08	0.12	0.11	-	0.39	0.39	0.30	-
Depth to water table (average from 19 piezometers)																
MAE [m]	0.79	0.88	0.80	0.94	0.78	0.83	0.80	0.90	0.77	0.80	0.78	0.87	0.80	0.88	0.80	0.97
RMSE [m]	0.93	1.02	0.94	1.07	0.91	0.97	0.93	1.03	0.90	0.94	0.91	1.01	0.94	1.03	0.94	1.11

Optimal value of the MAE and RMSE is 0 and of NSE and KGE is 1.

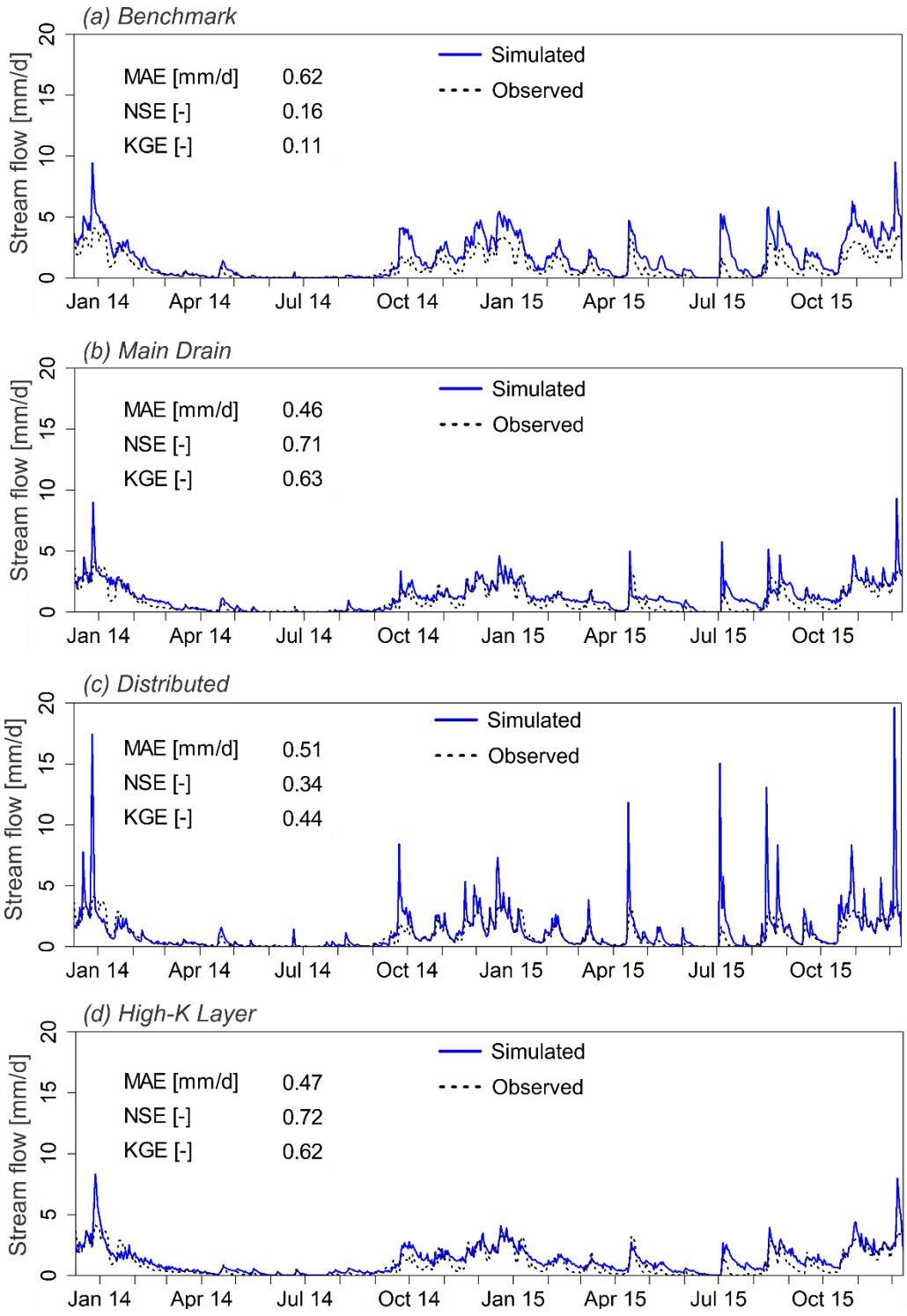

Figure 6.8 - Observed and simulated subcatchment stream discharge from January 2014 to January 2016 for the Benchmark, Main Drain, Distributed, and High-K Layer Models. Observed discharge is at the subcatchment station S2. MAE: Mean absolute error, NSE: Nash Sutcliffe efficiency, KGE: Kling-Gupta efficiency. MAE is calculated from daily discharges and NSE and KGE from weekly discharges.

6.4.2 Drain discharge

The cumulative volumes of the simulated drain discharge for the 2014-2015 period are underestimated compared to measured discharge for all drainage areas, except for D1 (Figure 6.9). All models simulated cumulative volumes at least 50% lower than measured for drainage areas D4, D6, D7 and D8, which have small areas compared to the others. Simulated volumes close to the measured ones were obtained for D3. Representing the entire drainage areas with tile drains in the Distributed Model contributed to the higher simulated volumes for D1, D2, D5 and D8 when compared to the Benchmark and Main Drain Models. Despite some differences in simulated discharge volumes between the models, their performance to reproduce measured discharge volumes is generally similar (Figure 6.9).

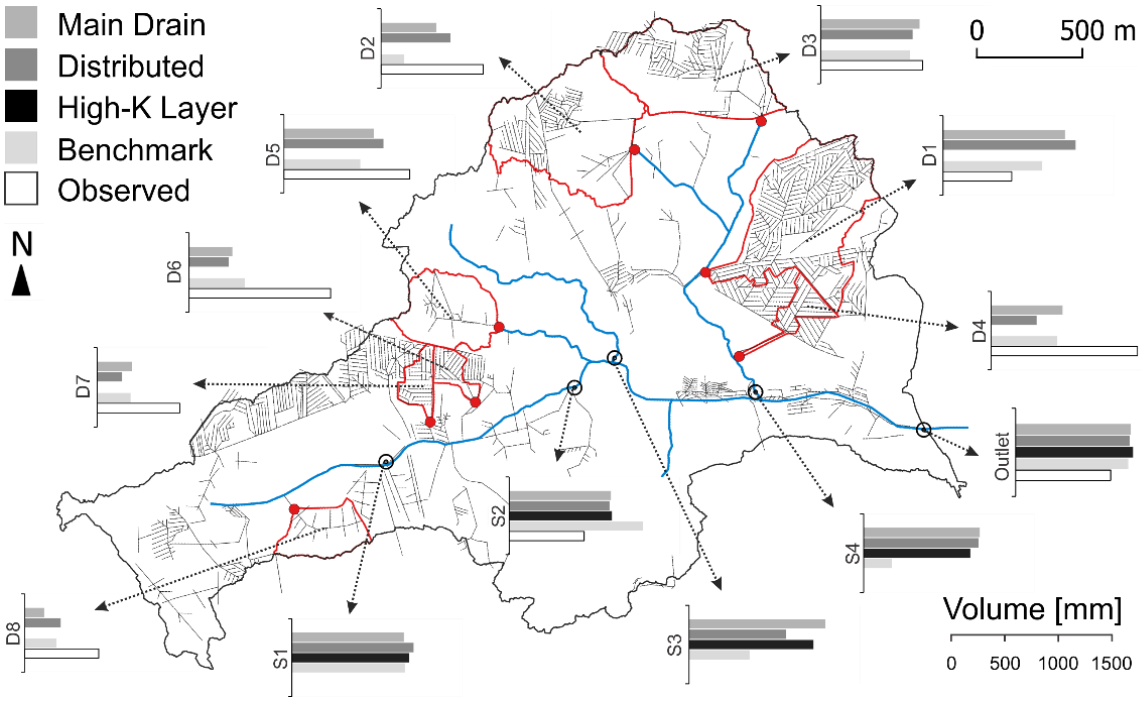

Figure 6.9 – Simulated and observed cumulative volumes during the 2014-2015 period at the drainage outlet stations D1 to D8 (red dots), stream stations S1 to S4 and the outlet (black dots). The cumulative volumes are presented in equivalent depth for the drainage and subcatchment areas. Tile drains and streams are represented as black and blue lines, respectively.

The simulated daily drain discharge using the different conceptual models for tile drains resulted in similar MAE and NSE for all drainage areas except for D1 and D2, where the Distributed and Benchmark Model, respectively, produce worse results compared to the Main Drain Model (Figure 6.10). On average, the MAE is around 1 mm/d for all models (Table 6.5). The NSE for all models ranged from -0.26 to 0.75 (Figure 6.10b), except for the Distributed Model in D1, where the NSE was -1.19. The Main Drain Model had the best NSE performance (0.30), followed by the Benchmark (0.27) and the Distributed (0.11) models. When excluding the drainage area D1, the average NSE were similar for all models, ranging

from 0.27 (Benchmark) to 0.34 (Main Drain). These results indicate that the Main Drain Model performed better than the other models to simulate drain discharge at the field scale. The calibration of the Main Drain Model against stream discharge may have contributed to the better performance.

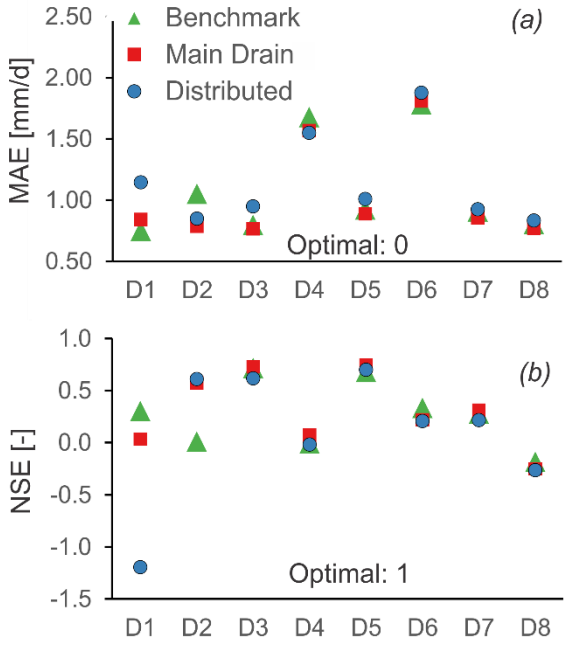

Figure 6.10 – Mean Absolute Error (MAE) of daily and Nash Sutcliffe efficiency (NSE) of weekly drain discharge for the drainage areas during the 2014-2015 period. NSE for the Distributed Model in D1 was too low (-3.5) and is not shown here.

Observed and simulated monthly drain discharge rates in the 2014-2015 period were plotted for drainage areas D1 to D8 in Figure 6.11. The drain discharge is frequently underestimated for drainage areas D2 to D8, especially in 2014 and for the first half of 2015, and overestimated for D1. Misrepresentation of drain discharge may be attributed to the lack of soil heterogeneity representation. The overestimation of the drain discharge in D1 may be largely affected by tile drains included in the maps but never installed in the field as observed during field work by Hansen et al. (2019a). Furthermore, the installation of tile drains started as early as 1940 and many tile drains represented in the model may actually be damaged or disconnected from the gauging station.

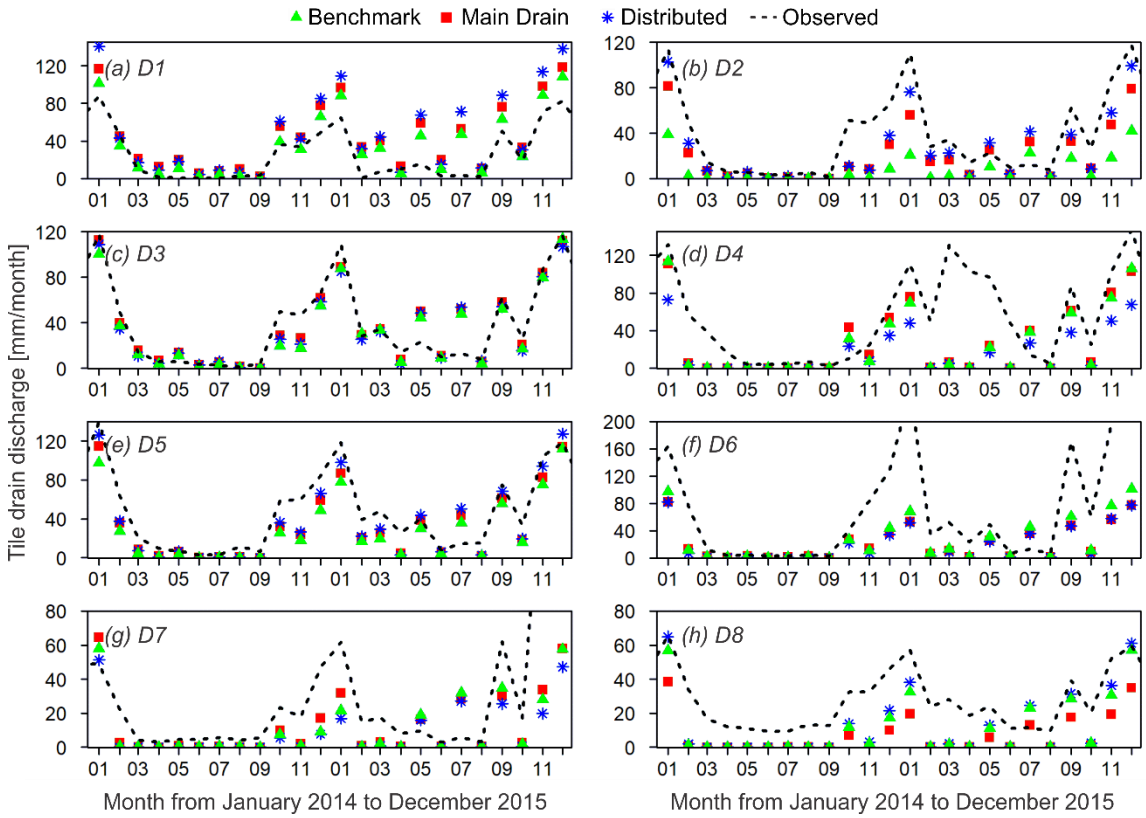

Figure 6.11 - Observed and simulated monthly drain discharge (Q) from January 2014 to December 2015 for the drainage areas D1 to D8 using the four different modeling approaches to represent tile drains. Observed data were measured at outlet of the tile drainage system.

We investigated the simulation of the drain discharge using the alternative soil models presented in Section 6.3.10. We observed that a homogeneous soil composed of one single layer and the heterogeneous soil model 1 performed worse than the homogenous soil layers model to simulate drain discharge. The heterogeneous soil model 2, however, had a comparable performance to the layered model, with a little improvement of the MAE, NSE and KGE (Table 6.5). For the Main Drain Model, when the homogeneous soil was applied, the drain discharge was better simulated in D1 (NSE=0.61) compared to the homogeneous soil layers model and the heterogeneous soil model 2 (NSE around 0 for both models). When the homogeneous soil layers model and the heterogeneous soil model 2 were applied, better results were obtained in D5 (NSE higher than 0.70) compared to the other soil models (NSE=0.16 for the homogeneous soil model and NSE=0.51 for the heterogeneous soil model 1).

6.4.3 Surface water depth

The surface water depth simulated by the four conceptual models for tile drains was evaluated in terms of the expected behavior for tile-drained catchments since no measured data was available for an error performance analysis. All models simulated realistic spatial and temporal patterns for the surface water depth for most of the 2014-2015 period, with dry surface conditions in the drainage areas and higher

surface water levels in the stream paths. However, the water flow connection was better simulated for the main stream than for the tributaries. During the summer of 2014 and 2015, the simulated surface water depths were near zero for all models except in some stream stretches and in the wetland (western part of the catchment). For dryer days, such as 15th June 2014, no model simulated the water flow connection along all the streams, when low precipitation during the summer results in much less simulated runoff (Figure 6.7) and tile drainage (Figure 6.11).

Figure 6.12 presents the simulated surface water depth for a wet day during the winter (15th December 2015). The stream tributaries were dry for most of the simulation period. The simulated surface water depths were generally lower than the obstruction storage height of 0.01 m in the agricultural areas for all models, where no runoff was generated, except in some areas for the High-K Layer Model (Figure 6.12d). Values greater than 0.1 m were simulated around the streams on 15th December 2015, with higher water depth in the wetlands and near the outlet for all models. Contrary to the other models, the main drain paths can be identified in the Main Drain Model as locations with water depths below 0.001 in Figure 6.12b. The Distributed Model resulted in the driest conditions with surface water depths generally lower than 0.001 m on 15th December 2015 in the agricultural areas. These results indicate that implementing seepage nodes in all agricultural areas may limit surface water flow because the tile drains are overrepresented. The surface water depth simulated by the High-K Layer Model was generally higher than for the other models (Figure 6.12d). The High-K Layer Model shows the largest areas of surface water depths higher than 1 m in the wetland areas and 0.01 m in some tile drained agricultural areas on 15th December 2015. During the entire 2014-2015 period, the High-K Layer Model simulated surface water depths higher than 1 m in the wetland areas.

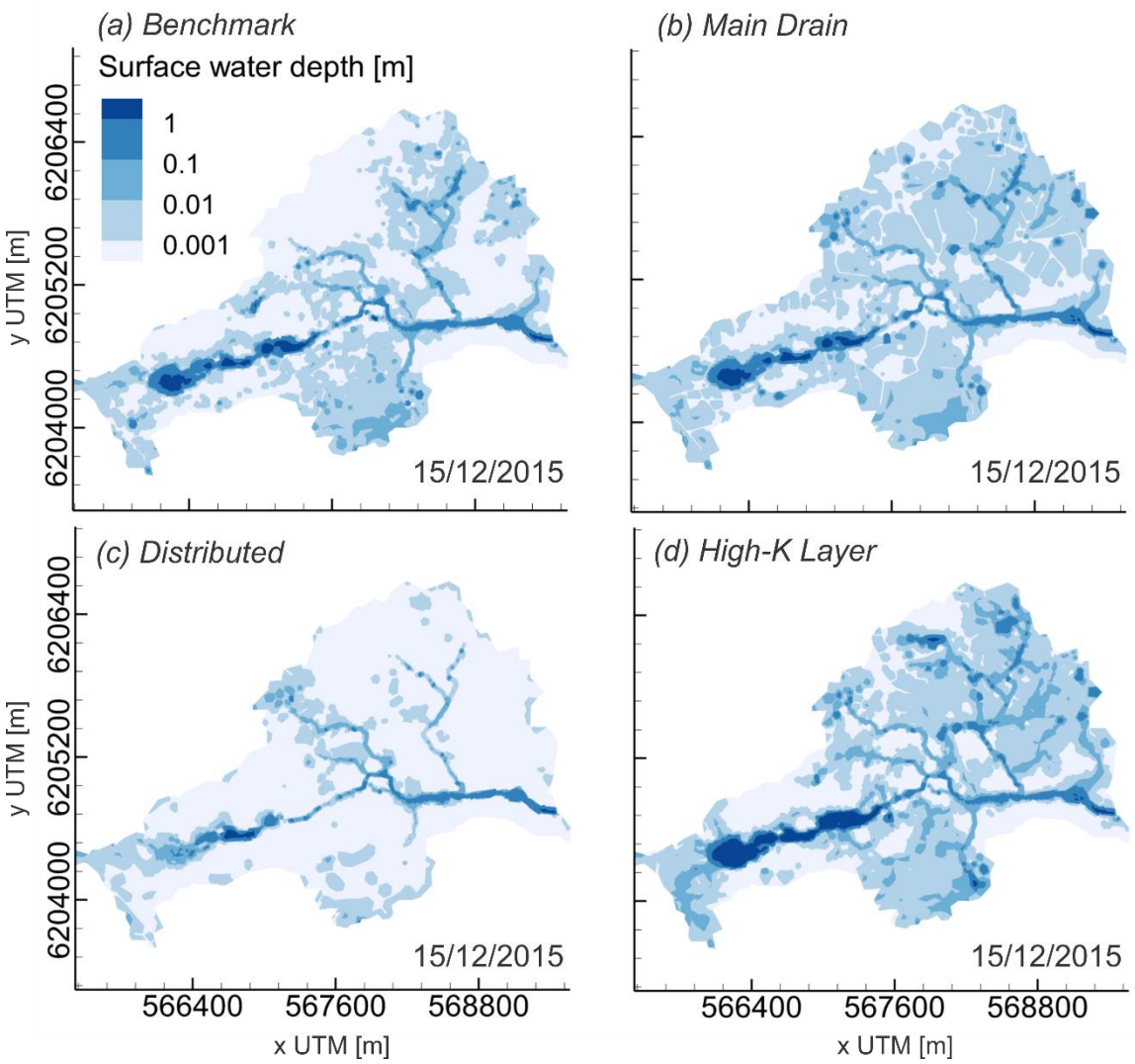

Figure 6.12 – Surface water depth for the (a) Benchmark, (b) Main drain, (c) Distributed and (d) High-K Layer Models on 15th December 2015 (wet season).

6.4.4 Depth to water table below ground

Observed versus simulated depths to the water table from ground surface for 9 piezometers are presented in Figure 6.13. Around 32 measurements were available for each piezometer for the 2014-2015 period. In piezometers P1, P7, P8, P11, P12, P14, P15, P17, and P19, the depths were overestimated (generally more than 2 m below ground surface) and they are not included in the figure. The Main Drain and High-K Layer Models simulated lower depths to water table compared to the Benchmark and Distributed Models. Most of the simulated depth to water table values were zero, with the water table reaching ground surface, in P10 and P18 for the Main Drain Model (Figure 6.13b) and in P2, P3, P9 and P10 for the High-K Layer Model (Figure 6.13d), where the piezometers are filled with water and interaction with the soil

surface may occur. Fully saturated piezometers and greater surface water depths where piezometers P2 and P3 are located is unlikely because of the large number if tile drains in that region (Figure 6.1c).

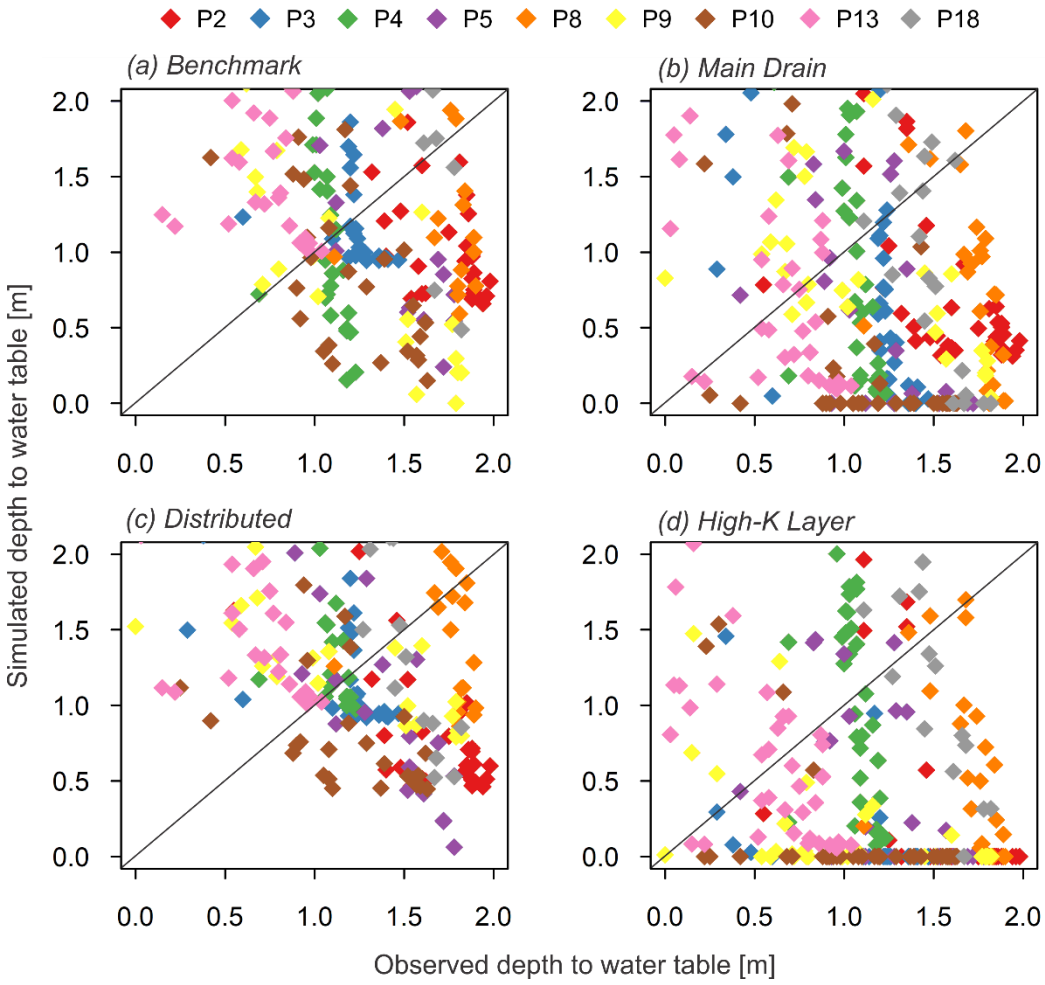

Figure 6.13 - Scatter plots of observed versus simulated depth to water table for 9 piezometers in Fensholt. The maximum depth shown is 2 m, which is the lowermost screen depth of the piezometers. For each plot, data points to the upper left of the diagonal line represent overestimated simulated values while data points to the lower right of the diagonal are underestimated simulated values.

The error analysis indicates that the depth to the water table was slightly better simulated using the Benchmark Model compared to the other models (Table 6.5). The average MAE and RMSE were above 0.79 and 0.93 for all models. These values are relatively high considering that depths to water table are around the drains level (1 m below ground surface). Field-scale models within the Fensholt catchment developed with finer grid resolution than our models simulated better MAE and RMSE (Boico et al., 2022b, Hansen et al., 2019a). However, our results are very satisfactory compared to modeling studies with similar mesh resolution (~50 m). Koch et al. (2019) simulated the depth to the shallow water table in a regional model in Denmark (Koch et al., 2019) and obtained a MAE of 0.76 m and a RMSE of 1.13 m, which are very similar than the errors calculated in our study. Hansen et al. (2013) calculated MAE

and RMSE equal to 1.03 m and 1.25 m, respectively, for a model calibrated with both stream discharge and hydraulic heads observations. These values are higher than the calculated for our models. The alternative soil models showed that only limited improvement was achieved using a single homogeneous soil layer and two different heterogeneous soil models to simulate the depth to water table (Table 6.5). Therefore, we conclude the performance of our models was satisfactory for simulating the depth to water table from 0 to 2 m below ground surface. No conclusion can be reached for depths to water table greater than 2 m since this is the lower limit for piezometer measurements.

6.5.5 Effect of soil heterogeneity in the simulations

The stream discharge at the outlet simulated using the four conceptual models for tile drains was similarly or slightly better simulated with the alternative soil models. The highest difference in the error performance was observed for the Distributed Model with the heterogeneous soil 1, where MAE, NSE and KGE improved by 0.09 mm/d, 0.20 and 0.18, respectively (Table 6.5). The four conceptual models had similar performance relative to each other regardless of the soil model, with the Benchmark Model performing better than the others to simulate the outlet stream discharge.

The Main Drain and High-K Layer Models showed better performance than the Benchmark and Distributed Models to simulate the subcatchment stream discharge with the alternative soil models. Simulated subcatchment discharge was only mildly affected by the soil models, except for the Benchmark Model that was improved when simulated with the heterogeneous soil 2 with MAE, NSE and KGE varying from 0.62 mm/d, 0.16 and 0.11 to 0.45 mm/d, 0.60 and 0.45. An improvement was generally observed for all conceptual models based on the heterogeneous soil model 2, where NSE was higher than 0.51 for all simulations.

Two of the alternative soil parameters showed worse performance to simulate the drain discharge (Table 6.5). Little variation in the error analysis was observed for the depth to water table, with MAE varying from 0.77 to 0.97 m and RMSE varying from 0.91 to 1.11 m.

The error analysis suggests that NSE and KGE, used to evaluate the performance of the discharge dynamics, are more sensitive to the alternative soils and the conceptual models for tile drains than the MAE. Drain discharge dynamics are more sensitive to the soil heterogeneity than the tile drainage conceptualization. However, the subcatchment stream discharge is more sensitive to the tile drainage conceptualization. The drainage conceptualization and soil heterogeneity effect on the outlet stream discharge are comparable. This suggests that at smaller scales (drainage area) heterogeneity was more relevant than the drainage conceptualization to improve model results. However, at the subcatchment

scale, the opposite was observed and, at the catchment scale, both criteria had a comparable effect. We highlight that this analysis comprises only 3 alternative soil models and is limited to the studied catchment.

6.5 Discussion

6.5.1 Drain discharge

We expected the best simulation performance for the Main Drain Model, with calibrated hydraulic parameters, and the Benchmark Model, where the location of all mapped tile drains was explicitly represented and the mesh was more refined. The error analysis showed that the performance of the Benchmark and Distributed Models when simulating drain discharge was generally similar or worse than the performance of the Main Drain Model (Table 6.5, Figure 6.10). The MAE of daily drain discharge for the drainage areas in the period of 2014-2015 indicated that the models performed equally well (Figure 6.10a). Despite some relevant differences in the NSE results (Figure 6.10b), with the Distributed and Benchmark Models showing worse performance for drainage areas D1 and D2, respectively, the cumulative drain discharge volumes simulated from all models were generally similar (Figure 6.9). These results suggest that more accurately representing the locations of the individual tile drains does not necessarily improve the simulation of drain discharge at the catchment scale.

Improvements in the drain discharge simulation may be obtained by a better representation of the spatial variability of the structure and hydraulic properties of the subsurface in the catchment. In a hydrological model study developed for drainage area D5 (Figure 6.1b), Boico et al. (2022b) concluded that including average soil hydraulic properties can be sufficient to simulate tile drain discharge for a heterogeneous tile drainage area. However, tile drain discharge may greatly vary due to different soil textures from one tile-drained field to another within the same catchment (Eastman et al., 2010). Some authors identified that tile drainage is controlled by the hydrogeological properties of the surficial geology (Bednorz et al., 2016; Hansen et al., 2019b, De Schepper et al., 2017). The homogeneous soil layers model as included in our models may have hindered the local tile drainage simulation, since homogeneous soil layers are unlikely in Danish clayey till catchments.

We evaluated drain discharge simulations using four alternative soil models (Section 6.3.10) with the four conceptual models for tile drains (a total of 16 models). We concluded that drain discharge are sensitive to soil heterogeneity in the first 1.5 m from surface, regardless of which tile drain conceptualization was adopted (Table 6.5), suggesting that specific soil properties are relevant to simulate drain discharge. The heterogeneous soil models consist of random K fields developed based on the mean and variance of hydraulic conductivity values, resulting in inaccurate discharges for some drainage areas. Soil zonation can be specified in the catchment based on borehole and geophysical data to reduce parameter

uncertainty. However, this information is rarely available and field-scale heterogeneity is difficult to implement in the model at the catchment scale. We argue this is the main reason why the models were not able to reproduce the spatial dynamics of hydraulic heads, which influences the accuracy of the drain discharge simulations. Hansen et al. (2019b) evaluated drain discharge simulations varying the geological model below 3 m. In their study, the weekly NSE varied from 0.47 to 0.92 using different geological models, indicating that geological units located below 3 m also affect the simulated drain discharge. Our simulations suggest that drain discharge are more sensitive to the spatial variability of the soil parameters than the stream discharge. In this regard, a better representation of the tile drainage systems and the implementation of a drain conductance term may not overcome the lack of heterogeneity representation within the catchment.

6.5.2 Surface water

The four models performed satisfactorily to simulate the outlet stream discharge and could be recommended almost interchangeably. Simulated stream discharges at the outlet were less impacted by the conceptualization of the tile drains than the depth to water table, drain discharge and surface water depth in agricultural areas. One possible reason is that the outlet discharges represent the cumulative effect of hydrological processes taking place upstream, while piezometers, subcatchment stations and drainage areas are more sensitive to local conditions such as the mesh refinement, the number of tile drains, soil properties and topography.

Greater discrepancies were observed for the simulated subcatchment stream discharge. The Main Drain Model had a performance comparable to that of the High-K Layer Model, but the Benchmark and Distributed Models simulated distinct subcatchment stream discharge dynamics. The low stream discharges at the subcatchment station (S2) were better simulated by the Distributed Model, followed by the Benchmark, while the peaks were overestimated in all models. One possible reason that the Distributed Model simulated realistic low discharge at station S2 is that areas near the gauging station may include more tile drains than are shown in Figure 6.1b. In that case, representing tile drains in all agricultural areas may include tile drains omitted in the Main Drain and Benchmark Models. The High-K Layer Model creates preferential horizontal flow paths at the drain depth all over the catchment area. However, compared to the other models, it does not limit the water table rise above the drains level and water resurgence may occur near station S2 despite the presence of tile drains. Actually, simulations revealed that for wet conditions in winter, the surface water depth simulated by the High-K Layer Model was unexpectedly higher than 0.1 m in some tile-drained areas, which is not the case in the other models. Also, simulated depths to water table were often equal to zero near the tile drains, indicating that the water table is not adequately controlled by the drains. Simulations suggest that applying a high-

permeability layer is not the best suited concept to simulate the surface water depth conditions in tile-drained agricultural areas.

The cumulative stream discharge for the subcatchments is presented in Figure 6.9 for the entire 2014-2015 period. The tributary streams simulated different behavior between the four conceptualizations for tile drains, specially for the Benchmark Model, that simulated lower cumulated discharge volumes than the other models. Since the tributary streams were often dry during the 2-year simulation period, the simulated stream flow at stations S3 and S4 do not represent the continuous water flow coming from upstream, but water exfiltrated from the subsurface generating surface runoff near the stream station. Surface-subsurface water exchange and surface runoff generation are affected by the difference in the cell areas between the more refined mesh of the Benchmark Model and the coarser mesh of the other models (Figure 6.5). The larger cell elements of the coarser mesh have flatter topography, which reduces the representation of plan curvatures and local slopes, implying greater overland flow (Sulis et al., 2011), and possibly increasing the stream discharge at S3 and S4 when using the coarser mesh.

6.5.3 Depth to groundwater

The difficulty in simulating the water table behavior could be caused by specifying homogeneous soil layers for the entire catchment. In a hydrological model study developed for drainage area D5, Boico et al. (2022b) stated that including local soil heterogeneity in drainage area D5 results in a markedly different spatial resolution in hydraulic heads compared to the homogeneous approach. Analogous to the previous study, the piezometers in our studied catchment are installed from ground surface to a depth of 2 m, and the water table is expected to vary around 1 m below the ground. Hence, the soil properties may have great influence on the measured depths to water table. We demonstrated, however, that similar error performance was obtained with the implementation of three different soil models (one homogeneous and two heterogeneous). One of the reasons of the similar results is the coarser resolution of the model, that may not capture the water table fluctuation compared to the field-scale model developed by Boico et al. (2022b). Furthermore, in a modeling study in a clayey till catchment in Denmark, Hansen et al. (2013) argued that the misrepresentation of heterogeneity in the geological model was the main reason why their model was not able to reproduce the spatial dynamics in hydraulic heads. In this study, we applied the geological model developed in a larger scale model of approximately 101 km^2 area (He et. al., 2015), which may provide coarse information for our catchment-scale model.

The High-K Layer Model underestimates the depths to water table in many piezometers, probably due to the saturation of the high-permeability layer, along with the water table rise above the level of tile drains as mentioned in Section 6.5.2. In the models that used seepage nodes, fully saturated conditions only occur below the tile drains nodes. Hence, models with many seepage nodes such as the Distributed

Model and the Benchmark (Figure 6.4) simulated higher depths to water table below ground in the agricultural areas (Figure 6.13a and c).

6.5.4 Limitations of the model application

The time lag between the transfer of water from the soil to the drain and the release of water from the drain to the outlet cannot be simulated using seepage nodes. However, typical drain water velocities from 0.05 to 1.5 m/s (Szejba and Bajkowski, 2019; Sammons et al., 2005) are relatively high and the time lag of drainage flow may be short, which justifies our assumption to neglect this time-lag. We assumed that using the sum of discharge at all active seepage nodes into a drainage area was a suitable approximation to represent the cumulative drain discharge. However, tile drain flow lag time may be a crucial parameter to calibrate a model to tile drain discharge (Du et al., 2019).

We considered that the simulation times of the models were too long (around 2 to 3 days for a 2-year simulation) for automatic calibration using a parameter estimation software, such as PEST (Doherty, 1994, 2018). A manual trial-and-error calibration was therefore adopted, resulting in realistic simulations for the surface water discharge and saturation. We acknowledge, however, that automatic calibration including soft knowledge is more likely to result in a unique solution and enhance the forecast of the model (Hunt et al., 2020) and that the application of cloud computing can be used for rapid calibration of highly parameterized models (Berg et al., 2019).

In an integrated surface-subsurface flow model of a 4.2 km² catchment with similar mesh configuration than in our study, Partington et al. (2013) stated that a better spatial discretization in the wetlands and streams would enhance the simulation of the surface-subsurface water exchange, such as the groundwater discharges and rainfall infiltration in the wetlands. The Fensholt catchment contains large wetland areas and the stream widths are less than 3 m, requiring extreme refined meshes. Here the mesh had a maximum 10 m length around the streams and it is rarely smaller than 5 m, so we expect some discrepancy in the simulation of wetlands and streams for a hydrologic year.

The current version of HydroGeoSphere cannot simultaneously implement the return flow from the drainage system to the surface and an equivalent conductance term for tile drains. Over time, many tile drains will become clogged with roots or sediment, and the drain walls will become less permeable. Including a tile drain conductance term would certainly lower the drain discharge estimation and generate more flooding conditions in the winter, as stated by (Colombani et al., 2016). New releases may allow a more comprehensive application of the present study where the drain resistance to flow is also implemented in the model.

The simulation times for the High-K and Benchmark Models were around 1 day longer than the Main Drain and Distributed Models (Table 6.5). An explanation for the longer simulation times is the mesh refinement of the Benchmark Model and the numerical challenges due to high water table fluctuation and surface-subsurface water exchange in some areas of the catchment when using the High-K model. However, the simulation times may be reduced for the High-K Layer and Distributed Models by further simplifying the numerical mesh, since no refinement is necessary around the tile drain paths.

The number of alternative soil conceptualizations in our study is very limited and only useful as a reference to evaluate the parameters uncertainty in tile drainage modeling at the catchment scale. We suggest the implementation of different conceptual models to better represent the space of plausible heterogeneity structures and the variability of hydraulic parameter values. However, non-uniqueness is inherent to highly parameterized models (Refsgaard et al 2012; Zhou et al., 2014; Hill et al., 2016; Delottier et al., 2017; Aster et al., 2018) and may arise even with improvements in the model structure and parameter values.

6.6 Conclusion

We investigated two novel conceptual models for tile drains where seepage nodes are implemented in a model for the main collector drains and in anther where they are distributed over the entire agricultural area at the drain depth, applied in an agricultural catchment in Denmark. These conceptualizations were compared to a complex model representing all tile drain paths with seepage nodes and a commonly used model with a high-permeability layer. The four models performed satisfactorily to simulate the outlet stream discharge and could be recommended almost interchangeably. Results indicated that the three models using the seepage nodes concept i) simulated similar monthly discharges and cumulative discharge volumes for most of the studied tile-drained areas and ii) simulated realistic surface water depths in tile-drained fields with no runoff or ponding water. When seepage nodes were applied over all agricultural areas in the model, the simulated low stream discharge was in very good agreement with measured data. This model, and the model with seepage nodes representing the main drain paths, run around 35% faster than the model explicitly representing all tile drains for the same period. They are therefore better candidates for an automated model calibration.

Satisfactory results were obtained for the depth to water table below ground for the mesh resolution of our model study (~50m), specially for the models using the seepage nodes concept to simulate tile drains. A better reproduction of the shallow water table fluctuation may be necessary for a proper simulation of drain discharge, since tile drains are installed to lower the shallow water table level around 1 m below ground surface. However, all models had deficiencies to simulate drain discharge and the shallow depth

to water table at the tile drain level, highlighting the difficulty to use such a catchment model to accurately simulate the depth to water table at specific locations.

Four alternative soil models were developed to evaluate the effect of soil heterogeneity on the simulations. The drain discharge dynamics were more sensitive to the soil heterogeneity than the tile drainage conceptualization, suggesting that specific soil properties are relevant to simulate drain discharge.

When maps of the drain locations are available, but the modeling study is time constrained, the inclusion of only the main collector drains proposed by De Schepper et al. (2015; 2017) for an entire catchment proved suitable for simulating stream and drain discharge. Despite the availability of tile drain maps, including seepage nodes distributed over all agricultural areas is also a suitable approach. We suggest future research on artificial drainage systems in agricultural environments to focus on model calibration with a parameter estimation software to overcome the lack of representation of soil hydraulic properties.

Conclusions and perspectives

This PhD research evaluated the performance of hydrological models to simulate tile drain discharge, shallow groundwater dynamics, solute transport and stream discharge at the field and catchment scales. Subsurface drainage and solute mass discharge rates were simulated with fully-coupled 3D groundwater and surface water flow models under variably-saturated conditions. Extensive hydrological, geophysical and tile drain data were used to evaluate the effect of heterogeneity, macropores and the conceptualization of the tile drainage network in hydrological-solute models developed for two fields and a catchment with complex tile drainage systems. For large-scale hydrological modeling, the accuracy of the simulations is a trade-off with the computational processing times. The seepage node boundary condition was found to be suitable to simulate tile drainage and mass discharge and to explicitly represent drain locations while maintaining reasonable computational times and mesh refinement, for both field and catchment scales.

Tile drainage, hydraulic head and stream discharge simulation

The use of seepage nodes to represent tile drains in hydrological models allows for a physically-based, yet computationally-efficient representation of surface water flow in tile-drained fields. The seasonal variation of drain discharge was reasonably well simulated for a tile-drained agricultural field with significant hydrogeological heterogeneity (Chapter 4). However, difficulties encountered when developing a suitable conceptual model for a field with a steep slope and a dense drainage network (Chapter 5) hindered the simulation of some drain discharge peaks and the shallow hydraulic heads. Similar to the soil hydraulic properties, the arrangement of macropores in the field may vary with position along the hillslope, changing the residence time of the water in the system. The uniform distribution of macropores may have affected the simulation of drain discharge, hydraulic heads, and mass discharge in the field with a steep slope.

The inclusion of only the main collector drains proposed by De Schepper et al. (2015; 2017) for an entire catchment and the inclusion of seepage nodes distributed over all agricultural areas proved suitable for simulating stream and drain discharge. Furthermore, both models resulted in shorter computational times compared to a benchmark model representing the entire drainage system with seepage nodes, indicating they are better candidates for use in model calibration. These conceptualizations and the high-permeability layer to represent tile drains could be recommended almost interchangeably to simulate observed outlet stream discharge. The four conceptual models for tile drains applied at the catchment scale generally underestimated the drain discharge volumes. However, cumulative volumes simulated from all models were generally similar, suggesting that more accurately representing the locations of the

individual tile drains does not necessarily improve the simulation of drain discharge at the catchment scale.

Solute transport simulation

Proper simulation of the drain discharge and shallow hydraulic heads are essential for the simulation of the solute mass discharges. The hydrological-solute transport model (Chapter 5) was developed using a 3D surface and subsurface water flow model and included more soil layers than Varvaris et al. (2021b). The arrival time of bromide was accurately simulated in our model. However, a better representation of the spatial variation of the soil properties and macropores may be necessary to more accurately simulate the Br concentration dynamics at the drain outlet.

The solute mass transport simulations were most sensitive to the resistance of the drain wall and velocities in the topsoil layer. The calibrated parameters conformed with the expected anisotropy patterns at the study site. However, the model has homogeneous soil layers and a static macropore structure that can introduce uncertainties in the estimated parameters.

The explicit representation of tile drains using seepage nodes in the numerical model successfully captured the transport behavior around the location of tile drains at the field scale. This conceptualization simplifies the process of including tile drains in large-scale models and ensures fast computation times, representing an advance in modelling of tile-drained agricultural systems.

The models with homogeneous soil layers demonstrate coarse agreement with the observed spatial distribution of hydraulic heads, which is important when simulating nutrient reduction and transport processes dependent on water table elevation and moisture content. A better representation of the subsurface flow dynamics will improve subsequent simulations of the transport and fate of leached agrochemicals such as nitrate or phosphate.

Heterogeneity in tile-drained landscapes

This study demonstrated that depth-specific electrical conductivity estimates can be used with borehole data for mapping heterogeneities in clayey till soils. Simulations showed that including the topsoil heterogeneity improved the simulation of hydraulic heads and water table fluctuations, particularly where clay-rich zones had been identified, and generated flooded areas that are more representative of those observed during the wet seasons. Including average hydraulic properties of the soil layers in a 3D hydrological model was suitable to simulate tile drain discharge for a heterogeneous clayey-till field in Denmark. However, the homogeneous soil layers model may have hindered the tile drainage simulation for a dense tile-drained field with steep slopes (Chapter 5) and a catchment scale model (Chapter 6). At

the catchment scale, the drain discharge dynamics were more sensitive to the soil heterogeneity than the tile drainage conceptualization, suggesting that specific soil properties are relevant to simulate drain discharge. We argue that the incomplete representation of soil heterogeneity in the field-scale model with steep slopes and the catchment-scale model is the main reason for the difficulty in reproducing the shallow water levels in the piezometers and, consequently, the tile drain discharge.

The single porosity with immobile zone conceptual model

The implicit representation of macropores through calibration was suitable for hydrological simulations at the field and catchment scales. However, a dual-continuum approach for representing preferential flow paths through macropores was necessary to simulate solute mass discharge at the drain outlet. The single porosity with immobile zone conceptual model was simple to implement at the field scale and performed well when simulating the bromide concentration in the first two months after the tracer application. However, we cannot confirm the hypothesis that a single porosity with immobile zone conceptual model is adequate to simulate the Br peaks at the drain outlet and the late-time Br mass. A better representation of the soil heterogeneity and the spatial variation of the macropore density at the field-scale would be relevant to improve the hydrological and solute transport simulations. Improvements in the matrix diffusion and macropore advective transport may require a more robust dual continuum approach such as a dual permeability model. However, increasing model complexity may impair the modeler's understanding of the hydrological processes in tile-drained systems due to equifinality.

Perspectives for future research on tile drainage modeling

The delineated zones in Chapter 4 were based on sparse borehole data and EC estimates. However, the topography also plays an important role in recharge and surface runoff. Depression zones may affect the soil properties and alter the hydraulic heads and surface-subsurface water exchange. Future work could focus on delineating soil zones also based on topography.

Tile drain discharge is highly dependent on climate conditions (Williams et al., 2015; King et al., 2014). Climate interacts with topography and soil heterogeneity, affecting the temporal and spatial dynamics of the shallow water table, controlling tile drainage. We suggest simulating climate change scenarios to assess their influence on hydraulic heads and tile drainage in tile-drained catchments.

Nitrate concentrations in tile drainage water, piezometers and surface water could be used to develop hydrological and nitrate models to evaluate the potential of water contamination in tile-drained agricultural lands. However, nitrate transport modeling is complex due to the uncertainty on the spatial distribution of nitrate reduction in the subsurface and the lack of data on the history of the fertilizer

application in space and time (Refsgaard et al., 1999; 2014; Hansen et al., 2014). Future research could evaluate simplified approaches for nitrate flux modeling by applying a nitrogen budget method and integrating advection-dispersion equations in the model. Furthermore, scenarios of fertilizer application could be established to study the effect of new policies on surface and groundwater contamination.

Future modeling studies can simulate solute transport at the catchment scale using the simplified conceptual models for tile drains developed in Chapter 6. Since data on tile drain location is rarely available, the utilization of simplified conceptual models is inevitable. The comparison of different tile drainage conceptualizations to simulate solute transport in agricultural catchments is valuable for assessing the uncertainty in solute mass predictions using different approaches.

Finally, we suggest future research on artificial drainage systems in agricultural catchments with a focus on model calibration with parameter estimation software to overcome the lack of inclusion of heterogeneity in soil hydraulic properties.

Bibliography

Abbaspour, K. C., Kohler, A., S□ imu□ nek, J., Fritsch, M., Schulin, R. (2001). Application of a two-dimensional model to simulate flow and transport in a macroporous agricultural soil with tile drains. European Journal of Soil Science, 52(3), 433-447. doi:10.1046/j.1365-2389.2001.00389.x

Abrahamsen, P., Hansen, S. (2000). Daisy: an open soil-crop-atmosphere system model. Environmental Modelling and Software, 15(3), 313-330. doi:10.1016/S1364-8152(00)00003-7

Ajami, H., McCabe, M. F., Evans, J. P., Stisen, S. (2014). Assessing the impact of model spin-up on surface water-groundwater interactions using an integrated hydrologic model. Water Resour. Res., 50, 2636-2656. doi:10.1002/2013WR014258.

Akay, O., Fox, G. A., Šimůnek, J. (2008). Numerical Simulation of Flow Dynamics during Macropore–Subsurface Drain Interactions Using HYDRUS. Vadose Zone Journal, 7(3), 909-909. doi:10.2136/vzj2007.0148

Ala-Aho, P., Soulsby, C., Wang, H., Tetzlaff, D. (2017). Integrated surface-subsurface model to investigate the role of groundwater in headwater catchment runoff generation: A minimalist approach to parameterisation. Journal of Hydrology, 547(C), 664-677. doi:10.1016/j.jhydrol.2017.02.023

Almasri, M. N., Kaluarachchi, J. J. (2007). Modeling nitrate contamination of groundwater in agricultural watersheds. Journal of Hydrology, 343(3), 211-229. doi:10.1016/j.jhydrol.2007.06.016

Amado, A. A., Schilling, K., Jones, C., Thomas, N., Weber, L. (2017). Estimation of tile drainage contribution to streamflow and nutrient loads at the watershed scale based on continuously monitored data. Environmental Monitoring and Assessment, 189(9), 1-13. doi:10.1007/s10661-017-6139-4

Anderson, M. P., Woessner, W. W., Hunt, R. J. (2015). Applied Groundwater Modeling: Simulation of Flow and Advective Transport (Second ed.): Academic Press.

Aquanty Inc. (2017). HydroGeoSphere User Manual, 9–53. Retrieved from https://static1.squarespace.com/static/54611cc8e4b0f88a2c1abc57/t/581756cc03596e7961d2980d/1477924562972/hydrosphere_user.pdf

Arenas Amado, A., Schilling, K. E., Jones, C. S., Thomas, N., Weber, L. J. (2017). Estimation of tile drainage contribution to streamflow and nutrient loads at the watershed scale based on continuously

monitored data. Environmental Monitoring and Assessment, 189(9), 426. doi:10.1007/s10661-017-6139-4

Arnold, J. G., Srinivasan, R., Muttiah, R. S., Williams, J. R. (1998). Large area hydrologic modeling and assessment part I: Model development. Journal of the American Water Resources Association, 34(1), 73-89. doi:10.1111/j.1752-1688.1998.tb05961.x

Arrey, I. A., Odiyo, J. O., Makungo, R., Kataka, M. O. (2018). Effect of hysteresis on water flow in the vadose zone under natural boundary conditions, Siloam Village case study, South Africa. Journal of Hydroinformatics, 20(1), 134-148. doi:10.2166/hydro.2017.091

Aster, R. C., Borchers, B., Thurber, C. H. (2018). Parameter estimation and inverse problems. (Third edition. ed.). Retrieved from https://www.sciencedirect.com/science/book/9780128046517. doi: 10.1016/C2015-0-02458-3

Auken, E., Christiansen, A. V., Kirkegaard, C., Fiandaca, G., Schamper, C., Behroozmand, A. A., Binley, A., Nielsen, E., Effersø, F., Christensen, N. B., Sørensen, K., Foged, Nikolaj Vignoli, G. (2015). An overview of a highly versatile forward and stable inverse algorithm for airborne, ground-based and borehole electromagnetic and electric data. Exploration geophysics., 46(3), 223-235.

Auken, E., Viezzoli, A., Christensen, A. (2009). A single software for processing, inversion, and presentation of AEM data of different systems: the Aarhus Workbench. ASEG Extended Abstracts, 2009(1), 1. doi:10.1071/ASEG2009ab062

Ayars, J. E., Christen, E. W., Hornbuckle, J. W. (2006). Controlled drainage for improved water management in arid regions irrigated agriculture. Agricultural Water Management, 86(1), 128-139. doi:10.1016/j.agwat.2006.07.004

Bailey, R. T., Bieger, K., Flores, L., Tomer, M. (2022). Evaluating the contribution of subsurface drainage to watershed water yield using SWAT+ with groundwater modeling. Science of the Total Environment, 802. doi:10.1016/j.scitotenv.2021.149962

Bednorz, D., Tauchnitz, N., Christen, O., Rupp, H., Meissner, R. (2016). The Impact of Soil Heterogeneity on Nitrate Dynamic and Losses in Tile-Drained Arable Fields. Water, Air, and Soil Pollution, 227(10), 1-18. doi:10.1007/s11270-016-3095-5

Berg, S. J., Grosso, N. R., Sherrier, M. P., Mudrick, K., Ohr, M., Hwang, H.-T., Park, Y-J, Callaghan, M. V., Frey, S. K., Sudicky, E. A. (2019). Natural Stimuli Calibration with Fining Direction Regularization in an Integrated Hydrologic Model. Ground Water, 57(1), 21. doi:10.1111/gwat.12842

Berg, S. J., Sudicky, E. A. (2019). Toward Large-Scale Integrated Surface and Subsurface Modeling. Ground Water, 57(1), 1. doi:10.1111/gwat.12844

Beven, K. (2006). A manifesto for the equifinality thesis. Journal of Hydrology, 320(1), 18-36. doi:10.1016/j.jhydrol.2005.07.007

Beven, K., Freer, J. (2001). Equifinality, data assimilation, and uncertainty estimation in mechanistic modelling of complex environmental systems using the GLUE methodology. Journal of Hydrology, 249(1), 11-29. doi:10.1016/S0022-1694(01)00421-8

Bieger, K., Arnold, J. G., Rathjens, H., White, M. J., Bosch, D. D., Allen, P. M., Volk, M., Srinivasan, R. (2017). Introduction to SWAT+, A Completely Restructured Version of the Soil and Water Assessment Tool. JAWRA Journal of the American Water Resources Association, 53(1), 115-130. doi:10.1111/1752-1688.12482

Bishop, J. M., Callaghan, M. V., Cey, E. E., Bentley, L. R. (2015). Measurement and simulation of subsurface tracermigration to tile drains in low permeability,macroporous soil. Water Resources Research, 51, 9127-9140. doi:10.1002/2014WR016259

Blann, K. L., Anderson, J. L., Sands, G. R., Vondracek, B. (2009). Effects of Agricultural Drainage on Aquatic Ecosystems: A Review. Critical Reviews in Environmental Science and Technology, 39(11), 909-1001. doi:10.1080/10643380801977966

Blöschl, G., Sivapalan, M. (1995). Scale issues in hydrological modelling: A review. Hydrological Processes, 9(3-4), 251-290. doi:10.1002/hyp.3360090305

Boico, V. F., Therrien, R., Delottier, H., Young, N. L., Højberg, A. L. (2022a). Comparing alternative conceptual models for tile drains and soil heterogeneity for the simulation of tile drainage in agricultural catchments. Journal of Hydrology, 612(Part A). doi:10.1016/j.jhydrol.2022.128120

Boico, V. F., Therrien, R., Højberg, A. L., Iversen, B. V., Koganti, T., Varvaris, I. (2022b). Using depth specific electrical conductivity estimates to improve hydrological simulations in a heterogeneous tile-drained field. Journal of Hydrology, 604. doi:10.1016/j.jhydrol.2021.127232

Boland-Brien, S. J., Basu, N. B., Schilling, K. E. (2014). Homogenization of spatial patterns of hydrologic response in artificially drained agricultural catchments. Hydrological Processes, 28(19), 5010-5020. doi:10.1002/hyp.9967

Boles, C. M. W., Frankenberger, J. R., Moriasi, D. N. (2015). Tile drainage simulation in SWAT 2012: Parameterization and evaluation in an Indiana watershed. Transactions of the ASABE, 58(5), 1201-1213.

Bonton, A., Bouchard, C., Rouleau, A., Rodriguez, M. J., Therrien, R. (2012). Calibration and validation of an integrated nitrate transport model within a well capture zone. Journal of Contaminant Hydrology, 128(1-4), 1-18. doi:10.1016/j.jconhyd.2011.10.007

Børgesen, C., Schaap, M. (2005). Point and parameter pedotransfer functions for water retention predictions for Danish soils. Geoderma (Amsterdam), 127(1-2), 154-167.

Bouraoui, F., Vachaud, G., Haverkamp, R., Normand, B. (1997). A distributed physical approach for surface-subsurface water transport modeling in agricultural watersheds. Journal of Hydrology, 203(1), 79-92. doi:10.1016/S0022-1694(97)00085-1

Branger, F., Tournebize, J., Carluer, N., Kao, C., Braud, I., Vauclin, M. (2009). A simplified modelling approach for pesticide transport in a tile-drained field: The PESTDRAIN model. Agricultural Water Management, 96(3), 415-428. doi:10.1016/j.agwat.2008.09.005

Brown, C. D., van Beinum, W. (2009). Pesticide transport via sub-surface drains in Europe. Environmental Pollution, 157(12), 3314-3324. doi:10.1016/j.envpol.2009.06.029

Burrows, W., Doherty, J., 2015. Efficient Calibration/Uncertainty Analysis Using Paired Complex/Surrogate Models. Groundwater 53, 531–541. doi:10.1111/gwat.12257

Callegary, J. B., Ferré, T. P. A., and Groom, R. W. (2007). Vertical Spatial Sensitivity and Exploration Depth of Low-Induction-Number Electromagnetic-Induction Instruments. Vadose Zone Journal, 6(1), 158-167. doi:10.2136/vzj2006.0120

Callegary, J. B., Ferré, T. P. A., Groom, R. W. (2012). Three-Dimensional Sensitivity Distribution and Sample Volume of Low-Induction-Number Electromagnetic-Induction Instruments. Soil Science Society of America Journal, 76(1), 85-91. doi:10.2136/sssaj2011.0003

Camporese, M., Paniconi, C., Putti, M., McDonnell, J. J. (2019). Fill and Spill Hillslope Runoff Representation With a Richards Equation-Based Model. Water Resources Research, 55(11), 8445-8462. doi:10.1029/2019WR025726

Carle, S. F. (1999). T-PROGS: Transition probability geostatistical software (version 2.1). University of California.

Carluer, N., De Marsily, G. (2004). Assessment and modelling of the influence of man-made networks on the hydrology of a small watershed: Implications for fast flow components, water quality and landscape management. Journal of Hydrology, 285(1-4), 76-95. doi:10.1016/j.jhydrol.2003.08.008

Chae, G.-T., Kim, K., Yun, S.-T., Kim, K.-H., Kim, S.-O., Choi, B.-Y., Kim, H.-S., Rhee, C. W. (2004). Hydrogeochemistry of alluvial groundwaters in an agricultural area: an implication for groundwater contamination susceptibility. Chemosphere, 55(3), 369-378. doi:10.1016/j.chemosphere.2003.11.001

Chow, R., Frind, M. E., Frind, E. O., Jones, J. P., Sousa, M. R., Rudolph, D. L., Molson, J. W., Nowak, W. (2016). Delineating baseflow contribution areas for streams – A model and methods comparison. Journal of Contaminant Hydrology, 195, 11-22. doi:10.1016/j.jconhyd.2016.11.001

Christiansen, A., Pedersen, J., Auken, E., Soe, N., Holst, M., Kristiansen, S. M. (2016). Improved Geoarchaeological Mapping with Electromagnetic Induction Instruments from Dedicated Processing and Inversion. REMOTE SENSING, 8(12). doi:10.3390/rs8121022

Christiansen, J. S., Thorsen, M., Clausen, T., Hansen, S., Christian Refsgaard, J. (2004). Modelling of macropore flow and transport processes at catchment scale. Journal of Hydrology, 299(1-2), 136-158. doi:10.1016/j.jhydrol.2004.04.029

Cle□ ment, J.-C., Aquilina, L., Bour, O., Plaine, K., Burt, T. P., Pinay, G. (2003). Hydrological flowpaths and nitrate removal rates within a riparian floodplain along a fourth-order stream in Brittany (France). Hydrological Processes, 17(6), 1177-1195. doi:10.1002/hyp.1192

Cochand, F., Therrien, R., Lemieux, J.-M. (2018). Integrated Hydrological Modeling of Climate Change Impacts in a Snow-Influenced Catchment. Ground Water, 57(1). doi:10.1111/gwat.12848

Corwin, D. L., Lesch, S. M. (2004). Apparent soil electrical conductivity measurements in agriculture. Computers and Electronics in Agriculture. doi:10.1016/j.compag.2004.11.005

Davis, D. M., Gowda, P. H., Mulla, D. J., Randall, G. W. (2000). Modeling Nitrate Nitrogen Leaching in Response to Nitrogen Fertilizer Rate and Tile Drain Depth or Spacing for Southern Minnesota, USA. Journal of environmental quality, 29(5), 1568-1581. doi:10.2134/jeq2000.00472425002900050026x

Davis, J. H., Griffith, S. M., Wigington, P. J. (2011). Surface Water and Groundwater Nitrogen Dynamics in a Well Drained Riparian Forest within a Poorly Drained Agricultural Landscape. Journal of environmental quality, 40(2), 505-516. doi:10.2134/jeq2010.0310

De Schepper, G., Therrien, R., Refsgaard, J. C., Hansen, A. L. (2015). Simulating coupled surface and subsurface water flow in a tile-drained agricultural catchment. Journal of Hydrology, 521, 374-388. doi:10.1016/j.jhydrol.2014.12.035

De Schepper, G., Therrien, R., Refsgaard, J. C., He, X., Kjærgaard, C., Iversen, B. V. (2017). Simulating seasonal variations of tile drainage discharge in an agricultural catchment. Water Resources Research, 3896-3920. doi:10.1002/2016WR020209

Delottier, H., Pryet, A., Dupuy, A. (2017). Why Should Practitioners be Concerned about Predictive Uncertainty of Groundwater Management Models? Water Resources Management : An International Journal - Published for the European Water Resources Association (EWRA), 31(1), 61-73. doi:10.1007/s11269-016-1508-2

Doherty, J. (1994). PEST: A Unique Computer Program for Model-independent Parameter Optimisation. Water Down Under, 94, 551–554.

Doherty, J. (2018). PEST, Model-Independent Parameter Estimation User Manual. Brisbane, Australia: Watermark Numerical Computing.

Doherty, J. (2016a). PEST: Model-independent parameter estimation. User Manual Part 1: PEST, SENSAN and Global Optimisers - 6th Edition published in 2016, http://www.pesthomepage.org/Downloads.php, watermark numerical computing, brisbane, australia ed.

Doherty, J. (2016b). PEST: Model-independent parameter estimation. User Manual Part 2: PEST Utility Support Software - 6th Edition published in 2016, http://www.pesthomepage.org/Downloads.php, watermark numerical computing, brisbane, australia ed.

Doherty, J., Hunt, R. J. (2009). Two statistics for evaluating parameter identifiability and error reduction. Journal of Hydrology, 366(1), 119-127. doi:10.1016/j.jhydrol.2008.12.018

Dorner, J., Horn, R. (2006). Anisotropy of pore functions in structured Stagnic Luvisols in the Weichselian moraine region in N Germany. Journal of Plant Nutrition and Soil Science, 169(2), 213-220.

Du, B., Saleh, A., Jaynes, D. B., Arnold, J. G. (2006). Evaluation of SWAT in Simulating Nitrate Nitrogen and Atrazine Fates in a Watershed with Tiles and Potholes. TRANSACTIONS- ASABE, 49(4), 949-1068.

Dualem Inc. (2008). DUALEM-21S user's manual. Dualem Inc., Milton, ON, Canada. 2008.

Earthdata. (2015). MODIS Collection 6 (C6) LAI / FPAR Product User ' s Guide. Retrieved from https://lpdaac.usgs.gov/documents/2/mod15_user_guide.pdf

Eastman, M., Gollamudi, A., Stämpfli, N., Madramootoo, C. A., Sarangi, A. (2010). Comparative evaluation of phosphorus losses from subsurface and naturally drained agricultural fields in the Pike River watershed of Quebec, Canada. Agricultural Water Management, 97(5), 596-604. doi:10.1016/j.agwat.2009.11.010

Ebel, B. A., Loague, K. (2006). Physics-based hydrologic-response simulation: Seeing through the fog of equifinality. Hydrological Processes, 20(13), 2887-2900. doi:10.1002/hyp.6388

Eidem, J., Simpkins, W., Burkart, M. (1999). Geology, groundwater flow, and water quality in the Walnut Creek watershed. Journal of environmental quality, 28(1), 60-69. doi:10.2134/jeq1999.00472425002800010006x

Evans, R. O., Wayne Skaggs, R., Wendell Gilliam, J. (1995). Controlled versus Conventional Drainage Effects on Water Quality. Journal of irrigation and drainage engineering, 121(4), 271-276. doi:10.1061/(ASCE)0733-9437(1995)121:4(271)

European Union. (2008). The Water Framework Directive. Retrieved from http://ec.europa.eu/environment/water/participation/pdf/waternotes/water_note9_other_water_legislation.pdf

Fleckenstein, J. H., Niswonger, R. G., Fogg, G. E. (2006). River-aquifer interactions, geologic heterogeneity, and low-flow management. Ground Water, 44(6), 837–852. https://doi.org/10.1111/j.1745-6584.2006.00190.x

Ford, W., King, K., Williams, M., Williams, J., Fausey, N. (2015). Sensitivity Analysis of the Agricultural Policy/Environmental eXtender (APEX) for Phosphorus Loads in Tile-Drained Landscapes. Journal of environmental quality, 44(4), 1099-1110. doi:10.2134/jeq2014.12.0527

Francesconi, W., Smith, D. R., Heathman, G. C., Wang, X., Williams, C. O. (2014). Monitoring and APEX Modeling of No-Till and Reduced-Till in Tile-Drained Agricultural Landscapes for Water Quality. TRANSACTIONS- ASABE, 57(3), 777-790.

Frederiksen Rasmus Rumph, R. R., Frederiksen, R. R., Molina-Navarro, E. (2021). The importance of subsurface drainage on model performance and water balance in an agricultural catchment using SWAT and SWAT-MODFLOW. Agricultural Water Management, 255.

Frei, S., Fleckenstein, J. H. (2014). Representing effects of micro-topography on runoff generation and sub-surface flow patterns by using superficial rill/depression storage height variations. Environmental Modelling Software, 52, 5-18. doi:10.1016/j.envsoft.2013.10.007

Frey, S. K., Hwang, H. T., Park, Y. J., Hussain, S. I., Gottschall, N., Edwards, M., Lapen, D. R. (2016). Dual permeability modeling of tile drain management influences on hydrologic and nutrient transport characteristics in macroporous soil. Journal of Hydrology, 535, 392-406. doi:10.1016/j.jhydrol.2016.01.073

Frey, S. K., Rudolph, D. L., Lapen, D. R., Ball Coelho, B. R. (2012). Viscosity dependent dual-permeability modeling of liquid manure movement in layered, macroporous, tile drained soil. Water Resources Research, 48(3). doi:10.1029/2011WR010809

Gärdenäs, A. I., Šimůnek, J., Jarvis, N., van Genuchten, M. T. (2006). Two-dimensional modelling of preferential water flow and pesticide transport from a tile-drained field. Journal of Hydrology, 329(3-4), 647-660. doi:10.1016/j.jhydrol.2006.03.021

Gerke, H. H., van Genuchten, M. T. (1993). Dual porosity model for simulating the prefrential movement of water and solutes in structured porous media. Water Resources Research, 29(2), 305-319.

Gerrits, A. M. J., Pfister, L., Savenije, H. H. G. (2010). Spatial and temporal variability of canopy and forest floor interception in a beech forest. Hydrological Processes, 24(21), 3011-3025. doi:10.1002/hyp.7712

Goderniaux, P., Brouyère, S., Fowler, H. J., Blenkinsop, S., Therrien, R., Orban, P., Dassargues, A. (2009). Large scale surface–subsurface hydrological model to assess climate change impacts on groundwater reserves. Journal of Hydrology, 373(1), 122-138. doi:https://doi.org/10.1016/j.jhydrol.2009.04.017

Gramlich, A., Stoll, S., Stamm, C., Walter, T., Prasuhn, V. (2018). Effects of artificial land drainage on hydrology, nutrient and pesticide fluxes from agricultural fields - A review. Agriculture, Ecosystems and Environment, 266, 84-99. doi:10.1016/j.agee.2018.04.005

Gupta, H. V., Kling, H., Yilmaz, K. K., Martinez, G. F. (2009). Decomposition of the mean squared error and NSE performance criteria: Implications for improving hydrological modelling. Journal of Hydrology, 377(1-2), 80-91. doi:10.1016/j.jhydrol.2009.08.003

Hansen, A. L., Christensen, B. S. B., Ernstsen, V., He, X., Refsgaard, J. C. (2014). A concept for estimating depth of the redox interface for catchment-scale nitrate modelling in a till area in Denmark. Hydrogeology Journal, 22(7), 1639-1655. doi:10.1007/s10040-014-1152-y

Hansen, A.L., Jakobsen, R., Refsgaard, J.C., Højberg, A.L., Iversen, B.V., Kjaergaard, C. (2019a). Groundwater dynamics and effect of tile drainage on water flow across the redox interface in a Danish Weichsel till area. Adv. Water Resour. 123, 23–39. doi:10.1016/j.advwatres.2018.10.022.

Hansen, A. L., Refsgaard, J. C., Baun Christensen, B. S., Jensen, K. H. (2013). Importance of including small-scale tile drain discharge in the calibration of a coupled groundwater-surface water catchment model. Water Resources Research, 49(1), 585-603. doi:10.1029/2011WR011783

Hansen, A.L., Storgaard, A., He, X., Højberg, A.L., Refsgaard, J.C., Iversen, B.V., Kjaergaard, C. (2019b). Importance of geological information for assessing drain flow in a Danish till landscape. Hydrol. Process. 33, 450–462. doi:10.1002/ hyp.13338.

Hansen, J. R., Refsgaard, J. C., Ernstsen, V., Hansen, S., Styczen, M., Poulsen, R. N. (2009). An integrated and physically based nitrogen cycle catchment model. Hydrology Research, 40, 347-347. doi:10.2166/nh.2009.035

Haws, N. W., Rao, P. S. C., Simunek, J., Poyer, I. C. (2005). Single-porosity and dual-porosity modeling of water flow and solute transport in subsurface-drained fields using effective field-scale parameters. Journal of Hydrology, 313(3-4), 257-273. doi:10.1016/j.jhydrol.2005.03.035

He, X., Højberg, A. L., Jørgensen, F., Refsgaard, J. C. (2015). Assessing hydrological model predictive uncertainty using stochastically generated geological models. Hydrological Processes, 29(19), 4293-4311. doi:10.1002/hyp.10488

He, X., Koch, J., Sonnenborg, T. O., Flemming, J., Schamper, C., Refsgaard, J. C. (2014). Transition probability-based stochastic geological modeling using airborne geophysical data and borehole data. Water Resources Research, 1-23. doi:10.1002/2013WR014593.Received

Heil, K., Schmidhalter, U. (2012). Characterisation of soil texture variability using the apparent soil electrical conductivity at a highly variable site. Computers and Geosciences, 39, 98-110. doi:10.1016/j.cageo.2011.06.017

Hill, A. R. (2019). Groundwater nitrate removal in riparian buffer zones: a review of research progress in the past 20 years. Biogeochemistry : An International Journal, 143(3), 347-369. doi:10.1007/s10533-019-00566-5

Hill, A. R. (1996). Nitrate Removal in Stream Riparian Zones. Journal of Environment Quality, 25(4), 743-743. doi:10.2134/jeq1996.00472425002500040014x

Hill, M. C. (2006). The practical use of simplicity in developing ground water models. Ground Water, 44(6), 775-781. doi:10.1111/j.1745-6584.2006.00227.x

Hill, M.C., Kavetski D., Clark M., Ye M., Arabi M., Lu D., Foglia L., Mehl S. (2016) Practical use of computationally frugal model analysis methods, Groundwater, 54(2): 159-170.

Hill, M. C., Tiedeman, C. R. (2007). Effective groundwater model calibration with analysis of data, sensitivities, predictions, and uncertainty. Hoboken, N.J.: Wiley-Interscience.

Hinsby, K., Troldborg, L., Purtschert, R., Corcho, J. A. A. (2006). Integrated dynamic modelling of tracer transport and long-term groundwater/surface water interaction using four 30 year 3H time series and multiple tracers for groundwater dating. Retrieved from: http://www-pub.iaea.org/MTCD/Publications/PDF/te_1507_web/PDF/TE_1507.pdf

Holbak, M., Abrahamsen, P., Diamantopoulos, E. (2021). A Physically Based Model for Preferential Water Flow and Solute Transport in Drained Agricultural Fields. Water Resources Research, 57(3). doi:10.1029/2020WR027954

Houmark-Nielsen, M., Henrik Kjær, K. (2003). Southwest Scandinavia, 40-15 kyr BP: palaeogeography and environmental change. Journal of Quaternary Science, 18(8), 769-786. doi:10.1002/jqs.802

Huang, J., Monteiro Santos, F. A., Triantafilis, J. (2016). Mapping soil water dynamics and a moving wetting front by spatiotemporal inversion of electromagnetic induction data. Water Resources Research, 52(11), 9131-9145. doi:10.1002/2016WR019330

Huang, J., Pedrera-Parrilla, A., Vanderlinden, K., Taguas, E. V., Gómez, J. A., Triantafilis, J. (2017). Potential to map depth-specific soil organic matter content across an olive grove using quasi-2d and quasi-3d inversion of DUALEM-21 data. Catena, 152(C), 207-217. doi:10.1016/j.catena.2017.01.017

Hümann, M., Schüler, G., Müller, C., Schneider, R., Johst, M., Caspari, T. (2011). Identification of runoff processes - The impact of different forest types and soil properties on runoff formation and floods. Journal of Hydrology, 409(3), 637-649. doi:10.1016/j.jhydrol.2011.08.067

Hunt, R. J., Fienen, M. N., White, J. T. (2020). Revisiting "An Exercise in Groundwater Model Calibration and Prediction" After 30 Years: Insights and New Directions. Ground Water, 58(2), 168-182. doi:10.1111/gwat.12907

Hwang, H.-T., Frey, S. K., Park, Y.-J., Pintar, K. D. M., Lapen, D. R., Thomas, J. L., Spoelstra, J., Schiff, S. L., Brown, S. J., Sudicky, E. A. (2019). Estimating cumulative wastewater treatment plant discharge influences on acesulfame and Escherichia coli in a highly impacted watershed with a fully-integrated modelling approach. Water Research, 157, 647-662. doi:10.1016/j.watres.2019.03.041

Iversen, B. V., Børgesen, C. D., Lægdsmand, M., Greve, M. H., Heckrath, G., Kjærgaard, C. (2011). Risk Predicting of Macropore Flow using Pedotransfer Functions, Textural Maps, and Modeling. Vadose Zone Journal, 10(4), 1185-1185. doi:10.2136/vzj2010.0140

Iversen, B. V., Moldrup, P., Loll, P. (2004). Runoff modelling at two field slopes: use of in situ measurements of air permeability to characterize spatial variability of saturated hydraulic conductivity. Hydrological Processes, 18(5), 1009-1026. doi:10.1002/hyp.1455

Jarvis, N. J. (2007). A review of non-equilibrium water flow and solute transport in soil macropores: Principles, controlling factors and consequences for water quality. European Journal of Soil Science, 58(3), 523-546. doi:10.1111/j.1365-2389.2007.00915.x

Jarvis, N. J. (1998a). Modeling the impact of preferential flow on nonpoint source pollution. In: Selim, H.M., Ma, L. (Eds.), Physical Nonequilibrium in Soils: Modeling and Application, Ann Arbor Press, Chelsea, MI, pp. 195–221.

Jarvis, N. J. (1998b). Physical Nonequilibrium in Soils: Modeling and Application. Chelsea, MI.

Jarvis, N. J. (2020). A review of non-equilibrium water flow and solute transport in soil macropores: principles, controlling factors and consequences for water quality. European Journal of Soil Science, 71(3), 279-302. doi:10.1111/ejss.12973

Jensen, P. N., Boutrup, S., Svendsen, L. M., Blicher-Mathiasen, G., Wiberg-Larsen, P., Bjerring, R., Hansen, J. W., Ellermann, T., Thorling, L., Holm, A. G. (2013). Vandmiljø og natur 2012, NOVANA Tilstand og udvikling - faglig sammenfatning (Aquatic environment and Nature, NOVANA. State and trends - technical summary). Retrieved from http://dce2.au.dk/pub/SR78.pdf

Ju nior, R. P., Smelt, J. H., Boesten, J. J., Hendriks, R. F., van der Zee, S. E. (2004). Preferential flow of bromide, bentazon, and imidacloprid in a Dutch clay soil. Journal of environmental quality, 33(4), 1473-1486. doi:10.2134/jeq2004.1473

Kalita, P. K., Ward, A. D., Kanwar, R. S., McCool, D. K. (1998). Simulation of pesticide concentrations in groundwater using Agricultural Drainage and Pesticide Transport (ADAPT) model. Agricultural Water Management, 36(1), 23-44. doi:10.1016/S0378-3774(97)00056-5

Kaluarachchi, J. J., Parker, J. C. (1987). Effects of hysteresis with air entrapment on water flow in the unsaturated zone. Water Resources Research, 23(10), 1967-1976. doi:10.1029/WR023i010p01967

Kaown, D., Koh, D.-C., Mayer, B., Lee, K.-K. (2009). Identification of nitrate and sulfate sources in groundwater using dual stable isotope approaches for an agricultural area with different land use (Chuncheon, mid-eastern Korea). Agriculture, Ecosystems and Environment, 132(3), 223-231. doi:10.1016/j.agee.2009.04.004

Kazemi, H. V., Anderson, S. H., Goyne, K. W., Gantzer, C. J. (2008). Atrazine and alachlor transport in claypan soils as influenced by differential antecedent soil water content. Journal of environmental quality, 37(4), 1599-1607. doi:10.2134/jeq2007.0470

Kennedy, C. D., Bataille, C., Liu, Z., Ale, S., VanDeVelde, J., Roswell, C. R., Bowling, L. C., Bowen, G. J. (2012). Dynamics of nitrate and chloride during storm events in agricultural catchments with different

subsurface drainage intensity (Indiana, USA). Journal of Hydrology, 466-467, 1-10. doi:https://doi.org/10.1016/j.jhydrol.2012.05.002

Khongnawang, T., Zare, E., Zhao, D., Srihabun, P., Triantafilis, J. (2019). Three-Dimensional Mapping of Clay and Cation Exchange Capacity of Sandy and Infertile Soil Using EM38 and Inversion Software. Sensors (Basel, Switzerland), 19(18). doi:10.3390/s19183936

Kiesel, J., Fohrer, N., Schmalz, B., White, M. J. (2010). Incorporating landscape depressions and tile drainages of a northern German lowland catchment into a semi-distributed model. Hydrological Processes, 24(11), 1472-1486. doi:10.1002/hyp.7607

Kim, K.-H., Yun, S.-T., Choi, B.-Y., Chae, G.-T., Joo, Y., Kim, K., Kim, H.-S. (2009). Hydrochemical and multivariate statistical interpretations of spatial controls of nitrate concentrations in a shallow alluvial aquifer around oxbow lakes (Osong area, central Korea). Journal of Contaminant Hydrology, 107(3-4), 114-127. doi:10.1016/j.jconhyd.2009.04.007

King, K. W., Fausey, N. R., Williams, M. R. (2014). Effect of subsurface drainage on streamflow in an agricultural headwater watershed. Journal of Hydrology, 519(PA), 438-445. doi:10.1016/j.jhydrol.2014.07.035

Kirkham, D. (1949). Flow of ponded water into drain tubes in soil overlying an impervious layer. Eos, Transactions American Geophysical Union, 30(3), 369-385. doi:10.1029/TR030i003p00369

Kladivko, E. J., Frankenberger, J. R., Jaynes, D. B., Meek, D. W., Jenkinson, B. J., Fausey, N. R. (2004). Nitrate leaching to subsurface drains as affected by drain spacing and changes in crop production system. Journal of environmental quality, 33(5), 1803-1813

Klaus, J., Zehe, E. (2011). A novel explicit approach to model bromide and pesticide transport in connected soil structures. Hydrology and Earth System Sciences, 15(7), 2127-2144. doi:10.5194/hess-15-2127-2011

Klaus, J., Zehe, E. (2010). Modelling rapid flow response of a tile-drained field site using a 2D physically based model: assessment of 'equifinal' model setups. Hydrological Processes, 24, 1595-1609.

Klint, K., Gravesen, P. (1999). Fractures and biopores in Weichselian clayey till aquitards at Flakkebjerg, Denmark. Nordic Hydrology, 30(4-5), 267-284. doi:10.2166/nh.1999.0015

Klute, A., Dirksen, C. (1986). Hydraulic conductivity and diffusivity. Laboratory methods (A. Klute Ed.). Madison: SSSA Book Series, Soil Science Society of America.

Knoben, W. J. M., Freer, J. E., Woods, R. A. (2019). Technical note: Inherent benchmark or not? Comparing Nash–Sutcliffe and Kling–Gupta efficiency scores. Hydrology and Earth System Sciences, 23(10), 4323-4331. doi:10.5194/hess-23-4323-2019

Koch, S., Bauwe, A., Lennartz, B. (2013). Application of the SWAT model for a tile-drained lowland catchment in north-eastern Germany on subbasin scale. Water Resources Management, 27(3), 791-805. doi:10.1007/s11269-012-0215-x

Koch, J., Berger, H., Henriksen, H. J., Sonnenborg, T. O. (2019). Modelling of the shallow water table at high spatial resolution using random forests. Hydrology and Earth System Sciences, 23(11), 4603-4619. doi:10.5194/hess-23-4603-2019

Koganti, T., Moral, F. J., Rebollo, F. J., Huang, J., Triantafilis, J. (2017). Mapping cation exchange capacity using a Veris-3100 instrument and invVERIS modelling software. Science of the Total Environment, 599-600, 2156-2165. doi:10.1016/j.scitotenv.2017.05.074

Koganti, T., Narjary, B., Zare, E., Pathan, A. L., Huang, J., Triantafilis, J. (2018). Quantitative mapping of soil salinity using the DUALEM-21S instrument and EM inversion software. Land Degradation and Development, 29(6), 1768-1781. doi:10.1002/ldr.2973

Köhne, J. M., Köhne, S., S□ imu□ nek, J. (2004). Inverse Mobile-Immobile Modeling of Transport During Transient Flow: Effects of Between-Domain Transfer and Initial Water Content. Vadose Zone Journal, 3(4), 1309-1321. doi: 10.2136/vzj2004.1309

Kokulan, V., Akinremi, O., Moulin, A. P., Kumaragamage, D. (2018). Importance of terrain attributes in relation to the spatial distribution of soil properties at the micro scale: a case study. Canadian Journal of Soil Science, 98, 292-305. doi:10.1139/cjss-2017-0128

Konikow, L. F. (2011). The Secret to Successful Solute-Transport Modeling. Ground Water, 49(2), 144-159. doi:10.1111/j.1745-6584.2010.00764.x

Konyha, K. D., Skaggs, R. W., Gilliam, J. W. (1992). Effects of Drainage and Water-Management Practices on Hydrology. Journal of irrigation and drainage engineering, 118(5), 807-819. doi:10.1061/(ASCE)0733-9437(1992)118:5(807)

Krause, P., Boyle, D. P., Bäse, F. Comparison of different efficiency criteria for hydrological model assessment. Advances in Geosciences, 5, 89-97.

Kristensen, K. J., Jensen, S. E. (1975). A model for estimating actual evapotranspiration from potential evapotranspiration. Nordic Hydrology, 6, 170-188. doi:10.2166/nh.1975.012

Kroes, J. G., Van Dam, J. C., Bartholomeus, R. P., Groenendijk, P., Heinen, M., Hendriks, R. F. A., Mulder, H. M., Supit, I., Van Walsum, P. E. V. (2017). SWAP version 4: Theory description and user manual. Retrieved from Wageningen: www.wur.eu/environmental-research

Kruger, J., Franko, U., Fank, J., Stelzl, E., Dietrich, P., Pohle, M., Werban, U. (2013). Linking Geophysics and Soil Function Modeling-An Application Study for Biomass Production. Vadose Zone Journal, 12(4). doi:10.2136/vzj2013.01.0015

Labolle, E. M., Fogg, G. E. (2001). Role of molecular diffusion in contaminant migration and recovery in an alluvial aquifer system. Transport in Porous Media, 42(1), 155–179. https://doi.org/10.1007/978-94-017-1278-1_8

Lasserre, F., Razack, M., Banton, O. (1999). A GIS-linked model for the assessment of nitrate contamination in groundwater. Journal of Hydrology, 224(3), 81-90. doi:10.1016/S0022-1694(99)00130-4

Lemieux, J. M., Sudicky, E. A., Peltier, W. R., Tarasov, L. (2008). Dynamics of groundwater recharge and seepage over the Canadian landscape during the Wisconsinian glaciation. Journal of Geophysical Research: Earth Surface, 113(F1). doi:10.1029/2007JF000838

Lesaffre, B., Zimmer, D. (1988). Subsurface Drainage Peak Flows in Shallow Soil. Journal of irrigation and drainage engineering, 114(3), 387-406. doi:10.1061/(ASCE)0733-9437(1988)114:3(387)

Li, Q., Unger, A. J. A., Sudicky, E. A., Kassenaar, D., Wexler, E. J., Shikaze, S. (2008). Simulating the multi-seasonal response of a large-scale watershed with a 3D physically-based hydrologic model. Journal of Hydrology, 357(3), 317-336. doi:https://doi.org/10.1016/j.jhydrol.2008.05.024

Li, Z., Zhang, J. (2001). Calculation of Field Manning's Roughness Coefficient. Agricultural Water Management, 49(2), 153-161. doi:10.1016/S0378-3774(00)00139-6

Likos, W. J., Lu, N., Godt, J. W. (2014). Hysteresis and Uncertainty in Soil Water-Retention Curve Parameters. Journal of Geotechnical and Geoenvironmental Engineering, 140(4), 04013050. doi:10.1061/(ASCE)GT.1943-5606.0001071

Lin, H. C., Richards, D. R., Yeh, G. T., Cheng, J. R., Cheng, H. P., Jones, N. L. (1997). FEMWATER: A three-dimensional finite element computer model for simulating density dependent flow and transport in variably saturated media. Technical Report CHL-97-12, Waterways Experiment Station, U.S. Army Corps of Engineers, Vicksburg, MS, USA. 143 p. Retrieved from: homepage.usask.ca/ mjr347/gwres/femwref.pdf.

Ma, L., Malone, R. W., Heilman, P., Ahuja, L. R., Meade, T. (2007). Sensitivity of tile drainage flow and crop yield on measured and calibrated soil hydraulic properties. Geoderma, 140(3), 284-296.

Macrae, M. L., English, M. C., Schiff, S. L., Stone, M. (2007). Intra-annual variability in the contribution of tile drains to basin discharge and phosphorus export in a first-order agricultural catchment. Agricultural Water Management, 92(3), 171-182. doi:10.1016/j.agwat.2007.05.015

Maurer, T. (1997). Physikalisch begründete zeitkontinuierliche Modellierung des Wassertransports in kleinen ländlichen Einzugsgebieten. Mitteilungen des Instituts f{ü}r Hydrologie und Wasserwirtschaft. Heft 61. Thesis(November), 251-251.

Maxwell, R. M. (2013). A terrain-following grid transform and preconditioner for parallel, large-scale, integrated hydrologic modeling. Advances in Water Resources, 53, 109-117. doi:10.1016/j.advwatres.2012.10.001

McNeill, J. D. (1980). Electromagnetic terrain conductivity measurement at low induction numbers. Retrieved from Geonics Limited, Ontario, Canada.

Meals, D. W., Dressing, S. A., Davenport, T. E. (2010). Lag Time in Water Quality Response to Best Management Practices: A Review. Journal of environmental quality, 39(1), 85-96. doi:10.2134/jeq2009.0108

Merrick, D. P., Merrick, N. P. (2015). AlgoMesh: A new software tool for building unstructured grid models. Paper presented at the Modflow and More 2015, Golden, Colorado: Colorado School of Mines.

Merz, B., Bárdossy, A. (1998). Effects of spatial variability on the rainfall runoff process in a small loess catchment. Journal of Hydrology, 212(1/4), 304-317. doi:10.1016/S0022-1694(98)00213-3

Merz, B., Plate, E. J. (1997). An analysis of the effects of spatial variability of soil and soil moisture on runoff. Water Resources Research, 33(12), 2909-2922. doi:10.1029/97WR02204

Mohanty, B. P., Bowman, R. S., Hendrickx, J. M. H., Simunek, J., van Genuchten, M. T. (1998). Preferential transport of nitrate to a tile drain in an intermittent-flood-irrigated field: Model development and experimental evaluation. Water Resources Research, 34(5), 1061-1076. doi:10.1029/98WR00294

Mole nat, J., Gascuel-Odoux, C. (2002). Modelling flow and nitrate transport in groundwater for the prediction of water travel times and of consequences of land use evolution on water quality. Hydrological Processes, 16(2), 479-492. doi:10.1002/hyp.328

Molina-Navarro, E., Andersen, H. E., Nielsen, A., Thodsen, H., Trolle, D. (2017). The impact of the objective function in multi-site and multi-variable calibration of the SWAT model. Environmental Modelling and Software, 93, 255-267. doi:10.1016/j.envsoft.2017.03.018

Molina-Navarro, E., Bailey, R. T., Andersen, H. E., Thodsen, H., Nielsen, A., Park, S., Jensen, J. S., Jensen, J. B., Trolle, D. (2019). Comparison of abstraction scenarios simulated by SWAT and SWAT-MODFLOW. Hydrological Sciences Journal, 64(4), 434-454. doi:10.1080/02626667.2019.1590583

Møller, A. B., Beucher, A., Iversen, B. V., Greve, M. H. (2018). Predicting artificially drained areas by means of a selective model ensemble. Geoderma, 320, 30-42. doi:10.1016/j.geoderma.2018.01.018

Møller, A. B., Koganti, T., Beucher, A. l., Iversen, B. V., Greve, M. H. (2021). Downscaling digital soil maps using electromagnetic induction and aerial imagery. Geoderma, 385. doi:10.1016/j.geoderma.2020.114852

Morbidelli Renato, R., Morbidelli, R., Saltalippi, C., Govindaraju, R. S. (2018). Role of slope on infiltration: A review. Journal of Hydrology, 557, 878-886. doi:10.1016/j.jhydrol.2018.01.019

Moriasi, D., Arnold, J., Van Liew, M., Bingner, R., Harmel, R., Veith, T. (2007). Model evaluation guidelines for systematic quantification of accuracy in watershed simulations. Transactions of the ASABE, 50, 885-900.

Mualem, Y. (1976). A new model for predicting the hydraulic conductivity of unsaturated porous media. Water Resources Research, 12(3), 513-522. doi:10.1029/WR012i003p00513

Muma, M., Gumiere, S. J., Rousseau, A. N. (2014). Comprehensive analysis of the CATHY model sensitivity to soil hydrodynamic properties of a tile-drained, agricultural micro-watershed. Hydrological Sciences Journal, 59(8), 1606-1623.

Muma, M., Rousseau, A. N., Gumiere, S. J. (2016). Modeling of subsurface agricultural drainage using two hydrological models with different conceptual approaches as well as dimensions and spatial scales. Canadian Water Resources Journal, 42(1), 38-53. doi:10.1080/07011784.2016.1231014

Munz, M., Oswald, S.E., Schmidt, C., 2017. Coupled Long-Term Simulation of Reach-Scale Water and Heat Fluxes Across the River-Groundwater Interface for Retrieving Hyporheic Residence Times and Temperature Dynamics. Water Resour. Res. 53, 8900–8924. doi:10.1002/2017WR020667

Nangia, V., Gowda, P. H., Mulla, D. J., Sands, G. R. (2010). Modeling Impacts of Tile Drain Spacing and Depth on Nitrate-Nitrogen Losses. Vadose Zone Journal, 9(1), 61-72. doi:10.2136/vzj2008.0158

Nash, J. E., Sutcliffe, J. V. (1970). River Flow Forecasting Through Conceptual Models Part I-a Discussion of Principles*. Journal of Hydrology, 10, 282-290. doi:10.1016/0022-1694(70)90255-6

Nilsson, B., Sidle, R. C., Klint, K. E., Bøggild, C. E., Broholm, K. (2001). Mass transport and scale-dependent hydraulic tests in a heterogeneous glacial till–sandy aquifer system. Journal of Hydrology, 243(3), 162-179. doi:10.1016/S0022-1694(00)00416-9

Nimmo, J. R. (2012). Preferential flow occurs in unsaturated conditions. Hydrological Processes, 26(5), 786-789. doi:10.1002/hyp.8380

Nogueira, G.E.H., Schmidt, C., Brunner, P., Graeber, D., Fleckenstein, J.H., 2021. Transit-time and temperature control the spatial patterns of aerobic respiration and denitrification in the riparian zone. Water Resour. Res. https://doi.org/10.1029/2021WR030117

Nolan, B.T., Malone, R.W., Doherty, J.E., Barbash, J.E., Ma, L., Shaner, D.L. (2015). Data worth and prediction uncertainty for pesticide transport and fate models in Nebraska and Maryland, United States. Pest Manag. Sci. 71, 972–985. doi:10.1002/ps.3875

Noorduijn, S. L., Refsgaard, J. C., Petersen, R. J., Højberg, A. L. (2021). Downscaling a national hydrological model to subgrid scale. Journal of Hydrology. doi:10.1016/j.jhydrol.2021.126796

Nousiainen, R., Warsta, L., Turunen, M., Huitu, H., Koivusalo, H., Pesonen, L. (2015). Analyzing subsurface drain network performance in an agricultural monitoring site with a three-dimensional hydrological model. Journal of Hydrology, 529(P1), 82-93. doi:10.1016/j.jhydrol.2015.07.018

O'Connell, E., Ewen, J., O'Donnell, G., Quinn, P. (2007). Is there a link between agricultural land-use management and flooding? Hydrology and Earth System Sciences, 11(1), 96-107. doi:10.5194/hess-11-96-2007

Oosterbaan, R. J. (2002). SaltMod. Description of principles, user manual and examples of application. Technical report, International Institute for Land Reclmatation and Improvement, Wageningen, The Netherlands. 77 p. Retrieved from: www.waterlog.info/pdf/saltmod.pdf.

Ovesen, N. B., and Poulsen, J. R. (2016), (In Danish) Hydrometriske stationer, databehandling og beregninger, QH-station. Teknisk anvisning nr. B05 version 1.0.

Palosuo, T., Kersebaum, K. C., Angulo, C., Hlavinka, P., Moriondo, M., Olesen, J. E., Çaldağ, B. (2011). Simulation of winter wheat yield and its variability in different climates of Europe: A comparison of eight crop growth models. European Journal of Agronomy, 35(3), 103-114. doi:10.1016/j.eja.2011.05.001

Panday, S., Huyakorn, P. S. (2004). A fully coupled physically-based spatially-distributed model for evaluating surface/subsurface flow. Advances in Water Resources, 27(4), 361-382. doi:10.1016/j.advwatres.2004.02.016

Partington, D., Brunner, P., Frei, S., Simmons, C. T., Werner, A. D., Therrien, R., Maier, H. R., Dansy, G. C., Fleckenstein, J. H. (2013). Interpreting streamflow generation mechanisms from integrated surface-subsurface flow models of a riparian wetland and catchment. Water Resources Research, 49(9), 5501-5519. doi:10.1002/wrcr.20405

Petersen, C. T., Trautner, A., Hansen, S. (2008). Spatio-temporal variation of anisotropy of saturated hydraulic conductivity in a tilled sandy loam soil. Soil and Tillage Research, 100(1-2), 108-113. doi:10.1016/j.still.2008.05.004

Petersen, R. J., Prinds, C., Iversen, B. v., Engesgaard, P., Jessen, S., Kjaergaard, C. (2020). Riparian Lowlands in Clay Till Landscapes: Part I—Heterogeneity of Flow Paths and Water Balances. Water Resources Research, 56(4), n/a-n/a. doi:10.1029/2019WR025808

Postma, D., Boesen, C., Kristiansen, H., Larsen, F. (1991). Nitrate Reduction in an Unconfined Sandy Aquifer: Water Chemistry, Reduction Processes, and Geochemical Modeling. Water Resources Research, 27(8), 2027-2045. doi:10.1029/91WR00989

Prinds, C., Petersen, R.J., Greve, M.H., Iversen, B.V. (2019). Locating tile drainage outlets and surface flow in riparian lowlands using thermal infrared and RGB-NIR remote sensing. Geogr. Tidsskr. - Danish J. Geogr. 119, 94–105. doi:10.1080/ 00167223.2019.1573408.

Prinds, C., Petersen, R.J., Greve, M.H., Iversen, B.V. (2020). Three-dimensional voxel geological model of a riparian lowland and surrounding catchment using a multi- geophysical approach. J. Appl. Geophys. 174, 1–38. doi:10.1016/j. jappgeo.2020.103965.

Radcliffe, D. E., Reid, D. K., Blombäck, K., Bolster, C. H., Collick, A. S., Easton, Z. M., Francesconi, W., Fuka, D. R., Johnsson, H., King, K., Larsbo, M., Youssef, M. A., Mulkey, A. S., Nelson, N. O., Persson, K., Ramirez-Avila, J. J., Schmieder, F., Smith, D. R. (2015). Applicability of Models to Predict Phosphorus Losses in Drained Fields: A Review. Journal of Environment Quality, 44(2), 614-614. doi:10.2134/jeq2014.05.0220

Refsgaard, J. C., Auken, E., Bamberg, C. A., Christensen, B. S. B., Clausen, T., Dalgaard, E., Effersø, F., Ernstsen, V., Gertz, F., Hansen, A. L., He, X., Jacobsen, B. H., Jensen, K. H., Jørgensen, F., Jørgensen, L. F., Koch, J., Nilsson, B., Petersen, C., De Schepper, G., Schamper, C., Sørensen, K. I., Therrien, R., Thirup, C., Viezzoli, A. (2014). Nitrate reduction in geologically heterogeneous catchments - A framework for assessing the scale of predictive capability of hydrological models. Science of the Total Environment, 468-469, 1278-1288. doi:10.1016/j.scitotenv.2013.07.042

Refsgaard, J. C., Christensen, S., Sonnenborg, T. O., Seifert, D., Højberg, A. L., Troldborg, L. (2012). Review of strategies for handling geological uncertainty in groundwater flow and transport modeling. Advances in Water Resources, 36, 36-50. doi:10.1016/j.advwatres.2011.04.006

Refsgaard, J., Hansen, A., Højberg, A., Olesen, J., Hashemi, F., Wachniew, P., Chubarenko, B. (2019). Spatially differentiated regulation: Can it save the Baltic Sea from excessive N-loads? Ambio, 48(11), 1278-1289. doi:10.1007/s13280-019-01195-w

Refsgaard, J. C., Storm, B. (1995). MIKE SHE. In V. P. Singh (Ed.), Computer Models of Watershed Hydrology (pp. 809-846). CO, USA: Water Resource Publications.

Reichenberger, S., Bach, M., Skitschak, A., Frede, H.-G. (2007). Mitigation strategies to reduce pesticide inputs into ground- and surface water and their effectiveness; A review. Science of the Total Environment, 384(1), 1-35. doi:10.1016/j.scitotenv.2007.04.046

Robin, M. J. L., Gutjahr, A. L., Sudicky, E. A. (1993). Cross-correlated random field generation with the direct Fourier transform method. Water Resources Research, 29(7), 2385-2397. Retrieved from http://www.agu.org/pubs/crossref/1993/93WR00386.shtml

Robinet, J. r. m., von Hebel, C., Govers, G., van der Kruk, J., Minella, J. P. G., Schlesner, A., Ameijeiras-Marin□ o,Y., Vanderborght, J. (2018). Spatial variability of soil water content and soil electrical conductivity across scales derived from Electromagnetic Induction and Time Domain Reflectometry. Geoderma, 314, 160-174. doi:10.1016/j.geoderma.2017.10.045

Robinson, M. and Rycroft, D. W. (1999). The impact of drainage on streamflow. In Skaggs, R. W., Van Schilfgaarde, J., Bartels, J. M., Hatfield, J. L., Volenec, J. J., Bigham, J. M. (1999). Agricultural drainage [1 online resource (xxv, 1328 pages) : illustrations]. doi:10.2134/agronmonogr38

Rodvang, S. J., Simpkins, W. W. (2001). Agricultural contaminants in Quaternary aquitards: A review of occurrence and fate in North America. Hydrogeology Journal, 9(1), 44-59. doi:10.1007/s100400000114

Rosenbom, A. E., Olsen, P., Plauborg, F., Grant, R., Juhler, R. K., Brüsch, W., Kjær, J. (2015). Pesticide leaching through sandy and loamy fields - Long-term lessons learnt from the Danish Pesticide Leaching Assessment Programme. Environmental Pollution, 201, 75-90. doi:10.1016/j.envpol.2015.03.002

Rozemeijer, J. C., Van Der Velde, Y., McLaren, R. G., Van Geer, F. C., Broers, H. P., Bierkens, M. F. P. (2010a). Integrated modeling of groundwater-surface water interactions in a tile-drained agricultural field: The importance of directly measured flow route contributions. Water Resources Research, 46(11), 1-10. doi:10.1029/2010WR009155

Rozemeijer, J. C., Van Der Velde, Y., Van Geer, F. C., Bierkens, M. F. P., Broers, H. P. (2010b). Direct measurements of the tile drain and groundwater flow route contributions to surface water contamination: From field-scale concentration patterns in groundwater to catchment-scale surface water quality. Environmental Pollution, 158(12), 3571-3579. doi:10.1016/j.envpol.2010.08.014Sammons, R. J., Mohtar, R. H., Northcott, W. J. (2005). Modeling subsurface drainage flow of a tile-drained small watershed using DRAINMOD. Applied Engineering in Agriculture, 21(5), 815-834.

Salo, H., Warsta, L., Turunen, M., Nurminen, J., Myllys, M. (2017). Simulating 3-D water flow in subsurface drain trenches and surrounding soils in a clayey field. Soil and Tillage Research, 168, 20-32.

Sammons, R. J., Mohtar, R. H., Northcott, W. J. (2005). Modeling subsurface drainage flow of a tile-drained small watershed using DRAINMOD. Applied Engineering in Agriculture, 21(5), 815-834.

Schilling, K. E., Gassman, P. W., Arenas-Amado, A., Jones, C. S., Arnold, J. (2019). Quantifying the contribution of tile drainage to basin-scale water yield using analytical and numerical models. The Science of the total environment, 657, 297-309. doi:10.1016/j.scitotenv.2018.11.340

Schilling, K. E., Helmers, M. (2008). Effects of subsurface drainage tiles on streamflow in Iowa agricultural watersheds: Exploratory hydrograph analysis. Hydrological Processes, 22(23), 4497-4506.

Schilling, K. E., Jindal, P., Basu, N. B., Helmers, M. J. (2012). Impact of artificial subsurface drainage on groundwater travel times and baseflow discharge in an agricultural watershed, Iowa (USA). Hydrological Processes, 26(20), 3092-3100. doi:10.1002/hyp.8337

Schilling, K. E., Libra, R. D. (2003). Increased baseflow in Iowa over the second half of the 20th century. JAWRA Journal of the American Water Resources Association, 39(4), 851-860. doi:10.1111/j.1752-1688.2003.tb04410.x

Sheets, K. R., Hendricks, J. M. H. (1995). Noninvasive Soil Water Content Measurement Using Electromagnetic Induction. Water Resources Research, 31(10), 2401-2409. doi:10.1029/95WR01949

S imu nek, J., Genuchten, M. T. (2008). Modeling Nonequilibrium Flow and Transport Processes Using HYDRUS. Vadose Zone Journal, 7(2), 782-797. doi:10.2136/vzj2007.0074

Šimůnek, J., Huang, K., van Genuchten, M.Th. (1995). The SWMS-3D code for simulating water flow and solute transport in three-dimensional variably-saturated media. Version 1.0. Research Report No. 139, US Salinity Laboratory, Riverside, CA.

Šimůnek, J., Jarvis, N. J., van Genuchten, M. T., Gärdenäs, A. (2003). Review and comparison of models for describing non-equilibrium and preferential flow and transport in the vadose zone. Journal of Hydrology, 272(1), 14-35. doi:10.1016/S0022-1694(02)00252-4

Šimůnek, J., van Genuchten, M. T., Šejna, M. (2016). Recent developments and applications of the HYDRUS computer software packages. Vadose Zone Journal, 15(7). doi:10.2136/vzj2016.04.003

Šimůnek, J., van Genuchten, M. T., Šejna, M. (2006). The HYDRUS software package for simulating two- and three-dimensional movement of water, heat, and multiple solutes in variably-saturated media.

Technical Manual, Version 1.0, PC Progress, Prague, Czech Republic. 213 p. Retrieved from: www.pc-progress.com/en/Default.aspx?Downloads.

Skaggs, R. W. (1978). A water management model for shallow water table soils. North Carolina. University. Water Resources Research(14).

Skaggs, R. W., Brevé, M. A., Gilliam, J. W. (1994). Hydrologic and water quality impacts of agricultural drainage. Critical Reviews in Environmental Science and Technology, 24(1), 1-32. doi:10.1080/10643389409388459

Skaggs, R. W., Chescheir, G. M. (2003). Effects of Subsurface Drain Depth on Nitrogen Losses from Drained Lands. Transactions of the ASAE, 46(2), 237-244.

Skaggs, R. W., Youssef, M. A., Chescheir, G. M. (2012). DRAINMOD: Model use, calibration, and validation. Transactions of the ASABE, 55(4), 1509-1522.

Sloan, B. P., Basu, N. B., Mantilla, R. (2016). Hydrologic impacts of subsurface drainage at the field scale: Climate, landscape and anthropogenic controls. Agricultural Water Management, 165, 1-10. doi:10.1016/j.agwat.2015.10.008

Sloan, B. P., Mantilla, R., Fonley, M., Basu, N. B. (2017). Hydrologic impacts of subsurface drainage from the field to watershed scale. Hydrological Processes, 31(17), 3017-3028. doi:10.1002/hyp.11218

Stamm, C., Flu□ hler, H., Ga□ chter, R., Leuenberger, J., Wunderli, H. (1998). Preferential Transport of Phosphorus in Drained Grassland Soils. Journal of environmental quality, 27(3), 515-522. doi:10.2134/jeq1998.00472425002700030006x

Stamm, C., Sermet, R., Leuenberger, J., Wunderli, H., Wydler, H., Flühler, H., Gehre, M. (2002). Multiple tracing of fast solute transport in a drained grassland soil. Geoderma, 109(3-4), 245-268. doi:10.1016/S0016-7061(02)00178-7

Sudicky, E. A. (1990). The Laplace Transform Galerkin technique for efficient time-continuous solution of solute transport in double-porosity media. Geoderma, 46(1), 209-232. doi:10.1016/0016-7061(90)90016-3

Sulis, M., Paniconi, C., Camporese, M. (2011). Impact of grid resolution on the integrated and distributed response of a coupled surface-subsurface hydrological model for the des Anglais catchment, Quebec. Hydrological Processes, 25(12), 1853-1865. doi:10.1002/hyp.7941

Szejba, D., Bajkowski, S. (2019). Determination of Tile Drain Discharge under Variable Hydraulic Conditions. Water, 11(1).

Tang, X. Y., Zhu, B., Katou, H. (2012). A review of rapid transport of pesticides from sloping farmland to surface waters: Processes and mitigation strategies. Journal of Environmental Sciences, 24(3), 351-361. doi:10.1016/S1001-0742(11)60753-5

Tedeschi, A., Beltrán, A., and Araguésa, R. (2001). Irrigation management and hydrosalinity balance in a semi-arid area of the middle Ebro River Basin (Spain). Agr. Water Manage., 49(1):31–50. doi:10.1016/S0378-3774(00)00117-7.

Therrien, R., McLaren, R. G., Sudicky, E. A., Panday, S. M. (2010). HydroGeoSphere: A three-dimensional numerical model describing fully-integrated subsurface and surface flow and solute transport.

Thodsen, H., Andersen, H. E., Blicher-Mathiesen, G., Trolle, D. (2015). The combined effects of fertilizer reduction on high risk areas and increased fertilization on low risk areas, investigated using the SWAT model for a Danish catchment. Acta Agriculturae Scandinavica, Section B - Soil & Plant Science, 65(sup2), 217-227. doi:10.1080/09064710.2015.1010564

Thomas, N. W., Arenas, A. A., Schilling, K. E., Weber, L. J. (2016). Numerical investigation of the spatial scale and time dependency of tile drainage contribution to stream flow. Journal of Hydrology, 538, 651-666. doi:10.1016/j.jhydrol.2016.04.055

Tiemeyer, B., Moussa, R., Lennartz, B., Voltz, M. (2007). MHYDAS-DRAIN: A spatially distributed model for small, artificially drained lowland catchments. Ecological Modelling, 209(1), 2-20. doi:10.1016/j.ecolmodel.2007.07.003

Tolboll, R., Christensen, N. (2007). Sensitivity functions of frequency-domain magnetic dipole-dipole systems. GEOPHYSICS, 72(2), F45-F56. doi:10.1190/1.2409623

Turunen, M., Warsta, L., Paasonen-Kivekas, M., Nurminen, J., Myllys, M. (2013). Modeling water balance and effects of different subsurface drainage methods on water outflow components in a clayey agricultural field in boreal conditions. Agricultural Water Management, 121, 135-148.

van Der Velde, Y., Rozemeijer, J., de Rooij, G., van Geer, F., Broers, H. (2010). Field-Scale Measurements for Separation of Catchment Discharge into Flow Route Contributions. Vadose Zone Journal, 9(1), 25-35. doi:10.2136/vzj2008.0141

van Genuchten, M. T., Leij F., Yates S. (1991). The RETC code for quantifying the hydraulic functions of unsaturated soils. IAG-DW12933934. USEPA, Robert S. Kerr Environ. Res. Lab., Ada, OK, the U.S.A.

van Genuchten, M. T., Wierenga, P. J. (1976). Mass Transfer Studies in Sorbing Porous Media I. Analytical Solutions. Soil Science Society of America Journal, 40(4), 473-480. doi:10.2136/sssaj1976.03615995004000040011x

Varvaris, I., Børgesen, C. D., Kjærgaard, C., Iversen, B. V. (2018). Three Two-Dimensional Approaches for Simulating the Water Flow Dynamics in a Heterogeneous Tile-Drained Agricultural Field in Denmark. Soil Science Society of America Journal, 82(6), 1367-1383. doi:10.2136/sssaj2018.05.0190

Varvaris, I., Pittaki-Chrysodonta, Z., Børgesen, C. D., Iversen, B. V. (2021a). Parameterization of two-dimensional approaches in HYDRUS-2D: Part 1. Simulating water flow dynamics at the field scale. Soil Science Society of America Journal, 85(5), 1578-1599. doi:10.1002/saj2.20307

Varvaris, I., Pittaki-Chrysodonta, Z., Børgesen, C. D., Iversen, B. V. (2021b). Parameterization of two-dimensional approaches in HYDRUS-2D. Part 2: Solute transport on field and column-scale. Soil Science Society of America Journal. doi:10.1002/saj2.20262

Varvaris, I., Pittaki - Chrysodonta, Z., Moldrup, P., Jonge, L. W., Iversen, B. V. (2019). Combining Visible−Near-Infrared and Pedotransfer Functions for Parameterization of Tile Drain Flow Simulations. Vadose Zone Journal, 18(1), 1-12. doi:10.2136/vzj2018.09.0171

Vervloet, L. S. C., Binning, P. J., Børgesen, C. D., Højberg, A. L. (2018). Delay in catchment nitrogen load to streams following restrictions on fertilizer application. Science of the Total Environment, 627, 1154-1166. doi:10.1016/j.scitotenv.2018.01.255

Viezzoli, A., Christiansen, A., Auken, E., Sorensen, K. (2008). Quasi-3D modeling of airborne TEM data by spatially constrained inversion. GEOPHYSICS, 73(3), F105-F113. doi:10.1190/1.2895521

Vogel, T., Gerke, H. H., Zhang, R., Van Genuchten, M. T. (2000). Modeling flow and transport in a two-dimensional dual-permeability system with spatially variable hydraulic properties. Journal of Hydrology, 238(1-2), 78-89. doi:10.1016/S0022-1694(00)00327-9

Voss, C. I. and Provost, A. M. (2010). SUTRA, A model for saturated-unsaturated variable density ground-water flow with solute or energy transport. Water-resources investigations report 02-4231, U.S. Geological Survey, Reston, VA, USA. 291 p.

Walker, S. E., Mitchell, J. K., Hirschi, M. C., Johnsen, K. E. (2000). Sensitivity analysis of the root zone water quality model. Transactions of the ASAE, 43(4), 841-846.

Wang, W., Oswald, S.E., Gräff, T., Lensing, H.J., Liu, T., Strasser, D., Munz, M. (2020). Impact of river reconstruction on groundwater flow during bank filtration assessed by transient three-dimensional modelling of flow and heat transport. Hydrogeol. J. 28, 2633–2634. doi:10.1007/s10040-020-02221-y

Wang, Mosley, C. T., Frankenberger, J. R., Kladivko, E. J. (2006). Subsurface drain flow and crop yield predictions for different drain spacings using DRAINMOD. Agricultural Water Management, 79(2), 113-136.

Wang, Z., Zhang, T. Q., Tan, C. S., Taylor, R. A. J., Wang, X., Qi, Z. M., Welacky, T. (2018). Simulating crop yield, surface runoff, tile drainage and phosphorus loss in a clay loam soil of the Lake Erie region using EPIC. Agricultural Water Management, 204, 212-221. doi:10.1016/j.agwat.2018.04.021

Warsta, L., Karvonen, T., Koivusalo, H., Paasonen-Kivekäs, M., Taskinen, A. (2013). Simulation of water balance in a clayey, subsurface drained agricultural field with three-dimensional FLUSH model. Journal of Hydrology, 476, 395-409. doi:10.1016/j.jhydrol.2012.10.053

Werner, B., Tracy, J., Johnson, W. C., Voldseth, R. A., Guntenspergen, G. R., Millett, B. (2016). Modeling the Effects of Tile Drain Placement on the Hydrologic Function of Farmed Prairie Wetlands. Journal of the American Water Resources Association, 52(6), 1482-1492. doi:10.1111/1752-1688.12471

Wiberg-Larsen, P., Windolf, J., Bøgestrand, J., Baattrup-Pedersen, A., Astrup Kristensen, E., Erik Larsen, S., Thodsen, H., Bering Ovesen, N., Bjerring, R., Kronvang, B., Blicher-Mathiesen, G., Kjeldgaard, A. (2013). Videnskabelig rapport fra DCE – Nationalt Center for Miljø og Energi. Retrieved from http://dce2.au.dk/pub/SR75.pdf

Williams, M. R., King, K. W., Ford, W., Buda, A. R., Kennedy, C. D. (2016). Effect of tillage on macropore flow and phosphorus transport to tile drains. Water Resources Research, 52(4), 2868-2882. doi:10.1002/2015WR017650

Woolhiser, D. A., Smith, R. E., Giraldez, J. V. (1996). Effects of Spatial Variability of Saturated Hydraulic Conductivity on Hortonian Overland Flow. Water Resouces Research, 32(3), 671-678. doi:10.1029/95WR03108

Wriedt, G., Spindler, J., Neef, T., Meißner, R., Rode, M. (2007). Groundwater dynamics and channel activity as major controls of in-stream nitrate concentrations in a lowland catchment system? Journal of Hydrology, 343(3), 154-168. doi:10.1016/j.jhydrol.2007.06.010

Xu, T., Gómez-Hernández, J.J., 2016. Characterization of non-Gaussian conductivities and porosities with hydraulic heads, solute concentrations, and water temperatures. Water Resour. Res. 52, 6111–6136. doi:10.1002/2016WR019011

Yuan, Y., Bingner, R. L., Theurer, F. D. (2006). Subsurface Flow Component for AnnAGNPS. Applied Engineering in Agriculture, 22(2), 231-242.

Zehe, E., Flühler, H. (2001). Preferential transport of isoproturon at a plot scale and a field scale tile-drained site. Journal of Hydrology, 247(1), 100-115. doi:10.1016/S0022-1694(01)00370-5

Zehe, E., Maurer, T., Ihringer, J., Plate, E. (2001). Modeling water flow and mass transport in a loess catchment. Physics and Chemistry of the Earth, Part B: Hydrology, Oceans and Atmosphere, 26(7-8), 487-507. doi:10.1016/S1464-1909(01)00041-7

Zhou, H., Go□ mez-Herna□ ndez, J. J., Li, L. (2014). Inverse methods in hydrogeology: Evolution and recent trends. Advances in Water Resources, 63, 22-37. doi:10.1016/j.advwatres.2013.10.014